

# Seismic Hazards in Southern California: Probable Earthquakes, 1994 to 2024

by Working Group on California Earthquake Probabilities<sup>1,2,3</sup>

**Abstract** We combine geodetic, geologic, and seismic information to estimate frequencies of damaging earthquakes in three types of seismotectonic zone. Type A zones contain faults for which paleoseismic data suffice to estimate conditional probabilities. Type B zones contain faults with insufficient data for conditional probability analysis. Type C zones contain diverse or hidden faults. Each zone is assumed to have randomly distributed earthquakes plus characteristic earthquakes on specific faults. Our “cascade” model allows for multiple-segment earthquakes. Within each zone, distributed earthquakes are assumed uniform in time and space, with a truncated Gutenberg–Richter magnitude distribution. Thus, seismic hazard is defined by the characteristic earthquake rate, the rate of all distributed events, and the limiting (characteristic) magnitude. Limiting magnitudes are determined from fault lengths, while earthquake rates are determined by observed seismicity and seismic moment rate.

We present a preferred seismic hazard model with lognormal recurrence and an alternate Poissonian model. The models predict 80 to 90% probability of an  $m \geq 7$  earthquake within southern California before 2024. The 17 January 1994 Northridge earthquake occurred within the 13% of southern California’s area having the highest moment rate density. The probability of 0.2  $g$  or greater shaking before 2024 exceeds 60% in the Ventura and San Bernardino areas, and 50% throughout the Transverse Ranges between Santa Barbara and San Bernardino.

The predicted seismicity exceeds that observed historically. This may imply that (1) we underestimate the maximum magnitudes, (2) significant strain may be released aseismically, or (3) seismicity may have been anomalously low since 1850.

## Introduction

This report has two primary purposes: (1) to update the data and review the methods for estimating probabilities of large earthquakes on the southern San Andreas and San Jacinto faults estimated in 1988 by the Working Group on California Earthquake Probabilities (WGCEP, 1988), and (2) to consider other potentially damaging earthquakes throughout southern California. This is the

second in a continuing series of reports on earthquake hazards in southern California prompted by the 1992  $m = 7.3$  Landers earthquake. It updates and expands upon a report entitled “Probabilities of Large Earthquakes Occurring in California on the San Andreas Fault,” prepared by WGCEP (1988). A previous report (available from the Southern California Earthquake Center) entitled “Future Seismic Hazards in Southern California: Phase I, Implications of the 1992 Landers Earthquake Sequence” dealt primarily with short-term hazards through 1993 posed by the Landers earthquake and its aftershocks.

This report is timely for several reasons: (1) new information exists on earthquake histories for the faults considered by WGCEP (1988), including the San Andreas; (2) we need to address the seismic hazard throughout southern California more broadly than WGCEP (1988); (3) we understand better the “blind” faults that

<sup>1</sup>Principal Authors: D. D. Jackson, K. Aki, C. A. Cornell, J. H. Dieterich, T. L. Henyey, M. Mahdyiar, D. Schwartz, and S. N. Ward.

<sup>2</sup>Contributors: D. Agnew, G. Davis, J. Davis, J. Dolan, P. Flores, M. Forrest, E. Hauksson, T. Heaton, G. Huftile, I. M. Idriss, K. Jackson, P. Jennings, L. Jones, Y. Kagan, E. Lehmer, K. McNally, J. McRaney, B. Minster, S. Park, M. Petersen, M. Reichle, T. Rockwell, S. Salyards, J. Savage, K. Sieh, J. Suppe, P. Ward, R. Weldon, S. Wesnousky, and R. Yeats.

<sup>3</sup>Coordinated by the Southern California Earthquake Center, on behalf of the United States Geological Survey and the California Office of Emergency Services. The Southern California Earthquake Center is a National Science Foundation Science and Technology Center.

do not break the surface, as well as numerous lesser faults that are individually not as hazardous, but pose a significant aggregated danger; (4) new geodetic data on crustal strain rates are rapidly becoming available; and (5) improvements have been made in seismological methods for studying recent earthquakes and in statistical methods for dealing with their uncertainties. Following the 1989 Loma Prieta earthquake, a similar reassessment of the chances for large earthquakes in northern California was made in a report entitled "Probabilities of Large Earthquakes in the San Francisco Bay Region, California" (USGS Circular 1053, 1990), prepared by the WGCEP (1990).

The Southern California Earthquake Center has coordinated the post-Landers series of reports at the request of the National Earthquake Prediction Evaluation Council (NEPEC) and the California Earthquake Prediction Evaluation Council (CEPEC). An *ad hoc* Working Group on Southern California Earthquake Probabilities was established to prepare this and the earlier report. For this study, NEPEC and CEPEC asked the working group to (1) include a regional perspective on the current tectonic environment, (2) review the methodology of the 1988 and 1990 reports and emphasize their differences from the current report, (3) consider new models for earthquake recurrence, (4) review newly available data for inclusion in updated probabilistic analyses, and (5) include examples of strong ground-motion predictions using existing models and attenuation relationships.

NEPEC was established in 1979 pursuant to the National Earthquake Hazards Reduction Act of 1977 to advise the Director of the United States Geological Survey (USGS) concerning any formal predictions or other information pertinent to potential significant earthquakes. CEPEC was established in 1976 under existing administrative authority as the successor to an advisory group formed in 1974. For the Director of the California Office of Emergency Services (OES), CEPEC evaluates predictions of earthquakes capable of causing damage in California, including the reliability of the data and scientific validity of the technique used to arrive at a specific prediction.

SCEC was established in 1991 under the National Science Foundation's Science and Technology Center Program and the USGS's component of the National Earthquake Hazards Reduction Program.

Preliminary versions of this report were presented to earthquake scientists and engineers at various meetings including a NEPEC meeting in June 1993, a joint NEPEC-CEPEC meeting in August 1993, a symposium during the Fall 1993 AGU meeting, and several SCEC workshops addressing various aspects of the study. The report has been reviewed jointly by both NEPEC and CEPEC to assess the extent of scientific consensus on its analytical approach and conclusions.

Estimates of seismic hazard depend on a knowledge

of potential earthquake sources, seismic wave paths, and local site conditions. This report contributes to an improved understanding of the first of these factors. The earthquake source potential in each of 65 seismotectonic zones in southern California is estimated by combining geologic, geodetic, and historical seismicity data. We present an up-to-date data base of fault information, with our best estimates of the size and frequency of future earthquakes. We also assess the likelihood of earthquake occurrence in areas where individual faults may not tell the whole story. We summarize the historical record of earthquake occurrence and report on the distribution of strain accumulation in the area. Finally, we show examples of how information in the data base can be used in seismic hazard estimation.

The total slip rate implied by the estimated earthquake frequency is roughly equal to the long-term plate tectonic slip rate, although departures in the frequency of earthquakes predicted from this rate may occur near the big restraining bend of the San Andreas in southern California. The current rate of plate tectonic slip can be estimated from geodetic measurements, and we assume that the strain accumulating in the brittle part of the crust is released seismically, except for the known creeping fault segments. This "slip budget" could be met by very large rare earthquakes or by more frequent moderate earthquakes. Thus, during the 30-yr time span of our forecast, the probability of an earthquake of a given magnitude depends on the assumed maximum earthquake in a given location.

## Tectonic Framework of Southern California

The tectonic framework physically links the geologic, geodetic, and seismological data on earthquake sources presented in this report. It constrains geodetic models of crustal deformation, where earthquakes are likely to occur, and what their mechanisms are likely to be.

Earthquakes and crustal deformation result from plate tectonic processes. These processes have been going on for hundreds of millions of years. They involve movements of large plates of lithosphere—slabs of the earth's outermost layers about 100-km thick and thousands of kilometers across. Three types of plate boundaries are recognized: (1) spreading ridges, where oceanic plates are formed and spread laterally away from each other; (2) transform faults, where two plates slide horizontally past each other along strike-slip faults; and (3) subduction zones, where one plate dives beneath another.

### California—On the Pacific–North American Plate Boundary

California has been the site of a plate boundary for more than 200 m.y., although its character has changed during this time. Figure 1 shows place names used

throughout the report, and Figure 2 interprets California's relationship to both ancient and present plate boundaries. Prior to about 25 m.y.a., the boundary was a subduction zone with an oceanic trench west of the continental margin (Fig. 2, dashed line with barbs)—similar to the present situation along the west coasts of Central and South America, as well as the Pacific Northwest. Much of California's geology reflects this early history of subduction. However, between 20 and 30 m.y.a., a segment of the East Pacific spreading ridge encountered the continent, annihilating itself and leading to formation of a transform fault boundary. Currently, the East Pacific Rise, as it is called, contacts North America at the tip of Baja California (Fig. 2), while a remnant of the spreading ridge still exists off the coasts of northern California, Oregon, and Washington.

The newly formed transform boundary, later to become the San Andreas fault, may have initially developed west of the continental margin, perhaps near the site of the original trench. However, about 5 m.y.a. it jumped ashore, began separating Baja California from mainland Mexico, and slid coastal California northward along the San Andreas fault system as we know it today. The rate at which coastal California and the rest of the Pacific plate is sliding past North America has been estimated by several different methods, including worldwide plate reconstructions, geodetic measurements, and geologic offsets. All are consistent, giving about 50 mm/yr over the last 5 m.y. or so. Since earthquake rupture is the primary consequence of the relative motion between two plates, California's seismicity should be compatible with the observed plate tectonic rate.

The on-land presence of this Pacific–North American plate boundary is responsible for southern California's faults and earthquakes. The boundary actually consists of a complex web of faults throughout most of the region (Fig. 3). As the principal member of this system, the San Andreas fault carries about 70% of the right-lateral strike-slip motion (~35 mm/yr) between the two plates. The remaining 30% is distributed on faults both to the east of the San Andreas (e.g., the Eastern Mojave Shear Zone—site of the 1992 Landers earthquake) and to the west, including the San Jacinto, Whittier–Elsinore, Newport–Inglewood, Palos Verdes, and offshore San Clemente faults.

#### The Big Bend in the San Andreas Fault

Southern California is complicated by considerable thrusting in addition to strike slip. Here the San Andreas fault, which carries the majority of the strike slip between the North American and Pacific plates, changes from a northwesterly trend, parallel to the relative plate motion, to a more westerly trend, making an angle of approximately 30° to the plate motion (Fig. 3). This “big bend” in the San Andreas causes a component of north–south convergence across the San Andreas in southern

California. Geodetic and geologic estimates of the convergence range from 5 to 20 mm/yr. The result has been the Transverse Ranges and numerous east–west-trending thrust faults, associated folds, and possible subhorizontal, mid-crustal detachment surfaces. The tectonic processes now operating in southern California are dominated by the intersection of the northwest-trending San Andreas family of faults (San Andreas, San Jacinto, Whittier–Elsinore, *etc.*) with the east–west-trending Transverse Ranges fault system. This complex plate boundary explains the distinct and more regionally distributed tectonic regime of southern California compared to those of the central and northern parts of the state.

The big bend in the San Andreas is due to a 160-km “left step” in the fault (Fig. 3). This left step occurs between the Coachella Valley and Carrizo segments of the San Andreas. Within the big bend, the fault consists of the Mojave and San Bernardino Mountains segments. Thrust faulting along the big bend occurs north of the San Andreas fault on the flanks of the San Bernardino Mountains, and south of the fault along the southern margin of the San Gabriel and Santa Monica Mountains, in the Los Angeles and Ventura basins, and throughout the western Transverse Ranges (Fig. 3). Many of these thrust faults break the earth's surface and place basement rocks over younger sedimentary rocks. Other faults are buried, forming the cores of large folds in the overlying rocks. These blind thrusts occur as segmented strands within zones of intense folding along the margins of major oil-bearing basins of coastal California.

#### Earthquakes and Mid-Crustal Detachment Surfaces

Earthquake hypocenters usually occur in the upper 10 to 15 km of the earth's crust (seismogenic zone) in southern California, even though the base of the crust (Moho) is at a depth of 25 to 30 km and lithospheric plates are believed to be about 100-km thick. What happens below the seismogenic zone? There is growing evidence that the lower crust is ductile and partially decoupled from the upper crust along one or more subhorizontal detachment surfaces. Faults that extend down into the lower crust may no longer be discrete fractures, but rather zones of distributed deformation unable to support stresses large enough to generate earthquakes. Also, in convergent zones, portions of the ductile lower crust and the underlying upper mantle may peel away from the remaining upper crust and sink into the deeper mantle. Seismic velocity tomography in southern California suggests that this process may be occurring beneath the central and eastern Transverse Ranges.

An emerging view of the thrust faults associated with the Transverse Ranges and oil-bearing basins posits that individual thrusts flatten out and merge into detachment surfaces at mid-crustal depths (Fig. 4). In this model, the Transverse Ranges resemble large crustal “flakes.” It is clear from the 1971 San Fernando, 1987 Whittier

Narrows, and 1994 Northridge earthquakes that many of these thrust faults are seismically active, but what fraction of Pacific–North American plate convergence occurs aseismically on these structures is unknown. Does slip on the detachment surfaces occur seismically or aseismically? These questions have profound implications for seismic hazard in southern California—especially in the populous Los Angeles and Ventura basins.

As noted earlier, the intersection of the northwest-trending San Andreas and east–west-trending Transverse Ranges fault systems dominates southern California's tectonics. The Transverse Ranges uplift is the most visible product of this deformation. Earthquakes, seemingly random in time and space, but more recently occurring in the Transverse Ranges seismic belt, effect this uplift and the continuing northwestward movement of coastal California. The major coastal basins, like Los Angeles and Ventura, that opened during an earlier phase of crustal extension before the modern San Andreas system formed 5 m.y.a., are now being squeezed into elongate troughs. These troughs are bounded by large fold and thrust belts as the Pacific and North American plates encounter each other along the big bend. Such belts probably deform both seismically and aseismically. Aseismic deformation should be restricted to the sedimentary section and to slip along deep, subhorizontal detachment surfaces below the brittle-ductile transition (the thickness,  $H$ , of brittle crust is assumed to be 11 km in this report). On the other hand, seismic slip will more likely occur on upward-branching buried thrust faults (Fig. 4), and along ramps and interconnecting flats of shallower detachments.

#### Conditional Probabilities for Earthquakes on Selected Faults in Southern California

In this chapter, we summarize the most recent geologic data on the major faults in southern California and update the 1988 Working Group estimates of the conditional probabilities of earthquake occurrence on various fault segments over the next 30 yr. We also describe methods for estimating earthquake recurrence times and magnitudes from geologic data.

##### Geologic Data Base: Rates and Dates for Faults with Conditional Probabilities

The 1988 Working Group estimated earthquake probabilities for the San Andreas, San Jacinto, and Imperial faults in southern California. Since then new studies have been performed on these and other major faults. In this section, we review and update the data for the San Andreas and San Jacinto, and we add new data for the Whittier–Elsinore fault.

Calculating conditional probabilities for a particular fault requires information on the recurrence interval, its uncertainty, and the elapsed time since the most recent

characteristic earthquake on the fault. Earthquake recurrence can be measured directly where the ages of successive earthquakes at a point on a fault can be dated using radiocarbon or other methods. It can also be calculated using estimates of fault-slip rate together with characteristic displacement. The 1988 report relied almost exclusively on recurrence intervals calculated from the slip rate and characteristic displacement, referring to this approach as the “direct method.” Paleoseismic interevent times were used only for the Coachella Valley segment of the San Andreas fault.

Since publication of the 1988 report, new geologic data on the dates of prehistoric earthquakes as well as characteristic displacement and slip rate have been obtained for several of these fault segments. Table 1 lists estimated slip rate, characteristic displacement, earthquake recurrence interval, date of the last characteristic earthquake, length of segment, and the latitude and longitude of the two points bounding each segment. Also shown are the uncertainties in some of these parameters. The slip rate, characteristic displacement, and mean recurrence time are described by a preferred value, and “positive” and “negative” uncertainties. For the first two, the lower limit is the preferred value minus the negative uncertainty, while the upper limit is the preferred value plus the positive uncertainty. The upper limit of the recurrence time is the ratio of the upper limit of mean displacement to the lower limit of slip rate, and so on. These errors are interpreted as two standard errors when used in estimating probabilities of fault rupture. The 1988 Working Group interpreted these errors as one standard deviation, but we feel that the geologists' error bounds are much more conservative than implied by WGCEP (1988).

In Appendix C we discuss in detail the 1988 report, the new geologic data, and the rationale for deriving the current values listed in Table 1. The differences between the two reports are summarized briefly below. One significant change from the 1988 report is inclusion of new recurrence data for the Elsinore fault zone. For those faults treated by the 1988 Working Group, we have made only modest changes, if any, to the basic input data (fault length, slip rate, last displacement, and earthquake dates). However, we calculate earthquake probabilities somewhat differently. As described in this section, we relax the assumption used in the 1988 report that ruptures on a given segment occur at regular recurrence intervals. We also allow for the fact that fault segments may fail either independently or when triggered by neighboring segments, as recent paleoseismic data suggest. The cascades model, described later in this section, accounts for this interaction between segments.

Conditional probabilities are calculated only for characteristic earthquakes in the type A zones. In general, each of the segments treated in the 1988 report, and the newly studied segments of the Whittier–Elsinore fault,

correspond to type A zones. However, a few of the segments treated in WGCEP (1988) are designated here as type B zones—characteristic earthquakes are assumed Poissonian, and no time-dependent conditional probabilities are computed. The Parkfield segment of the San Andreas fault is so treated because the aseismic period since the last earthquake in 1966 is inconsistent with the model used in the 1988 report. The Cholame segment is also treated as a type B zone because there is some doubt about whether it ever ruptures as a single segment. The Imperial fault is treated as a type B zone for the reason described later in this section.

San Andreas Fault

In the 1988 report, the central and southern San Andreas fault was divided into segments named Cholame, Carrizo, Mojave, San Bernardino Mountains, and Coachella Valley. This nomenclature is retained in the present report. Earthquake recurrence for each of the San Andreas segments in the 1988 report, except the Coachella Valley segment, is calculated from slip rate and characteristic displacement. Recurrence for Coachella Valley is based on intervals between dated earthquakes. However, new data on the timing of prehistoric earthquakes are available for the Carrizo, Mojave, and San Bernardino Mountain segments. One important difference between the two reports is that this more detailed earthquake chronology is now used to quantify recurrence for the Carrizo, Mojave, and San Bernardino

Mountains segments. A second concern is fault segmentation. Although fault segments are treated as independent sources of earthquakes, historical and paleoseismological observations show that ruptures may overlap and that some segments may not only produce their own earthquakes but also fail when large ruptures nucleate on adjacent segments and propagate into them. This is particularly true for long throughgoing strike-slip faults. The event dates from sites on the southern San Andreas fault at Wrightwood, Pallett Creek, and Indio clearly indicate a complex rupture history, with both independent and overlapping ruptures. For example, it appears that the San Bernardino Mountains segment produces its own earthquakes (the 1821 event) but also slips when ruptures extend into it from the north (the 1857 earthquake) or from the south (an event occurring about 1690). This variety complicates recurrence estimates and segmentation models. We deal with this problem in the section on cascading earthquakes.

*Cholame Segment.* The Cholame segment extends from Cholame southeastward for about 60 km. The 1988 Working Group used a value of  $4.75 \pm 2.0$  m for characteristic displacement and a slip rate of  $34 \pm 1.5$  mm/yr. There have been no new slip rate, earthquake recurrence, or characteristic displacement data for the Cholame segment since the 1988 report. We adopt the 1988 characteristic displacement value, but have increased the uncertainty in slip rate to  $\pm 5$  mm/yr. These

Table 1  
Input Data for Type A Fault Segments

Zone	Name	Vel. (mm/yr)	+	-	Disp. (m)	+	-	Tbar (yr)	+	-	Last Rupture	Length (km)	Lat. (NW)	Long. (NW)	Lat. (SE)	Long. (SE)
04	SACarriz	34	3	3	7.0	4.0	4.0	206	149	125	1857	121	35.348	119.903	34.783	118.807
05	SAMojave	30	8	8	4.5	1.5	1.5	150	123	71	1857	133	34.783	118.807	34.278	117.477
06	SASanBer	24	5	5	3.5	1.0	1.0	146	91	60	1812	78	34.278	117.477	34.034	116.670
07	SACoache	25	5	5	4.0	4.0	2.0	160	240	93	1690	114	34.034	116.670	33.360	115.722
	Total San Andreas											446				
08	SJSanBer	12	6	6	1.2	0.3	0.3	100	150	50	1890	35	34.245	117.508	34.017	117.237
09	SJSanJac	12	6	6	1.0	0.2	0.2	83	117	39	1918	42	34.017	117.237	33.740	116.917
10	SJAnza	12	7	5	3.0	1.0	1.0	250	321	145	1750	90	33.740	116.917	33.263	116.122
11	SJCoyCre	4	2	2	0.7	0.3	0.3	175	325	108	1892	40	33.457	116.508	33.200	116.194
12	SJBoreg	4	2	2	0.7	0.2	0.2	175	275	92	1968	29	33.200	116.194	33.011	115.975
13	SJSupMtn	4	2	2	2.0	0.3	0.3	500	650	217	1430	23	32.993	115.922	32.888	115.702
14	SJSupHil	4	2	2	1.0	0.3	0.3	250	400	133	1987	22	33.013	115.838	32.892	115.643
	Total San Jacinto											281				
15	Whittier	2.5	1	1	1.9	0.2	0.2	760	640	274	650	38	33.986	118.018	33.854	117.637
16	GlenIvy	5	2	2	1.6	0.4	0.4	310	340	146	1910	35	33.854	117.637	33.643	117.348
17	Temecula	5	2	2	1.2	0.3	0.3	240	260	111	1818	42	33.643	117.348	33.377	117.013
18	Julian	5	2	2	1.7	0.2	0.2	340	293	126	1892	75	33.377	117.013	32.965	116.362
19	CoyoteM	4	2	2	2.5	0.5	0.5	625	875	292	1892	38	32.965	116.362	32.779	116.006
	Total Whittier											228				
	Total											955				

values give an average recurrence interval of 140 yr. A question remains as to whether the Cholame segment produces its own events or only fails in conjunction with large 1857-type earthquakes. Because of these uncertainties, the zone containing the Cholame segment is treated as a type B zone.

*Carrizo Segment.* The Carrizo segment of the San Andreas fault is approximately 145-km long and extends from southeast of Cholame to about Three Points. The 1988 Working Group estimated a recurrence interval of 296 yr for this segment using a slip rate of  $34 \pm 1.5$  mm/yr and a characteristic displacement of  $9.5 \pm 2.0$  m. New dates of paleoearthquakes and new estimates of slip for the 1857 earthquake provide somewhat contradictory results among themselves and with the 1988 report. The new observations suggest the possibility of clustering and rupture overlap, and argue that our understanding of this segment, which traditionally has been considered the most stable in characteristic displacement and recurrence interval (large offsets and long intervals), is in a state of flux. We adopt the 1988 slip rate but the uncertainty is increased to  $\pm 3$  mm/yr. The characteristic displacement is equivocal, but we adopt  $7 \pm 4$  m to reflect the range of new estimates. This slip rate and characteristic displacement give a mean recurrence interval of 206 yr, similar to the average recurrence interval of 212 yr from one of the new event chronology studies. These recurrence intervals are significantly shorter than the value used in 1988.

*Mojave Segment.* The Mojave segment, as defined in the 1988 report and used here, extends some 100 km from about Three Points to a few kilometers northwest of Cajon Creek at the southern limit of the 1857 rupture. It contains the Pallett Creek paleoseismology site, where evidence of 11 surface-faulting earthquakes since about 529 A.D. had been found in trenches. These event dates give an average recurrence interval of 131 yr but also suggest that the interval between events varied markedly from the mean. The events occur as four groups or clusters with intervals of about 200 to 300 yr between clusters. In reviewing these data, the 1988 Working Group noted, somewhat paradoxically, that the segment with the most paleoseismic data at that time also appeared to exhibit great interevent variability. Because of this they chose to calculate recurrence using the previous (1857) displacement, rather than the dates of prehistoric earthquakes. Using a slip rate of  $30 \pm 5$  mm/yr and a characteristic displacement of  $4.5 \pm 1.0$  m, they derived a repeat time of 150 yr.

The present report retains the 1988 slip rate and characteristic displacement, but increases their uncertainties to  $\pm 8$  mm/yr and  $\pm 1.5$  m, respectively. Since the 1988 report there has been no new dating of prehistoric earthquakes on the Mojave segment. However, new

data for events at Wrightwood (20 km southeast of Pallett Creek) on the San Bernardino Mountains segment and statistical reevaluation of the published Pallett Creek dates suggest modest adjustment of the estimated earthquake dates. These analyses indicate the average recurrence interval for a surface-faulting event passing through Pallett Creek is 134 yr between about 644 A.D. and 1100 A.D., and 104 yr since. Unlike the 1988 report, we calculate the conditional probability using a weighted average method which incorporates the paleoseismic data, the displacement in the last event, and the slip rate.

*San Bernardino Mountains Segment.* This segment of the fault is delineated by the 1988 Working Group as a structurally complex zone between the Mojave and Coachella Valley segments with scant data on fault behavior. However, the San Bernardino Mountains segment has received the most study since the 1988 report. (Note: we assume that the Wrightwood paleoseismic site belongs to this segment.)

The 1988 Working Group used a slip rate of  $24 \pm 3$  mm/yr and a characteristic displacement of  $4 \pm 2$  m to calculate a recurrence interval of 167 yr, and suggested 1812 as a tentative date for the most recent event. The present report uses a slip rate of  $24 \pm 5$  mm/yr and a smaller characteristic displacement of  $3.5 \pm 1.0$  m to calculate an average recurrence interval of 146 yr. New observations at Wrightwood show that six surface-faulting events have occurred since 1192 A.D. The Wrightwood site appears to average one surface-rupturing earthquake every 133 yr since 1192 A.D. However, the most recent five events have been closer together, averaging 106 yr between events. It now appears that the most recent event was in 1812, which defines an elapsed time of 181 years. For this report we incorporate the new paleoseismicity data in our probability calculations.

*Coachella Valley.* The Coachella Valley segment comprises the southern 100 km of the fault and extends from San Geronio Pass in the northwest to the Salton Sea in the southeast. This segment has the longest elapsed time of any on the fault zone, last experiencing a large event around 1680. The 1988 Working Group used the paleoseismological event times at Indio of 1680, 1450, 1300, and 1020 to arrive at an average recurrence interval of 220 yr. There have been no new paleoseismic data for this segment since the 1988 report, although the new dating at Wrightwood suggests that events occurring there in 1690 and 1450 were equivalent to the 1680 and 1450 events at Indio, and thus may have ruptured simultaneously the Coachella Valley and San Bernardino Mountains segments of the fault. For the present report we adopt the 1988 Working Group values of slip rate, characteristic displacement, and earthquake dates.

### San Jacinto Fault

The San Jacinto fault system has been an important source of moderate to large earthquakes in southern California this century. The 1988 Working Group divided the fault into five segments using information on fault geometry, historical seismicity, and slip rate. The segments, from north to south, were named San Bernardino Valley, San Jacinto Valley, Anza, Borrego Mountain, and Superstition Hills. We increase the slip rate and change the estimate of characteristic displacement on those segments.

We add the Coyote Creek and Superstition Mountains segments. Also the Anza segment is redefined to include the Clark and Casa Loma faults. As a result, the estimate of its characteristic displacement is increased to  $3.0 \pm 1.0$  m from the  $1.4 \pm 0.4$  m value in the 1988 report. In addition, new studies near Anza indicate a slip rate of  $12 \pm 6$  mm/yr. This rate is now extended north to the San Bernardino Valley and San Jacinto Valley segments, and can be compared to the respective rates of  $8 \pm 3$  mm/yr and  $11 \pm 3$  mm/yr used in the 1988 report. Estimates of characteristic displacement for the San Bernardino Valley and San Jacinto Valley segments are decreased to reflect somewhat shorter rupture lengths. These changes lengthen the recurrence interval on the Anza segment from 142 to 250 yr, and shorten the estimates of recurrence on the San Bernardino Valley and San Jacinto Valley segments from 203 to 100 yr and from 184 to 83 yr, respectively.

### Imperial Fault

The Imperial fault is a complex structure with multiple modes of slip behavior. It has produced two large historical surface faulting earthquakes—an  $m = 6.9$  in 1940 and an  $m = 6.4$  in 1979. The 1979 event broke the northern 25 km of the 1940 rupture with a similar amount of surface offset. The 1988 Working Group noted that the long-term slip rate for the fault is not well determined, but assumed a value of  $30 \pm 5$  mm/yr, estimated a characteristic displacement of  $1.2 \pm 0.4$  m, and calculated a recurrence interval of 44 yr for the northern section only. Repeat times of 1940-type events are unknown. It is possible that the northern part of the fault, which had significantly lower slip than the southern part in 1940, is failing repeatedly at shorter intervals to fill a slip deficit. In the present report, we adopt the 1988 Working Group's recurrence interval for repeat of 1979-type events on the northern part of the fault. However, given this complicated history, we are not confident that slip can be explained adequately here by repeated occurrence of a single characteristic earthquake. For this reason we have not used the conditional probability methods for the Imperial fault, and we treat it as a type B zone.

### Elsinore Fault

This major northwest-trending strike-slip fault accommodates 10 to 15% of the plate-boundary slip in southern California and could produce earthquakes of magnitude 7 or larger. The fault can be traced about 250 km from Los Angeles across the United States–Mexico border into northern Baja California. Sufficient new data on its slip rate, earthquake recurrence, characteristic displacement, and segmentation have been gathered to warrant calculation of conditional probabilities.

In this report, the fault is divided into five segments (from north to south): Whittier, Glen Ivy, Temecula, Julian, and Coyote Mountain. Slip rates vary from about 2.5 mm/yr at the north end to about 5 mm/yr at the south end. The lower apparent slip rate on the Whittier segment may be related to branching of the fault or strain partitioning due to the more westerly trend of this segment. The San Andreas, San Jacinto, and Imperial faults are the only northwest-trending strike-slip faults in southern California having higher slip rates. Segment-specific mean repeat times range from 240 to about 760 yr and average around 400 yr. With the possible exceptions of the  $m \approx 7$  earthquake of 1892 on the Laguna Salada segment in Mexico and the  $m \approx 6$  1910 Temescal Valley event on the Glen Ivy segment, the Elsinore fault has not produced an earthquake with surface faulting during the past 200 yr.

### Characteristic Earthquakes and Magnitudes

Depending on the available data, we estimate the magnitude and expected recurrence time for ruptures on each fault segment by three different methods described below. Relevant data, in decreasing order of availability, include (1) the length or area of a fault segment, (2) the long-term slip rate,  $V$ , (3) the displacement,  $D$ , in the most recent earthquake, and (4) a list of dates of past earthquakes.

Our magnitude and recurrence time estimates are based on the "characteristic earthquake" hypothesis, in which the slip is dominated by earthquakes that rupture the entire segment, with a characteristic displacement,  $D$ . The magnitude of an earthquake rupturing a single segment is based on the "seismic moment,"  $M$ , of that earthquake,

$$M = \mu \cdot H \cdot L \cdot D, \quad (1)$$

where  $\mu$  is the rigidity of the crust (assumed to be  $3 \cdot 10^{10}$  Nm<sup>-2</sup>),  $H$  is the thickness of the brittle crust (here taken to be 11 km), and  $L$  is the length of the fault segment. The seismic moment is measured in units of Nm (Newton·meters). The predicted moment rate depends linearly on the assumed brittle thickness,  $H$ . Choosing  $H = 11$  km makes the total predicted seismic moment rate consistent with that from observed earthquakes since 1850.

If the brittle thickness is greater, then the predicted moment rate exceeds the observed, or in other words, earthquakes since 1850 have not released all of the accumulated seismic moment. The assumed thickness,  $H = 11$  km, is consistent with the deepest earthquakes in California if there is negligible seismic moment release in the upper few kilometers of crust.

The "moment magnitude,"  $m$ , is a logarithmic measure of the seismic moment:

$$m = 2/3 \cdot \log_{10}(M) - 6, \tag{2}$$

from which it follows that

$$M = 10^{1.5m+9}. \tag{3}$$

Below, we generalize the characteristic earthquake concept to include simultaneous ruptures of contiguous segments (Wesnousky, 1986). We presume that the displacements on each of the segments are equal to their respective characteristic displacements, so we simply add the seismic moments of all the affected segments and use equation (2) to compute the magnitude.

In using the characteristic earthquake hypothesis, we assume that we can recognize fault segments in advance. Long faults are generally assumed to be subdivided into segments. We presume segment boundaries exist where faults change direction, or where the displacement varied substantially in the last earthquake. The length of a

fault segment is generally estimated from the length of the surface trace if this length is less than about 100 km and details of the displacement distribution in the most recent earthquake are unknown.

### Conditional Probabilities for Selected Fault Segments

Probabilities for segment-rupturing earthquakes in the coming 30 yr have been obtained from the fault-segment data (type A zones, described later) presented in Table 1, using three different models. Results are summarized in Table 2 and Figure 5. In calculating these probabilities, we follow the general approach of the 1988 Working Group, with some variations. The methods and principal results are summarized here. The reader interested in additional detail is referred to Appendix A.

We assume that the probability of a segment-rupturing earthquake increases with elapsed time since the previous earthquake, as a result of continuing tectonic deformation which increases the stress on locked fault segments. The calculations require information on elapsed time since the previous earthquake and description of the probability density function for recurrence times for that segment. Following the precedent of the 1988 and 1990 Working Groups, we adopt a probability model which assumes a lognormal probability density function of earthquake recurrence intervals,  $T$ , with mean,  $\bar{T}$ , and intrinsic variability,  $\sigma_{\ln T}$  (the standard deviation of the natural logarithm of the random recurrence interval,  $T$ ).

Table 2  
Probabilities and Rates for Type A Fault Segments

Zone	Name	% Prob. T. Pred.	% Prob. Renew.	% Prob. Dates	% Prob. Mean	% Prob. WG (1988)	% Prob. Pois.	Rate Logn.	Rate Pois.	Rate Factor	MR. Logn.	MR. Pois.
04	SACarriz	19 ± 6	16 ± 13	18 ± 12	18 ± 9	10	14	7	5	1	1848	1358
05	SAMojave	31 ± 12	23 ± 16	24 ± 8	26 ± 11	30	18	10	7	1	1955	1317
06	SASanBer	33 ± 12	23 ± 15	27 ± 12	28 ± 13	20	19	11	7	2	1005	618
07	SACoache	22 ± 10	16 ± 11	32 ± 16	22 ± 12	40	17	8	6	1	1216	941
	Total San Andreas							36	25	0	6024	4233
08	SJSanBer	41 ± 16	31 ± 19	0 ± 0	37 ± 17	20	26	15	10	2	213	139
09	SJSanJac	46 ± 16	36 ± 22	0 ± 0	43 ± 18	10	30	19	12	2	257	166
10	SJAnza	18 ± 10	14 ± 11	28 ± 27	17 ± 12	30	11	6	4	2	555	356
11	SJCoyCre	19 ± 12	17 ± 15	0 ± 0	18 ± 13	0	16	7	6	1	63	53
12	SJBoreg	6 ± 7	8 ± 13	0 ± 0	6 ± 8	<10	16	2	6	0	14	38
13	SJSupMtn	10 ± 6	7 ± 6	0 ± 0	9 ± 6	0	6	3	2	2	46	30
14	SJSupHil	1 ± 5	3 ± 9	0 ± 0	2 ± 6	0	11	1	4	0	4	29
	Total San Jacinto							53	43		1152	812
15	Whittier	6 ± 3	4 ± 3	0 ± 0	5 ± 3	0	4	2	1	1	41	31
16	GlenIvy	12 ± 14	11 ± 18	0 ± 0	12 ± 15	0	9	4	3	1	74	58
17	Temecula	18 ± 9	14 ± 12	0 ± 0	16 ± 10	0	12	6	4	1	99	69
18	Julian	5 ± 4	6 ± 8	0 ± 0	5 ± 5	0	8	2	3	1	72	124
19	CoyoteM	1 ± 4	2 ± 5	0 ± 0	1 ± 4	0	5	1	2	0	16	50
	Total Whittier							14	13		301	332
	Total							102	81	1	7477	5377

For some fault segments we have estimated dates of several past earthquakes, which permit  $\bar{T}$  and  $\sigma_{\ln T_i}$  to be assessed using the method of Savage (1991), allowing for the open interval since the most recent event (Davis, P. *et al.*, 1989). Probabilities obtained using this approach are identified by the column heading, “Dates,” in Table 2.

For each segment we also estimate the expected time until the next rupture from the displacement in the last earthquake and the long-term slip rate. We use two separate techniques, each making different assumptions about the relationship between recurrence times and displacements. In the “time-predictable” model, referred to as the “direct” method in the 1988 report, the expected recurrence time is taken to be directly proportional to the displacement in the last earthquake; that is,

$$\bar{T} = D/V, \quad (4)$$

where  $\bar{T}$  is the expected time between successive earthquakes,  $D$  is the displacement in the earlier of the two, and  $V$  is the long-term slip rate. The uncertainty in the expected time comes only from the uncertainties in  $D$  and  $V$ , while the conditional probability must also include the intrinsic variability of the recurrence times. In a variant that we refer to as the “renewal” model, the mean recurrence time is assumed to be

$$\bar{T} = \bar{D}/V, \quad (5)$$

where  $\bar{D}$  is the mean displacement for earthquakes on the segment. The value of  $\bar{D}$  is estimated using the average of all known displacements on the segment. For all the segments considered here, only the last displacement is known, so that  $\bar{D}$  is assumed equal to  $D$ . Thus, the expected recurrence time is subject to an additional uncertainty due to the error in estimating the mean displacement from just one sample. We assume here that displacements on a segment are lognormally distributed, with a dimensionless variance equal to the intrinsic variability of recurrence times. Because of this additional variability, the renewal model usually predicts lower conditional probabilities than the time-predictable model.

Both the time-predictable and renewal models depend on the natural variability of the recurrence times, expressed here by  $\sigma_{\ln T_i}$ . On the basis of recent data and analyses, we have altered the treatment of  $\sigma_{\ln T_i}$  from that of the 1988 Working Group. They used a value of 0.21 for  $\sigma_{\ln T_i}$  from a study of circum-Pacific earthquakes by Nishenko and Buland (1987). However, the fault-segment recurrence times described in Appendix C, together with work by Savage (1991), suggest that  $\sigma_{\ln T_i}$  may not be as well constrained as supposed by the 1988 Working Group, and may also bring into question using

a single low value of 0.21 for all fault segments. We have adopted the significantly larger value,  $\sigma_{\ln T_i} = 0.5 \pm 0.2$ , for our calculations based on recurrence data along the southern San Andreas fault (described in Appendix C). As before, we develop a model uncertainty,  $\sigma_{\bar{T}}$ , to reflect incomplete information about the true value of  $\bar{T}$  (Appendix A). Note that the representation of  $\sigma_{\ln T_i}$  now additionally includes an indicated model uncertainty of  $\pm 0.2$  in  $\sigma_{\ln T_i}$ . The calculations of probability take these model and data uncertainties into account (see Appendix A).

The column labeled “Mean” in Table 2 gives the preferred result of these calculations, which consists of a weighted average from the three models, with weights proportional to the reciprocal of variance, assuming equal prior likelihood of each model. Of course, the “Dates” method is not included in the average when it is not available. Table 2 also includes the formal  $1 \sigma$  uncertainties in the probabilities that arise from the uncertain estimation of  $\bar{T}$  and  $\sigma_{\ln T_i}$ .

Probabilities estimated by the 1988 Working Group are also given in Table 2, labeled “WG88.” For the San Andreas, we do not consider the differences between our estimates and the previous ones to be significant. The 1988 Working Group reported probabilities only to the nearest 10% to indicate their estimation of significance. Probabilities for the Carizzo and San Bernardino Mountains segments are somewhat larger, and for the Coachella segment somewhat less than the 1988 Working Group probabilities. Our estimates of uncertainty in these values are generally a little over 10%.

The San Bernardino Valley and San Jacinto Valley segments of the San Jacinto fault are now estimated to have large probabilities of 37 and 43%, respectively—significant increases from the 1988 values. These increased probabilities result from increased slip rate estimates on those segments and decreased estimates of characteristic displacement. The Anza segment is assigned a lower probability of an earthquake because we increase the assigned segment length, which increases the assumed characteristic displacement.

Table 2 gives rupture probability on several fault segments not considered by the 1988 Working Group. These determinations follow recent geologic work described in Appendix C. Also shown in Table 2 are rupture probabilities, assumed independent of time, calculated using the Poisson model, abbreviated “%Prob/Pois.” For a Poisson process the probability that the next rupture will occur before time  $T$  is

$$P(t \leq T) = 1 - \exp(-r \cdot T), \quad (6)$$

where  $r = V/D = 1/\bar{T}$  is known as the rate parameter. The rate parameter, abbreviated “Rate/Pois,” is also shown in Table 2 (note that this rate is given in units of ruptures/thousand years). We have also calculated an

equivalent rate for the preferred mean probability, given by

$$r = -(1/T) \cdot \ln(1 - P), \quad (7)$$

where  $P$  is the weighted average conditional 30-yr probability labeled “%Prob/Mean.” The corresponding equivalent rate is given in the column labeled “Rate/Logn.” For the time-dependent models, the true rate varies with time, and the value given in Table 2 is an average for the 30-yr time span covered by this report.

The quantity “Rate/factor” in Table 2 is the ratio of the time-dependent Logn rate to that calculated using the Poisson model. For most fault segments the time-dependent probabilities exceed those from the Poisson model because, barring systematic error, most fault segments are “overdue” in the sense that the elapsed time exceeds the estimated recurrence time.

#### Cascades: Simultaneous Ruptures of Contiguous Segments

Like the earthquakes in 1857 and about 1690 on the San Andreas fault, many past earthquakes ruptured more than one segment in a single event. We use the term “cascade” for an earthquake that ruptures one or more contiguous segments. To explain the long-term slip rate, it makes no difference whether these events are treated as cascades or as separate earthquakes on individual segments. However, for seismic hazard estimates there is a difference. If individual segments always rupture independently, then there will be more earthquakes per unit time. Thus, the frequency with which one segment triggers another becomes important.

Let us distinguish between the rupture rate on each segment and the earthquake rate for combined segments. For a fault with just two adjacent segments, “x” and “y,” we can identify three different types of “characteristic” earthquakes: (1) x fails alone, (2) y fails alone, and (3) x and y fail together. We will use the notation x, y, and xy to indicate these three possible events. The rupture rate on segment x, for example, will be the sum of the earthquake rates of x alone and x and y in combination. The earthquake rate for the fault will be the sum of the rates of all three types of events. If two segments always fail independently (as assumed in the 1988 Report), then the rate of multi-segment earthquakes is zero, and the total earthquake rate is the sum of the two segment rupture rates. If x and y sometimes fail at the same time, the earthquake rate will be less than the sum of the segment rupture rates.

Suppose that over the long term, segments x and y rupture at rates of 10 and 20 ruptures per 1000 yr, respectively. If these segments fail at separate times, then the earthquake rate would be the sum of the individual rates, or 30 events per 1000 yr. An alternative is that x always triggers y, so that x and y fail together at the rate

of 10 per 1000 yr, and y fails by itself at the rate of 10 per 1000 yr. In this second alternative, the earthquake rate is 20 per 1000 yr, while the rupture rates on the two segments are 10 and 20 per 1000 yr as given. This example illustrates that the rupture rates do not uniquely specify the earthquake rate, since two different scenarios are both consistent with the observed rupture rates. Of course, the second scenario implies some larger earthquakes than the first, since simultaneous rupture of two segments will cause a larger earthquake than failure of either segment alone.

In principle, paleoseismic data can reveal both the rupture and the earthquake rates, by providing both the dates and extent of past earthquakes. However, unless the entire earthquake history of a fault is known, geologic data cannot adequately define the cascade frequencies. Typically, the dates of past earthquakes on various segments have been too uncertain to determine whether two neighboring segments ruptured separately or together. Thus, in general, the segment rupture rates are better determined than the earthquake rates.

Consider a fault with  $n$  segments joined end to end. Then there will be  $m = n \cdot (n + 1)/2$  possible cascades involving only contiguous fault segments. In the example above,  $n = 2$ , and there are three possible types of earthquakes. The earthquake rupture probabilities (or equivalently, the rupture rates) on the  $n$  segments will not uniquely specify the  $m$  earthquake rates. However, the degree of interaction will affect the distribution of earthquake magnitudes, and so we might use information about the expected magnitude distribution (for example, the Gutenberg–Richter relationship up to some limiting magnitude) to infer the degree of interaction. In estimating the degree of interaction, we try to approximate this relationship, while maintaining agreement with the estimated rupture rates on individual segments. In practice, this requires minimizing the total earthquake rate, subject to prior constraints on individual segments. Otherwise, the model predicts fewer large earthquakes, and more smaller ones, than the Gutenberg–Richter relationship.

We first adopt a minimum rate for each possible cascade—equal to half the observed rate for multi-segment earthquakes that have actually been observed (e.g., the 1857 and 1690 earthquakes on the San Andreas), half the segment rupture rate for simple, one segment ruptures, and zero for multi-segment ruptures never observed. We then calculate the rupture rates for each segment, by summing minimum rates of all combination events involving each segment. Lastly, we subtract from the observed rupture rates the rupture rates predicted by the minimum cascade rates, and explain the remainder by the smallest possible total rate of events. To accomplish the last step, we rank the possible cascades in decreasing order of seismic moment, and for each possible event we choose the largest rate compatible with the re-

sidual rupture rates on the segments. By maximizing the rates of the largest earthquakes first, we minimize the total number of events, because it takes fewer large events to explain a given set of rupture rates.

By incorporating the cascades approach into our model, the resulting probabilities are lower than would be inferred by treating all segment ruptures as independent events. That is, the estimated rate of surface ruptures is explained by a smaller number of larger events, compared to the method used by the 1988 and 1990 working groups. For example, the cascade rate of 25 events per 1000 yr for the combined four segments of the San Andreas corresponds to a 30-yr probability of 53% that at least one characteristic earthquake will occur on the San Andreas. The sum of the rupture rates on these four segments is 36 per 1000 yr (Table 3), corresponding to a 30-yr probability of 66%, if interactions are not included.

Assuming a characteristic displacement for each segment may appear to contradict empirical relationships between displacement and fault length (e.g., Scholz, 1982; Wells and Coppersmith, 1994). However, multiple-segment earthquakes are relatively infrequent, and they may be underrepresented in the empirical relationships. Our assumption is based on the geological observation that displacements on a given segment tend to fall within a narrow range. Perhaps the best example of this is the northern section of the Imperial fault, which was displaced about 1 m in each of two quite different earthquakes ( $m = 6.9$  in 1940, and  $m = 6.4$  in 1979).

### Integrated Approach to Assessing Earthquake Potential

#### Beyond Rates and Dates: Additional Information on Earthquake Likelihood

The methods for calculating conditional probabilities described in the preceding section apply only to faults with sufficient paleoseismic data. To develop probabilistic methods for the remaining faults in southern California, we divide the region into 65 seismotectonic zones as shown in Figure 6. Of these, 16 contain the major segments of the southern San Andreas, San Jacinto, and Elsinore faults for which earthquake probabilities were calculated in the preceding section. They are called type A zones. Type B zones contain major faults with measurable slip rates but inadequate data on segmentation, displacement, or date of last earthquake. Type C zones are not dominated by any single major fault, but they may contain diverse or hidden faults. There are 25 type B and 24 type C zones. The majority of damaging earthquakes in southern California, including the 1933 Long Beach, the 1952 Kern County, the 1971 San Fernando, the 1987 Whittier Narrows, the 1992 Landers, and the

1994 Northridge earthquakes occurred in type B or type C zones.

In this section, we develop seismic source models for all zones. Earthquakes caused by the failure of fault segments as considered in the preceding section are called characteristic earthquakes. We also consider earthquakes not directly associated with a fault segment. We call them "distributed earthquakes," and include them for all zone types.

We first review earth science information which can be used to constrain parameters of characteristic and distributed earthquakes for all zone types. These data include the historical earthquake record, geodetic evidence of strain accumulation, geologic estimates of slip for lesser but important faults, and a developing knowledge base on surface and blind thrust faults.

#### The Historical Earthquake Record

The locations of previous earthquakes indicate where future earthquakes are likely to occur. Kagan and Jackson (1994) showed that large earthquakes occur preferentially near the sites of recent, previous large earthquakes. Thus, the locations of previous earthquakes provide a reasonable indicator of future events. The completeness and accuracy of available information on earthquakes have evolved with time. Two significant events that improved earthquake reporting were the population boom that began with the California gold rush in 1849, and the establishment of the Caltech seismological network in 1932. Since 1932, the catalog should be complete to  $m = 4$  and locations should be accurate to a few tens of kilometers. Of course, both magnitude and location estimates have improved steadily as stations were added to the network. Today, the threshold for complete reporting is about  $m = 2$ , and location uncertainties are a few kilometers in most locations.

We base our conclusions on the catalog of earthquakes presented in Table 4 (Fig. 7) for that portion of California north of latitude  $32^\circ$  and south of latitude  $36^\circ$ . This catalog is a modified and updated version of that assembled by Ellsworth (1990) in a more complete account of California's earthquake history than given here. Modifications include the following: we excluded earthquakes smaller than magnitude 6, we added earthquakes since 1990, and we used the revised magnitude estimates of Hutton and Jones (1993) for earthquakes after 1932. We also assume that no mainshock greater than magnitude 6 has escaped detection since 1850, although location errors might exceed 100 km in some places, and magnitude errors could approach a full magnitude unit. Aftershocks have not been excluded from the catalog, but some aftershocks of early large events almost certainly have escaped inclusion.

The largest known earthquake in southern California's history was in 1857. It ruptured the San Andreas fault for a distance of about 350 km from about Park-

Table 3  
Cascade Earthquake Rates

Fault	Zones	Length (km)	Disp. (m)	mw	Lognormal			Poissonian		
					Rupt. Rate	Rate Floor	Rate Est.	Rupt. Rate	Rate Floor	Rate Est.
San Andreas	04-05-06-07	446	4.9	7.90		0.25	1.80		0.25	0.68
	04-05-06	332	5.2	7.84		0.00	0.00		0.00	0.00
	04-05	254	5.7	7.79		1.50	1.50		1.50	1.65
	05-06-07	325	4.1	7.76		0.00	0.49		0.00	0.00
	05-06	211	4.1	7.64		1.00	1.16		1.00	1.00
	04	121	7.0	7.63	6.61	3.31	3.31	4.86	2.43	2.52
	06-07	192	3.8	7.59		1.75	1.75		1.75	1.75
	05	133	4.5	7.53	9.90	4.95	4.95	6.67	3.34	3.34
	07	114	4.0	7.45	8.08	4.04	4.04	6.25	3.13	3.82
06	78	3.5	7.30	11.15	5.58	5.95	6.86	3.43	3.43	
Total San Andreas					35.74	22.37	24.95	24.63	16.82	18.20
San Jacinto	08-09-10-11-12-13	268	1.7	7.45		0.00	1.07		0.00	1.00
	08-09-10-11-12-14	275	1.6	7.43		0.00	0.00		0.00	1.00
	09-10-11-12-14	233	1.8	7.42		0.00	0.00		0.00	0.00
	08-09-10-11-12	243	1.7	7.42		0.00	0.00		0.00	0.00
	09-10-11-12-14	240	1.7	7.40		0.00	0.00		0.00	0.00
	08-09-10-11	210	1.8	7.40		0.00	2.05		0.00	0.00
	10-11-12-13	188	2.0	7.39		0.00	0.00		0.00	0.00
	09-10-11-12	208	1.8	7.38		0.00	0.00		0.00	0.00
	08-09-10	170	2.1	7.38		0.00	0.00		0.00	0.00
	10-11-12-14	195	1.8	7.37		0.00	0.00		0.00	0.00
	09-10-11	175	2.0	7.37		0.00	0.00		0.00	0.00
	10-11-12	163	2.0	7.35		0.00	0.00		0.00	0.00
	09-10	135	2.3	7.34		0.00	0.00		0.00	0.00
	10-11	130	2.3	7.33		0.00	0.00		0.00	0.00
	10	90	3.0	7.30	6.23	3.11	3.11	4.00	2.00	2.00
	11-12-13	98	1.0	7.00		0.00	0.00		0.00	0.00
	08-09	80	1.1	6.96		0.00	4.57		0.00	3.00
	11-12-14	105	0.8	6.91		0.00	0.00		0.00	0.86
	12-13	58	1.3	6.89		0.00	0.00		0.00	0.00
	12-14	65	0.8	6.76		0.00	0.00		0.00	0.00
11-12	73	0.7	6.80		0.00	0.00		0.00	0.00	
13	25	2.0	6.79	3.02	1.51	1.96	2.00	1.00	1.00	
09	45	1.0	6.76	18.53	9.26	10.84	12.00	6.00	7.00	
08	35	1.2	6.76	15.38	7.69	7.69	10.00	5.00	5.00	
14	32	1.0	6.57	0.58	0.29	0.58	4.00	2.00	2.14	
11	40	0.7	6.64	6.77	3.39	3.66	5.71	2.86	2.86	
12	33	0.7	6.55	2.13	1.07	1.07	5.71	2.86	2.86	
Total San Jacinto					52.64	26.32	36.60	43.43	21.71	28.71
Whittier	15-16-17-18-19	228	1.8	7.41		0.00	0.25		0.00	0.66
	16-17-18-19	190	1.7	7.36		0.00	0.00		0.00	0.14
	15-16-17-18	190	1.6	7.33		0.00	0.61		0.00	0.00
	17-18-19	155	1.8	7.30		0.00	0.00		0.00	0.00
	18-19	113	2.0	7.24		0.25	0.25		0.80	0.80
	16-17-18	152	1.5	7.26		0.00	0.60		0.00	0.82
	17-18	117	1.5	7.18		0.00	0.00		0.00	0.47
	15-16-17	115	1.5	7.18		0.00	0.00		0.00	0.00
	18	75	1.7	7.08	1.71	0.00	0.00	2.94	0.00	0.05
	15-16	73	1.7	7.08		0.00	0.00		0.00	0.00
	19	38	2.5	7.00	0.50	0.00	0.00	1.60	0.00	0.00
	16-17	77	1.4	7.03		0.00	0.59		0.00	0.00
	15	38	1.9	6.92	1.72	0.86	0.86	1.32	0.66	0.66
	17	42	1.2	6.81	5.93	2.96	3.88	4.17	2.08	2.08
	16	35	1.6	6.84	4.12	2.06	2.06	3.23	1.61	1.61
Total Whittier					13.99	6.13	9.10	13.25	5.15	7.29
Total Cascades					102.37	54.82	70.64	81.31	43.68	54.20

field to Cajon Pass, with a right-lateral strike-slip displacement reaching 11 m in some places. The 1857 event is often used as an archetype for “the big one” in the popular press. Many seismologists now discourage this colloquial terminology, because it suggests that San Andreas earthquakes are much alike, and that there is only one such earthquake to worry about. In fact, many different earthquake scenarios are possible on the San Andreas, as discussed in the section on cascades, and we cannot conclude that any one earthquake,

however large, will preclude future damaging earthquakes.

The next largest earthquake since 1850 was the 1952 Kern County earthquake on the White Wolf fault. This event offers graphic evidence of the tectonic complexities caused by the big bend in the San Andreas fault. The White Wolf dips down to the south under the Tehachapi mountains, and one effect of the earthquake was to thrust the mountains up and to the north. The stresses that caused the earthquake undoubtedly resulted from the

Table 4  
Earthquake Catalog

Year	Mon	Day	Hour	Min	Lat (°)	min	Long (°)	min	<i>m</i>	Note*	Zone	Type
1852	11	29	20	0	32	30	115	0	6.5	b	64	C
1855	7	11	4	15	34	6	118	6	6.0	b	33	B
1857	1	9	16	0	35	42	120	18	7.8	a	3	B
1858	12	16	10	0	34	0	117	30	6.0	b	59	C
1862	5	27	20	0	32	42	117	12	6.0	b	22	B
1875	11	15	22	30	32	30	115	30	6.2	b	24	B
1883	9	5	12	30	34	12	119	54	6.2	b	55	C
1890	2	9	12	6	33	24	116	18	6.5	b	10	A
1892	2	24	7	20	32	33	115	38	7.0	b	24	B
1892	5	28	11	15	33	12	116	12	6.5	b	11	A
1894	7	30	5	12	34	18	117	36	6.0	b	5	A
1899	12	25	12	25	33	48	117	0	6.4	b	9	A
1901	3	3	7	45	36	0	120	30	6.4	b	1	B
1906	4	19	0	30	32	54	115	30	6.2	b	23	B
1908	11	4	8	37	36	0	117	0	6.0	b	61	C
1915	6	23	3	59	32	48	115	30	6.0	b	23	B
1916	11	10	9	11	35	30	116	0	6.1	b	62	C
1918	4	21	22	32	33	48	117	0	6.8	a	9	A
1922	3	10	11	21	36	0	120	30	6.1	a	1	B
1923	7	23	7	30	34	0	117	18	6.0	a	8	A
1925	6	29	14	42	34	18	119	48	6.9	a	55	C
1927	11	4	13	50	34	42	120	48	7.3	a	39	B
1933	3	11	1	54	33	37	117	58	6.2	a	20	B
1934	6	8	4	47	36	0	120	30	6.1	a	1	B
1937	3	25	16	49	33	24	116	16	6.0	b	10	A
1940	5	19	4	36	32	44	115	30	6.9	a	23	B
1942	10	21	16	22	33	3	116	5	6.6	a	12	A
1946	3	15	13	49	35	44	118	3	6.0	a	60	C
1947	4	10	15	58	34	59	116	33	6.6	a	47	C
1948	12	4	23	43	33	56	116	23	6.0	a	7	A
1952	7	21	11	52	35	0	119	1	7.5	a	25	B
1952	7	21	12	5	35	0	119	0	6.4	b	25	B
1952	7	29	7	3	35	23	118	51	6.3	a	53	C
1952	11	22	7	46	35	44	121	12	6.0	b	51	C
1954	3	19	9	54	33	17	116	11	6.4	a	10	A
1966	6	28	4	26	36	0	120	30	6.1	a	1	B
1968	4	9	2	28	33	11	116	8	6.5	a	12	A
1971	2	9	14	0	34	25	118	24	6.7	a	32	B
1979	10	15	23	16	32	36	115	18	6.4	a	23	B
1983	5	2	23	42	36	14	120	19	6.4	a	52	C
1986	7	8	9	20	34	0	116	36	6.2	a	7	A
1987	11	24	13	16	33	1	115	51	6.5	a	14	A
1992	4	23	4	50	33	58	116	19	6.1	c	64	C
1992	6	28	11	57	34	12	116	26	7.3	c	29	B
1992	6	28	15	5	34	12	116	50	6.2	c	42	C
1994	1	17	11	18	34	12	118	32	6.7	d	54	B

\* (a) Moment magnitude from Ellsworth (1990); (b) “M” from Ellsworth (1990); (c) Hauksson *et al.* (1993); and (d) Hauksson *et al.* (1994).

same plate motions causing slip on the San Andreas fault in the area of the "big bend" near Gorman. However, rates and dates on the San Andreas would not provide adequate information on the likelihood of this or similar events. The 1952 event taught us that thrust faults are important in southern California, that some of the largest earthquakes occur off the San Andreas, and that techniques beyond paleoseismology are required for comprehensive hazard assessment.

The third largest event on our list is the Landers earthquake of 1992. It was due to a right-lateral strike-slip rupture, close to but clearly not on the San Andreas fault. Seismological (Hauksson, 1994), geological (Sieh *et al.*, 1993), and geodetic studies (Hudnut *et al.*, 1994) all indicate that it was a complex event, rupturing several known and previously unknown fault segments. There was no evidence available before the earthquake to suggest that this group of fault segments would join to produce such a large earthquake. The Landers earthquake provides yet more evidence that large earthquakes occur off the San Andreas, and that it is not easy to foretell which faults are most likely to produce large earthquakes in our lifetimes.

The fourth largest event since 1850 was probably the so-called Lompoc earthquake of 1927. The earthquake occurred offshore, before the inception of the southern California seismic network, and its location and magnitude are uncertain. We know little about its focal mechanism. Since it triggered a tsunami, it may have been a thrust event, although submarine landslides triggered by strike-slip earthquakes may also cause tsunamis. In spite of these uncertainties, the 1927 event again shows that the San Andreas fault has no monopoly on producing large California earthquakes.

For most earthquakes prior to 1932, we lack the data to estimate magnitudes accurately. Exceptions include those earthquakes large enough to be detected by seismographs around the world, and those that left a clear surface trace from which the length and slip could be measured accurately. For the remaining earthquakes, we must estimate the magnitudes by comparing the sizes of the damaged areas with those of modern earthquakes of known magnitudes. With the exceptions noted below, the magnitudes for earthquakes before 1932 are determined from the area over which shaking of a given intensity, say Modified Mercalli Intensity VII, was experienced. The exceptions are the 1857 and 1872 earthquakes, whose moment magnitudes are estimated from the rupture length and surface displacement; and the 1927 earthquake, whose magnitude was estimated by instrumental recordings and from the size and duration of the tsunami it caused.

Because future earthquakes will not necessarily occur precisely where past ones have, forecasting requires a smoothed map of earthquake data (Kagan and Jackson, 1994). Statistical studies show that a function inversely

proportional to distance, out to some maximum distance,  $r_m$ , represents well the concentration of probability that a future earthquake will occur within a distance,  $r$ , of a previous one. A sum of such functions, each centered on the location of a past earthquake, with a weight proportional to its magnitude, provides one forecast in map form. In this report, we take  $r_m = 250$  km. This value is determined by maximum likelihood techniques using the Harvard catalog of Centroid Moment Tensor Solutions, 1977 through 1993 (e.g., Dziewonski *et al.*, 1993). The smoothed seismicity rate per unit area is then integrated over each zone to give the earthquake rate. This is combined with geologic and geodetic data to estimate regional earthquake potential as described later.

#### Regional Strain as a Measure of Earthquake Potential

With the exception of the "creeping" section of the San Andreas, faults that rupture in large earthquakes remain locked by friction between earthquakes, even though the crustal blocks separated by the faults continue to be deformed by tectonic forces. A consequence is that much of the differential strain occurs near the faults bounding the blocks. Geodetic measurements can reveal regions where locked faults are accumulating strain, even though those faults may not be exposed at the surface. Active faults may be hidden if they occur underwater or beneath deformable sediments that stretch or fold instead of breaking.

The creeping section of the San Andreas, which runs from about San Juan Bautista in the north to Parkfield in the south, slips continuously right up to the surface, so that only minor strain accumulates in the adjoining blocks. While this fault segment experiences many small earthquakes, the record size for any earthquake here is less than magnitude 6.0. Some other major exposed faults creep slightly, but their creep is generally insufficient to keep up with the relative block motion or prevent strain buildup on adjacent blocks. The relative importance of creep versus seismic strain accumulation and release on hidden faults remains a serious unanswered question.

Triangulation (Reid, 1910; Bowie, 1973; Thatcher, 1979) and trilateration measurements (Savage *et al.*, 1979; Lisowski *et al.*, 1991) have shown strain accumulation across the San Andreas, San Jacinto, Garlock, and other major faults, and how it is released in earthquakes on these structures. Little is known about the pattern of strain accumulation near lesser faults.

Both triangulation and trilateration methods require line-of-sight observations, imposing a constraint of about 40 km on the longest baselines observed. High-accuracy trilateration requires temperature and pressure measurements by aircraft along the line of sight, preventing measurements in some populated areas. Beginning in about 1975, Very Long Baseline Interferometry (VLBI) became accurate enough to measure strain over baselines with no length limitation. However, these measurements

require expensive and bulky antennas, so that VLBI measurements were made at only about 20 sites in southern California. Then, in 1986, the Global Positioning System (GPS) was first used to measure tectonic strains in California. This satellite system, originally for military navigation, now allows extremely accurate and cost-effective geodetic measurements. There is no need for line-of-sight observations between ground sites and no limitation on baseline length. Accurate strain-rate measurements require a sequence of observations covering several years, a requirement now met at a number of sites in southern California.

We use strain data to assess the seismic hazard of more obscure faults, including blind thrusts. Ward (1994) determined regional strain from GPS data in southern California, and interpolated these strains to provide average values in each of the 65 source zones. Ward used the geological data for slip rates on the San Andreas and San Jacinto faults to resolve the spatial ambiguities that result from the large spacing of relevant geodetic sites. The GPS and VLBI data show that the net displacement rate across southern California from about the middle of the Mojave desert to San Nicolas Island is about 40 mm/yr (Feigl *et al.*, 1993). Ward assigned about 75% of that rate to the San Andreas system, consistent with the slip rate determined by geological studies. He partitioned the remainder throughout southern California to fit the GPS data as well as possible.

Models which restrict the bulk of the regional strain accumulation and release to the biggest faults disagree in some important respects with recent geodetic observations. The geodetic data show a very broad region of strain accumulation in parts of southern California, whereas discrete fault models predict that the strain should be concentrated, for example, near the San Andreas fault. Figure 8 illustrates this difference. The squares are the observed velocities parallel to the San Andreas as a function of distance from the fault. Error bars indicate one standard deviation. The velocities were observed using GPS from 1987 to 1993 on a profile from San Nicolas Island, across the Mojave section of the San Andreas, to the central Mojave desert (Feigl *et al.*, 1993; Shen *et al.*, 1995). The triangles show the velocities predicted from the discrete fault model. All faults with slip rate greater than 3 mm/yr are included, and we assumed that all faults are locked to a depth of 20 km in this region. The locking depth of 20 km was chosen to minimize the discrepancy between geological prediction and geodetic observation. Had we used  $H = 11$  km, as we do elsewhere in the report, the discrepancy in Figure 8 would be even greater.

If the crustal strain in a region is purely elastic within an upper brittle layer of thickness,  $H$ , and purely inelastic below that depth, then straining also implies the accumulation of seismic moment. We express this mo-

ment accumulation by a simplified version of the Kostrov (1974) equation,

$$\dot{M} = 2\mu HA\dot{\epsilon}, \quad (8)$$

where  $\dot{M}$  is the rate of moment accumulation,  $A$  is the area of the region,  $\mu$  is the average rigidity of the crust, and  $\dot{\epsilon}$  is the average strain rate. In principle, both  $\dot{M}$  and  $\dot{\epsilon}$  are tensors. Here we use a scalar version, where  $\dot{\epsilon}$  is the maximum horizontal shear strain rate estimated from geodetic measurements or calculated from a dislocation model.

#### Faults with Slip Rates Exceeding 3 mm/yr

Segments of the San Andreas fault have slip rates of about 25 to 35 mm/yr, the San Jacinto fault-slip rate is about 12 mm/yr, and the slip rate for the Whittier–Elsinore fault averages around 5 mm/yr. These rates are geologically high and reflect recurrence intervals for large earthquakes of hundreds, rather than thousands, of years. During the past 10 yr, geological studies have shown that there are other important faults in southern California with relatively high rates of slip. In this report, we identify faults with slip rates of at least 3 mm/yr. While this is an arbitrary cutoff value, faults with this slip rate are also likely to have recurrence intervals of hundreds of years and, therefore, represent important sources of future large earthquakes. In Appendix C we discuss the Cucamonga, Garlock (east and west segments), Palos Verdes (north and south segments), Oak Ridge, San Cayetano, San Simeon, Sierra Madre, and Santa Susana faults. The faults have preferred slip rates of 3 to 7 mm/yr and estimated recurrence intervals of 225 to 685 yr. Each of these faults can generate magnitude 7 earthquakes but the historical record indicates that none has produced an event of this size in approximately the past 200 yr.

#### Surface and Blind Thrust Faults

Within southern California, northwest-trending strike-slip faults of the San Andreas system are clearly important sources of large-magnitude earthquakes. However, the big bend in the San Andreas (the primary plate boundary structure) has given rise to a strong component of north–south crustal compression in southern California which is accommodated by reverse and thrust faults. The 1971  $m = 6.7$  San Fernando earthquake and sections of the  $m = 7.5$  1952 Kern County earthquake were produced by reverse faults that produced mappable surface faulting. In contrast, the 1987  $m = 5.9$  Whittier Narrows and 1994  $m = 6.7$  Northridge earthquakes occurred on blind thrust faults that did not rupture to the surface.

*Surface Reverse and Thrust Faults.* Surface reverse and thrust faults can be mapped and their behavior quantified

in a manner similar to strike-slip faults. Numerous surface reverse and thrust faults have been studied within the Transverse Ranges. Although there are few fault-specific paleoseismic data on earthquake recurrence, there is sufficient stratigraphic, structural, and in a few cases geomorphic information for preliminary slip-rate calculations. Some of these faults, like the Cucamonga, Oak Ridge, San Cayetano, Sierra Madre, and Santa Susana, have slip rates in excess of 3 mm/yr and these are described separately in Appendix C. For this report, the earthquake potential of surface reverse and thrust faults has been treated by assigning them to the type B seismic source zones in the integrated seismic hazard model.

*Blind Thrust Faults.* Blind thrust faults are low-angle structures that do not cut the earth's surface. This makes it difficult to assess directly segmentation, recurrence intervals, characteristic displacement, and slip rate by traditional techniques such as trenching or microgeomorphic analysis. However, these faults do have surface expressions in the form of overlying folds that are known to grow during large earthquakes (Stein and Yeats, 1989). In the past decade, quantitative approaches have been developed that relate fold shape and growth rate to fault geometry and slip rate (Suppe, 1983; Suppe *et al.*, 1992). Specifically, kinematic and geometric modeling of active axial surfaces in fault-bend folds, based on shallow seismic reflection profiles and borehole stratigraphic data, allow the location, geometry, and cumulative slip of underlying blind thrust faults to be inferred.

Davis, T. *et al.* (1989), Shaw (1993), and Shaw and Suppe (1994a, b) have used this approach to infer the locations and geometries of major blind thrusts in coastal southern California and in the Los Angeles basin. Davis, T. *et al.* (1989) developed retrodeformable cross sections for the Palos Verdes anticlinorium, the central Los Angeles basin, the Santa Monica Mountains anticlinorium, the Verdugo-San Rafael Hills, and the San Gabriel Mountains. They proposed that the Los Angeles region is underlain by active thrust faults composed of inclined ramps and near-horizontal faults that root into a postulated basal detachment at mid-crustal depths. They suggest that during the past 2.2 to 4.0 m.y. these faults have accommodated 20 to 30 km of horizontal convergence between the Palos Verdes Peninsula and the San Andreas fault.

Dolan *et al.* (1994) summarized evidence for blind thrust faults in the Los Angeles basin and along the southern margin of the Transverse Ranges. Locations, estimated slip rates, and possible magnitudes for characteristic earthquakes (based on a provisional segmentation model) are shown in Figure 9. The Elysian Park, Santa Monica Mountains, and Compton-Los Alamitos blind thrust ramps are important members of this fault system in the Los Angeles basin. Hauksson and Jones (1989) conclude that the Elysian Park thrust caused the

1987 Whittier Narrows earthquake based on its focal mechanism and aftershock distribution. Dolan *et al.* suggest that the Santa Monica Mountains thrust ramp may be capable of producing earthquakes as large as  $m = 7.3$ . Shaw (1993) interprets the Compton-Los Alamitos fold trend as overlying a thrust ramp along the southwestern margin of the basin. They suggest that this ramp extends over 80 km from the Santa Monica bay coastline southeast into northwestern Orange County and may connect with the Elysian Park thrust to the northeast along a detachment below Los Angeles. Based on well data, they estimate that this buried thrust ramp has had an average slip rate of 1.3 mm/yr for the past 2.5 m.y. From the estimated fault rupture area, they propose that the fault ramp can produce earthquakes of  $m = 6.8$ . Lastly, in the Santa Barbara Channel, Shaw and Suppe (1994a) define the Channel Islands thrust ramp, which they divide into two segments on the basis of differing fold geometry south of Santa Barbara. They estimate a slip rate of about 1.3 mm/yr for the past 3.3 ma. Based on estimates of fault rupture area, they suggest that the Channel Islands thrust could produce earthquakes of  $m = 7.2$  to 7.4.

*Earthquake Hazards from Blind Thrust Faults.* Blind thrust faults have demonstrated their importance in regional seismic hazard. However, there is considerable uncertainty about their extent, geometry at depth, and the nature of the postulated regional detachment into which they might root. The relation between northwest-trending strike-slip faults and the thrust ramps raises questions about modeling ramp geometry in certain areas. For example, the Compton-Los Alamitos thrust ramp postulated by Shaw (1993) truncates the Palos Verdes fault at a depth of about 5 km. Shaw and Suppe (1994b) and Davis, T. *et al.* (1989) model the Palos Verdes fault as a west-dipping reverse fault that extends to a depth of about 5 km. However, recent geomorphic observations indicate that the Palos Verdes fault is a major right lateral strike-slip fault with a slip rate of about 3 mm/yr. Similarly, the Compton-Los Alamitos thrust is modeled as detaching the strike-slip Newport-Inglewood fault at a depth of about 8 km. In modeling the Elysian Park thrust, Davis, T. *et al.* (1989) require the Whittier fault to be inactive. However, as noted earlier, the Whittier fault is a major active strike-slip segment of the Elsinore fault.

At present there are no direct data on recurrence intervals or characteristic displacements for individual blind thrust segments. As noted, Shaw and Suppe (1994a, b) estimate long-term rates on the Channel Islands and Compton-Los Alamitos thrusts of 1.3 and 1.4 mm/yr, respectively. These rates are averaged over 2.5 to 3.3 m.y. For most blind thrust ramps there is much uncertainty as to when thrusting began. Because rates can change over time, slip rates averaged over millions of

years do not necessarily provide adequate constraints on present behavior. Slip during individual earthquakes cannot be directly measured from fold geometries. Shaw (1993) uses an estimated characteristic displacement of about 2 m for an expected magnitude 7.2 earthquake to calculate an average repeat time of about 1500 yr on the Channel Islands thrust. They also use a displacement range of 1.2 to 3.0 m from historical blind thrust events to calculate a recurrence interval of 850 to 2100 yr on the Compton–Los Alamitos thrust. If present slip rates are 1 to 2 mm/yr, the co-seismic slip of one to a few meters that occurs during moderate to large thrust events would give repeat times of one to a few thousand years.

The magnitude of an earthquake that a blind thrust can produce is a function of the fault's area and characteristic displacement. As modeled by Shaw and Suppe (1994a, b), areas of individual ramp segments can vary from about 250 km<sup>2</sup> (Whittier segment of the Elysian Park thrust) to about 2000 km<sup>2</sup> (Channel Islands thrust). This range indicates that we can expect earthquakes ranging in size from  $m = 6.4$  to perhaps as large as  $m = 7.5$  on individual blind thrust segments (e.g., Dolan *et al.*, 1994). However, because of the modeling and fault behavior uncertainties described here, we do not treat blind thrusts explicitly as individual structures with a specific magnitude and recurrence. However, the slip rates for blind thrusts are included in the estimates in Tables 5 and 6 for both type B and type C source zones.

#### Northridge Blind Thrust Fault: Implications for Earthquake Hazards

The  $m = 6.7$  17 January 1994 Northridge earthquake was produced by a south-dipping blind thrust fault that extended northward from beneath the San Fernando Valley to the Santa Susana Mountains. The Northridge blind thrust occurs in a structurally complex zone between the Sierra Madre fault zone to the east and the Oak Ridge and Santa Susana faults to the west. The eastern end of the 1994 rupture is south of, and actually extends below, the rupture of the 1971 earthquake. The earthquake nucleated at a depth of 19 km (Hauksson *et al.*, 1994). The displacement averaged about 1.5 m with a maximum of 3.5 m (Wald and Heaton, 1994), and most of the slip occurred at a depth between 6 and 13 km with little or no slip in the upper 5 km of the crust (Hudnut *et al.*, 1994). These interpretations of deep slip are consistent with the absence of primary co-seismic surface faulting (USGS Staff, 1994a, b).

Since the Northridge earthquake, there have been preliminary attempts to interpret the structure associated with the causative fault, which had not been mapped prior to the earthquake. Davis and Namson (1994), using oil company data, surface geology, and a balanced cross-sectional approach, suggest that the Santa Clara synclinorium, a major structure on the north side of the Santa Susana Mountains, is a fault propagation fold produced

by a southward-dipping thrust that roots into a mid-crustal detachment surface beneath the San Fernando Valley. In their model, the Santa Susana fault becomes a relatively minor structure in the hanging wall of the blind thrust. Yeats (1994), in an alternative interpretation using similar data, suggests that the Northridge blind thrust is an eastward continuation of the Oak Ridge fault of the Ventura basin, and argues that the fault imaged by the aftershocks has a moderate dip down to 18 km with no sign of flattening into a detachment. He concludes that reconstructions using balanced sections that do not involve the entire brittle crust are not applicable to this fault, and offers no suggestions as to how deformation associated with the Northridge blind thrust affects interpretations of the seismogenic potential of the Santa Susana fault. Suppe (personal comm.), in a modification of the Davis and Namson model, suggests that the Santa Susana is a wedge fault kinematically linked to the Northridge blind thrust.

None of the proposed models provides strong constraints on recurrence of earthquakes produced by the Northridge blind thrust. Davis and Namson suggest a recurrence interval of 3000 yr using geodetically modeled slip for the Northridge earthquake and an assumed minimum slip rate of 4 mm/yr for the past 2 to 3 m.y. However, it is highly uncertain that long-term rates are constant and present-day rates could vary significantly from the long-term average. Also, the characteristic displacement value has an uncertainty that will affect recurrence calculations. Yeats does not quantify the recurrence; however, he suggests from geomorphology that south-dipping faults in the San Fernando Valley slip more slowly than north-dipping faults and that Northridge-type earthquakes are relatively rare.

In summary, the 1994 Northridge earthquake reinforces the idea that blind thrusts and surface reverse faults in the Transverse Ranges will continue as important sources of future earthquakes. It does not fundamentally change our view of the earthquake hazards or the way in which blind thrusts are treated in this report. While the specific fault had not been known prior to the event, the location, magnitude, and style of the earthquake are typical for this region of compressional deformation. The differences regarding interpretations of the structure of the Northridge blind thrust, the inability to model its location before the Northridge earthquake, its relation to the brittle-ductile transition or a region-wide detachment, and a poor understanding of slip rates and recurrence intervals again highlight the uncertainties in quantifying the behavior of such faults throughout southern California.

#### Data Integration and Regional Earthquake Potential

The foregoing sections present important information, beyond the traditional paleoseismic data, that can

Table 5  
Preferred Seismic Source Model

Number	Name	Type	Area Km <sup>2</sup>	V	Length Km	M <sub>x</sub> Mod.	Rate Full 10 <sup>-3</sup> /yr	Rate Part 10 <sup>-3</sup> /yr	M <sub>f</sub> 10 <sup>15</sup> Nm/yr	M <sub>s</sub> 10 <sup>15</sup> Nm/yr	M <sub>d</sub> 10 <sup>15</sup> Nm/yr	M <sub>c</sub> 10 <sup>15</sup> Nm/yr	M <sub>m</sub> 10 <sup>15</sup> Nm/yr	f <sub>d</sub> 10 <sup>-3</sup> /yr	f <sub>c</sub> 10 <sup>-3</sup> /yr	a Dist.	
01	SACreepi	B	718	0	200	6.01	2.33	1.18	0	0	56	2	0	2	2.33	0.00	3.367
02	SAParkfi	B	881	34	30	6.79	3.05	1.32	347	337	70	11	331	342	3.05	21.79	3.484
03	SACHolam	B	1045	34	50	7.05	3.54	0.81	515	561	84	18	520	538	3.54	13.74	3.549
04	SACarriz	A	2265	34	121	7.51	8.19	3.05	1094	1358	193	29	1358	1387	3.05	cas	3.484
05	SAMojave	A	2847	30	133	7.56	8.67	3.27	1036	1317	200	34	1317	1350	3.27	cas	3.515
06	SASanBer	A	1799	24	78	7.28	4.78	2.35	585	618	112	17	618	634	2.35	cas	3.371
07	SACoachell	A	2793	25	114	7.48	5.62	3.85	860	941	134	36	941	976	3.85	cas	3.585
08	SJSanBer	A	409	12	35	6.87	1.19	0.47	109	139	28	2	139	140	0.47	cas	2.672
09	SJSanJac	A	820	12	42	6.96	2.41	1.19	129	166	57	5	166	172	1.19	cas	3.076
10	SJAnza	A	1482	12	90	7.36	3.65	2.12	281	356	87	17	356	373	2.12	cas	3.326
11	SJCoyCre	A	495	4	40	6.94	1.33	0.72	47	53	32	3	53	56	0.72	cas	2.857
12	SJBorreg	A	745	4	29	6.77	2.63	1.65	83	38	63	6	38	44	1.65	cas	3.217
13	SJSupMtn	A	415	4	23	6.65	1.3	1.08	81	30	31	3	30	33	1.08	cas	3.033
14	SJSupHil	A	332	4	22	6.63	1.03	0.73	50	29	25	2	29	31	0.73	cas	2.863
15	Whittier	A	1065	2.5	38	6.91	2.09	1.12	91	31	47	5	31	36	1.12	cas	3.049
16	GlenIvy	A	739	5	35	6.87	1.41	0.73	54	58	33	3	58	61	0.73	cas	2.863
17	Temecula	A	823	5	42	6.96	1.44	0.79	60	69	34	4	69	73	0.79	cas	2.898
18	Julian	A	1323	5	75	7.26	2.38	1.49	106	124	56	10	124	134	1.49	cas	3.173
19	CoyoteM	A	1162	4	38	6.91	2.65	1.97	72	50	63	8	50	58	1.97	cas	3.294
20	NewpIngl	B	1313	1	30	6.79	2.39	1.54	72	10	53	8	33	41	2.39	2.14	3.378
21	NIOffsho	B	1155	1.5	40	6.94	1.52	0.86	37	20	35	7	22	28	1.52	0.86	3.182
22	RoseCany	B	1661	1.5	40	6.94	1.97	1.33	45	20	46	9	24	32	1.97	0.94	3.294
23	Imperial	B	1497	30	90	7.36	4.24	4.04	720	891	102	33	772	806	4.24	7.15	3.627
24	LaguSala	B	1332	4	40	6.94	3.89	2.92	85	53	93	17	52	69	3.89	2.04	3.590
25	WhitWolf	B	2423	2	80	7.29	7.58	5	76	53	178	55	9	64	7.58	0.11	3.880
26	BigPine	B	568	1	40	6.94	1.48	0.66	11	13	34	6	6	12	1.48	0.22	3.170
27	GarlockW	B	1697	5	100	7.41	3.78	2.17	50	165	88	32	75	108	3.78	0.58	3.577
28	GarlockE	B	2813	7	130	7.55	3.47	2.66	80	300	82	35	155	190	3.47	0.74	3.540
29	PintoMtn	B	1226	2	30	6.79	2.48	1.97	17	20	59	9	10	18	2.48	0.64	3.394
30	Brawley	B	992	25	10	6.22	2.21	1.75	0	83	53	3	38	41	2.21	17.79	3.344
31	SierMadr	B	1879	3	81	7.30	4.5	2.25	83	80	99	33	49	82	4.5	0.55	3.653
32	SanGabFa	B	895	0.5	45	7.00	2.33	1.34	40	7	51	11	13	24	2.33	0.40	3.367
33	SaMoMali	B	1473	2	55	7.10	2.74	1.64	71	36	55	15	38	54	2.74	0.86	3.438
34	PaloVerd	B	1727	3	55	7.10	2.54	1.57	100	54	56	14	63	77	2.54	1.41	3.405
35	StaCruzI	B	1637	3	40	6.94	2.19	1.25	11	40	49	10	16	25	2.19	0.62	3.340
36	StaRosaI	C	1309	2	50	7.05	1.37	0.86	8	33	31	8	0	8	1.46	0.00	3.164
37	Rinconad	B	2563	1	40	6.94	4.48	2.53	64	13	107	20	19	39	4.48	0.75	3.651
38	HosgriN	B	2164	3	60	7.15	2.74	1.92	29	59	66	16	28	44	2.74	0.54	3.438
39	HosgriS	B	1778	3	60	7.15	2.48	1.47	21	59	59	15	26	40	2.48	0.49	3.394
40	StaYnez	B	4473	0.5	50	7.05	8.16	4.54	78	8	189	42	1	43	8.16	0.02	3.912
41	SierNeva	B	2082	1	50	7.05	3.66	2.98	13	17	86	19	0	19	3.66	0.00	3.563
42	SanBerMt	C	2039	2	20	6.58	4.69	2.87	37	13	110	25	0	25	9.54	0.00	3.980
43	MojaveW	C	5191	0.1	30	6.79	11.04	5.31	34	1	255	36	0	36	10.34	0.00	4.014
44	MojaveC	C	12736	5	70	7.23	18.7	12.42	83	116	438	103	0	103	15.64	0.00	4.194
45	Salton	C	1977	0.3	30	6.79	4.58	2.97	26	2	109	21	0	21	5.97	0.00	3.776
46	Ventura	C	1957	16	81	7.30	3.65	1.87	214	417	81	120	0	120	16.48	0.00	4.217
47	MojaveNE	C	4920	3	30	6.79	5.13	3.05	58	30	121	38	0	38	10.78	0.00	4.033
48	Coso	C	2161	0.5	20	6.58	3.23	2.81	14	3	76	11	0	11	4.34	0.00	3.637
49	SanGabMt	C	1060	0.5	15	6.43	2.88	1.35	33	2	65	19	0	19	9.54	0.00	3.980
50	CoasRanC	C	3293	0.5	40	6.94	7.92	3.23	62	7	189	48	0	48	11.03	0.00	4.042
51	CentCoas	C	3371	1	30	6.79	5.03	3.02	62	10	120	40	0	40	11.30	0.00	4.053
52	SanJoVaW	C	5854	2	30	6.79	14.87	7.34	39	20	353	46	0	46	12.96	0.00	4.113
53	SanJoVaC	C	7688	0.3	15	6.43	15.74	9.95	50	1	373	41	0	41	20.14	0.00	4.304
54	SimiSaFe	B	1388	2	30	6.79	2.91	1.85	135	20	55	10	67	77	2.91	4.42	3.464
55	StaBarCh	C	3754	1	50	7.05	5.32	3.38	223	17	122	125	0	125	24.22	0.00	4.384
56	OffsIsla	C	38124	4	50	7.05	23.37	14.43	247	66	513	184	0	184	35.56	0.00	4.551
57	OffshorC	C	22274	0.5	50	7.05	16.81	11.15	0	8	401	43	0	43	8.41	0.00	3.925
58	PeniRanW	C	9118	0.1	20	6.58	14.78	10.26	56	1	350	47	0	47	18.28	0.00	4.262
59	PeniRanC	C	3960	0.3	20	6.58	9.51	5.95	49	2	225	37	0	37	14.29	0.00	4.155
60	SoutSier	C	7530	0.3	20	6.58	14.38	10.49	91	2	338	64	0	64	24.89	0.00	4.396
61	BasiRang	C	11834	4	70	7.23	7.5	7.47	77	92	179	63	0	63	9.59	0.00	3.982
62	MojaveE	C	20564	0.3	50	7.05	8.49	6.81	131	4	203	87	0	87	16.91	0.00	4.228
63	ColoCorr	C	19376	0.5	40	6.94	13.31	10.84	115	7	319	87	0	87	19.76	0.00	4.296
64	SECorner	C	12564	1	40	6.94	18.95	16.18	83	13	454	83	0	83	18.94	0.00	4.277
65	TranRanW	C	5588	5	70	7.23	10.43	4.84	144	116	245	106	0	106	16.14	0.00	4.208
	All A		19514				50.77	26.58	4738	5377	1193	183	5377	5560	26.58	70.64	
	All B		41380				82.66	51.55	2700	2919	2172	451	2365	2816	82.66	78.79	
	All C		208242				241.68	158.85	1936	982	5670	1484	0	1484	346.51	0.00	
	Total		269136				375.11	236.98	9374	9277	9036	2118	7742	9860	455.75	149.43	

Table 6  
Alternate Seismic Source Model

Number	Name	Type	Area Km <sup>2</sup>	V mm/ yr	Length	M <sub>s</sub> Km	Rate Full 10 <sup>-3</sup> /yr	Rate Part 10 <sup>-3</sup> /yr	M <sub>0</sub> 10 <sup>15</sup> Nm/yr	M <sub>f</sub> 10 <sup>15</sup> Nm/yr	M <sub>s</sub> 10 <sup>15</sup> Nm/yr	M <sub>d</sub> 10 <sup>15</sup> Nm/yr	M <sub>c</sub> 10 <sup>15</sup> Nm/yr	M <sub>m</sub> 10 <sup>15</sup> Nm/yr	Rate 10 <sup>-3</sup> /yr	Rate 10 <sup>-3</sup> / yr	a Dist.
01	SACreepi	B	718	0	200	7.00	2.33	1.18	0	0	56	11	0	11	2.33	0.00	3.367
02	SAParkfi	B	881	34	30	7.29	3.05	1.32	347	337	70	22	320	342	3.05	3.74	3.484
03	SACHolam	B	1045	34	50	7.55	3.54	0.81	515	561	84	36	502	538	3.54	2.36	3.549
04	SACarriz	A	2265	34	121	8.01	8.19	3.05	1094	1358	193	56	1358	1414	3.05	cas	3.484
05	SAMojave	A	2847	30	133	8.06	8.67	3.27	1036	1317	200	64	1317	1381	3.27	cas	3.515
06	SASanBer	A	1799	24	78	7.78	4.78	2.35	585	618	112	32	618	650	2.35	cas	3.371
07	SACoachell	A	2793	25	114	7.98	5.62	3.85	860	941	134	68	941	1009	3.85	cas	3.585
08	SJSanBer	A	409	12	35	7.37	1.19	0.47	109	139	28	4	139	142	0.47	cas	2.672
09	SJSanJac	A	820	12	42	7.46	2.41	1.19	129	166	57	11	166	177	1.19	cas	3.076
10	SJAnza	A	1482	12	90	7.86	3.65	2.12	281	356	87	32	356	389	2.12	cas	3.326
11	SJCoyCre	A	495	4	40	7.44	1.33	0.72	47	53	32	6	53	59	0.72	cas	2.857
12	SJBorreg	A	745	4	29	7.27	2.63	1.65	83	38	63	12	38	50	1.65	cas	3.217
13	SJSupMtn	A	415	4	23	7.15	1.3	1.08	81	30	31	6	30	37	1.08	cas	3.033
14	SJSupHil	A	332	4	22	7.13	1.03	0.73	50	29	25	4	29	33	0.73	cas	2.863
15	Whittier	A	1065	2.5	38	7.41	2.09	1.12	91	31	47	9	31	41	1.12	cas	3.049
16	GlenIvy	A	739	5	35	7.37	1.41	0.73	54	58	33	6	58	64	0.73	cas	2.863
17	Temecula	A	823	5	42	7.46	1.44	0.79	60	69	34	7	69	76	0.79	cas	2.898
18	Julian	A	1323	5	75	7.76	2.38	1.49	106	124	56	20	124	144	1.49	cas	3.173
19	CoyoteM	A	1162	4	38	7.41	2.65	1.97	72	50	63	17	50	67	1.97	cas	3.294
20	NewpIngl	B	1313	1	30	7.29	2.39	1.54	72	10	53	17	24	41	2.39	0.28	3.378
21	NIOffsho	B	1155	1.5	40	7.44	1.52	0.86	37	20	35	13	15	28	1.52	0.11	3.182
22	RoseCany	B	1661	1.5	40	7.44	1.97	1.33	45	20	46	17	15	32	1.97	0.11	3.294
23	Imperial	B	1497	30	90	7.86	4.24	4.04	720	891	102	64	741	806	4.24	1.22	3.627
24	LaguSala	B	1332	4	40	7.44	3.89	2.92	85	53	93	34	35	69	3.89	0.24	3.590
25	WhitWolf	B	2423	2	80	7.79	7.58	5	76	53	178	106	0	106	7.58	0.00	3.880
26	BigPine	B	568	1	40	7.44	1.48	0.66	11	13	34	13	0	13	1.48	0.00	3.170
27	GarlockW	B	1697	5	100	7.91	3.78	2.17	50	165	88	61	46	108	3.78	0.06	3.577
28	GarlockE	B	2813	7	130	8.05	3.47	2.66	80	300	82	67	123	190	3.47	0.11	3.540
29	PintoMtn	B	1226	2	30	7.29	2.48	1.97	17	20	59	18	1	18	2.48	0.01	3.394
30	Brawley	B	992	25	10	7.00	2.21	1.75	0	83	53	11	31	41	2.21	0.97	3.344
31	SierMadr	B	1879	3	81	7.80	4.5	2.25	83	80	99	63	18	82	4.5	0.04	3.653
32	SanGabFa	B	895	0.5	45	7.50	2.33	1.34	40	7	51	22	1	24	2.33	0.01	3.367
33	SaMoMali	B	1473	2	55	7.60	2.74	1.64	71	36	55	30	24	54	2.74	0.09	3.438
34	PaloVerd	B	1727	3	55	7.60	2.54	1.57	100	54	56	28	50	77	2.54	0.20	3.405
35	StaCruzI	B	1637	3	40	7.44	2.19	1.25	11	40	49	19	6	25	2.19	0.04	3.340
36	StaRosaI	C	1309	2	50	7.55	1.37	0.86	8	33	31	11	0	11	1.08	0.00	3.032
37	Rinconad	B	2563	1	40	7.44	4.48	2.53	64	13	107	39	0	39	4.48	0.00	3.651
38	HosgriN	B	2164	3	60	7.65	2.74	1.92	29	59	66	32	13	44	2.74	0.04	3.438
39	HosgriS	B	1778	3	60	7.65	2.48	1.47	21	59	59	29	12	40	2.48	0.04	3.394
40	StaYnez	B	4473	0.5	50	7.55	8.16	4.54	78	8	189	83	0	83	8.16	0.00	3.912
41	SierNeva	B	2082	1	50	7.55	3.66	2.98	13	17	86	37	0	37	3.66	0.00	3.563
42	SanBerMt	C	2039	2	20	7.08	4.69	2.87	37	13	110	31	0	31	5.79	0.00	3.763
43	MojaveW	C	5191	0.1	30	7.29	11.04	5.31	34	1	255	57	0	57	7.89	0.00	3.897
44	MojaveC	C	12736	5	70	7.73	18.7	12.42	83	116	438	161	0	161	12.59	0.00	4.100
45	Salton	C	1977	0.3	30	7.29	4.58	2.97	26	2	109	29	0	29	4.10	0.00	3.613
46	Ventura	C	1957	16	81	7.80	3.65	1.87	214	417	81	133	0	133	9.41	0.00	3.974
47	MojaveNE	C	4920	3	30	7.29	5.13	3.05	58	30	121	47	0	47	6.60	0.00	3.820
48	Coso	C	2161	0.5	20	7.08	3.23	2.81	14	3	76	16	0	16	2.92	0.00	3.465
49	SanGabMt	C	1060	0.5	15	7.00	2.88	1.35	33	2	65	23	0	23	4.87	0.00	3.688
50	CoasRanC	C	3293	0.5	40	7.44	7.92	3.23	62	7	189	66	0	66	7.49	0.00	3.875
51	CentCoas	C	3371	1	30	7.29	5.03	3.02	62	10	120	49	0	49	6.83	0.00	3.835
52	SanJoVaW	C	5854	2	30	7.29	14.87	7.34	39	20	353	73	0	73	10.15	0.00	4.007
53	SanJoVaC	C	7688	0.3	15	7.00	15.74	9.95	50	1	373	63	0	63	13.07	0.00	4.116
54	SimiSaFe	B	1388	2	30	7.29	2.91	1.85	135	20	55	21	57	77	2.91	0.66	3.464
55	StaBarCh	C	3754	1	50	7.55	5.32	3.38	223	17	122	139	0	139	13.57	0.00	4.132
56	OffsIsla	C	38124	4	50	7.55	23.37	14.43	247	66	513	243	0	243	23.76	0.00	4.376
57	OffshorC	C	22274	0.5	50	7.55	16.81	11.15	0	8	401	86	0	86	8.41	0.00	3.925
58	PeniRanW	C	9118	0.1	20	7.08	14.78	10.26	56	1	350	68	0	68	12.61	0.00	4.101
59	PeniRanC	C	3960	0.3	20	7.08	9.51	5.95	49	2	225	50	0	50	9.32	0.00	3.969
60	SoutSier	C	7530	0.3	20	7.08	14.38	10.49	91	2	338	84	0	84	15.66	0.00	4.195
61	BasiRang	C	11834	4	70	7.73	7.5	7.47	77	92	179	87	0	87	6.75	0.00	3.829
62	MojaveE	C	20564	0.3	50	7.55	8.49	6.81	131	4	203	109	0	109	10.65	0.00	4.027
63	ColoCorr	C	19376	0.5	40	7.44	13.31	10.84	115	7	319	116	0	116	13.21	0.00	4.121
64	SECorner	C	12564	1	40	7.44	18.95	16.18	83	13	454	125	0	125	14.20	0.00	4.152
65	TranRanW	C	5588	5	70	7.73	10.43	4.84	144	116	245	139	0	139	10.83	0.00	4.035
	All A		19514				50.77	26.58	4738	5377	1193	355	5377	5731	26.58	70.64	
	All B		41380				82.66	51.55	2700	2919	2172	895	2032	2927	82.66	10.32	
	All C		208242				241.68	158.85	1936	982	5670	2004	0	2004	231.76	0.00	
	Total		269136				375.11	236.98	9374	9277	9036	3254	7409	10662	341.00	80.97	

improve our understanding of earthquake potential throughout southern California. We use the seismic moment (equation 1), which is directly related to parameters of the causative fault, to measure the seismic potential implied by the various kinds of information. Seismic moment can be measured by seismology (from the amplitude of seismic waves), geology (from the measured fault length and slip), or geodesy (by deducing potential fault slip on the rupture surfaces from observed ground displacements at the earth's surface). Similarly, the rate of seismic moment release in a region can be estimated from each of the three data sets. In this section we describe how we use these data sets to assign a rate of seismic moment release to each of the various seismotectonic zones.

We first identify the fault segments for which we could apply the conditional probability analysis. Each of these fault segments corresponds uniquely to a single type A zone. Then, for each of the 65 zones we estimate the rate of distributed earthquakes, assumed to be Poissonian in time, equally probable anywhere within a given zone, and having a modified Gutenberg–Richter magnitude distribution. The original Gutenberg–Richter distribution is given by

$$N(m) = 10^{a-b \cdot m}, \quad (9)$$

where  $N(m)$  is the annual number of earthquakes with magnitude equal to or greater than  $m$ . We use the moment magnitude for  $m$ , and assume that  $b$  is 1.0. In the modified form that we use (see Appendix D),  $N(m)$  decreases more rapidly for large  $m$ , approaching zero as  $m$  approaches the limiting magnitude  $m_x$ . In addition to the distribution described by the above formula, we allow for the occurrence of “extra” characteristic earthquakes with magnitude  $m_x$  at the annual rate  $f_c$ . Thus, for each zone, there are three parameters to be determined from the data:  $a$ ,  $m_x$ , and  $f_c$ .

For type A zones, we set  $f_c = 0$ , because characteristic earthquakes have already been accounted for by the cascade model, and we take  $m_x$  to be the characteristic magnitude from geological studies. We estimate the seismicity rate ( $a$  value) from the rate of observed  $m \geq 6$  earthquakes using the smoothed, modified Ellsworth catalog with large characteristic earthquakes removed. We removed the large earthquakes to avoid double-counting in the A zones, for which the characteristic earthquakes are treated separately.

For type B zones, geologists have documented faults that may have characteristic earthquakes, but information about their behavior is incomplete. Thus, we allow for characteristic earthquakes with the specified magnitude  $m_x$ . We fix the  $a$  value for distributed seismicity from the observed rate of  $m \geq 6$  earthquakes using the complete, smoothed catalog with all earthquakes included. The rate  $f_c$  of extra earthquakes is then set so

that the predicted seismic moment rate matches the “observed” moment rate. For these zones, we take the observed moment rate to be the average of the geological and geodetic estimates.

For type C zones, we lack direct evidence of a preferred characteristic earthquake, although the length of exposed fault segments may suggest an upper limit. For these zones we set  $f_c = 0$  (no characteristic earthquakes), and we set the seismicity rate to the average of the smoothed catalog seismicity rate and the value corresponding to the observed geodetic moment rate. In calculating the seismicity rate for a given moment rate, we need to assume the value of  $m_x$  (Appendix D).

Table 5 lists the seismicity parameters for each of the 65 zones. The first 10 columns are input data, and the following eight columns are derived from the input values. “Length” is the length (in kilometers) of the longest fault segment. “Area” is the total area (in  $\text{km}^2$ ) of the zone. “V” is the estimated slip rate (in  $\text{mm/yr}$ ) for the dominant fault in the type A and type B zones, and the estimated slip across the width of the zone for type C zones. Where oblique slip occurs, V represents the magnitude of the slip vector. For most zones the limiting magnitude,  $m_x$ , is estimated from the fault length using the regression formula of Wells and Coppersmith (1994), although it is revised upward for a few type C zones where the length of exposed faults did not adequately indicate the limiting earthquake magnitude. “Rate Full” is the rate  $r$  of  $m \geq 6$  earthquakes (in events per 1000 yr) predicted by the smoothed earthquake catalog. The choice of unit does not imply that the seismicity rates are constant for period of 1000 yr; rather they are chosen to make the values a convenient size. “Rate Part” is the smoothed seismicity rate  $r$  (again in events per 1000 yr) for the special catalog with characteristic earthquakes removed before smoothing. “ $\dot{M}_g$ ” is the moment rate (in units of  $10^{15} \text{ Nm/yr}$ ) for each zone estimated using the Kostrov formula (equation 8) and the geodetically measured strain rate for each zone. “ $\dot{M}_f$ ” is the moment rate estimated from the fault-slip rate, V,

$$\dot{M}_f = \mu H L V. \quad (10)$$

“ $\dot{M}_s$ ” is the moment rate implied by the smoothed complete catalog, assuming a generic value of  $m_x = 8.22$ , which is appropriate for the Harvard catalog of global earthquakes since 1977 (Kagan, 1993). “ $\dot{M}_d$ ” is the moment rate predicted by the model to result from distributed earthquakes. It is directly proportional to the predicted rate of distributed earthquakes, with a proportionality factor that increases with the limiting magnitude  $m_x$ . “ $\dot{M}_c$ ” is the characteristic earthquake moment rate predicted over the long term. For type A zones, it is computed directly from the fault-slip rate (in fact it

is equal to  $\dot{M}_p$ ) so it does not account for the accelerated probability of characteristic earthquakes on overdue fault segments. “ $\dot{M}_m$ ” is the total long-term moment rate predicted by the model (again neglecting the enhanced rate of predicted characteristic earthquakes in the overdue type A zones). For type A zones, the total moment rate for the model generally exceeds the geological estimate because the characteristic earthquakes fully account for the geological moment rate, and the moment rate of distributed earthquakes then contributes a small excess. “ $f_d$ ” is the predicted rate of distributed earthquakes, equal to or greater than magnitude 6, for each zone. “ $f_c$ ” is the predicted rate of characteristic earthquakes of magnitude  $m_x$ , in the type B zones only. In the type A zones, the rates and magnitudes of characteristic earthquakes are given by the cascade model, and in the type C zones there is no allowance for characteristic earthquakes. Finally, the column labeled “a/Dist” gives the  $a$  value of the modified Gutenberg–Richter distribution for distributed earthquakes only. The equations used for the calculations are given in Appendix D.

Entries at the bottom of Table 5 give sums of several quantities for each zone type, and for all zones together. Note that the geologic, geodetic, and seismic estimates of the moment rate are consistent for all of southern California. If we take the length of the plate boundary within southern California to be 500 km, the average relative plate motion to be 50 mm/yr, and assume  $\mu = 3 \cdot 10^{10}$  Nm<sup>-2</sup> and  $H = 11$  km, the expected moment rate contributed by plate tectonics can be calculated by equation (10) to be about  $8300 \cdot 10^{15}$  Nm/yr. This value is considered a lower estimate of the total seismic moment rate, as the elastic thickness of the crust may well exceed 11 km. Also, the estimate neglects the moment involved in crustal convergence, mountain building, and reshaping of the plates. The rate estimated from the seismic catalog using equation (3) is  $8300 \cdot 10^{15}$  Nm/yr. However, the distribution of moment rate differs among the three types of data. The smoothed seismicity catalog suggests a higher moment rate for the type C zones, while the geologic data puts most of the moment rate into the type A zones. Note that almost half of the seismically observed moment was released in the 1857 Fort Tejon earthquake on the San Andreas.

The geographic distribution of earthquake potential is perhaps best displayed in terms of the seismic moment per unit area, which after division by  $2\mu H$  is equal to the average strain rate (see equation 8). This representation is relatively insensitive to assumptions about the magnitude distribution. Figures 10 through 13 show the strain rate by zone derived from the geological, geodetic, and seismic data, and the combined form for input to the resulting hazard model of Table 5. The geological data (Fig. 10) indicate the equivalent rate for the Poissonian assumption; that is, they show the long-term rate, rather than the higher rate implied by the lognormal re-

currence hypothesis. The geological data show high strain rates in all of the type A zones, as well as type B zones Parkfield and Imperial.

The geodetic data (Fig. 11) generally agree with the geological data for the type A zones. This should be no surprise, as the geodetic data are interpreted with geologic slip rates where the geodetic data lacked adequate spatial resolution, especially along the San Andreas fault. However, the geodetic data show high strain rates in the Sierra Madre, San Gabriel, Santa Monica–Malibu, and Simi–San Fernando Valley zones where the geological slip rates imply lower strain. In the case of the seismic data (Fig. 12), the plotted strain rate assumes a uniform maximum magnitude, so that the strain rate is proportional to the seismicity rate per unit area. Only the seismicity rate itself is used in deriving the model parameters. Seismic strain rates are distributed more broadly than either the geologic or geodetic slip rates, primarily because of the smoothing applied to the catalog. The seismic strain rate exceeds the geologic rate in the White Wolf, Laguna Salada, San Gabriel, and Sierra Madre zones, where recent earthquakes have occurred despite low slip rates on the major faults in those zones. The combined strain-rate map or master model (Fig. 13) is not a simple average of the others, because of different assumptions made in the different zone types. Nevertheless, it is apparent that the master model is a compromise, gaining robustness by including three major categories of data.

Figure 14 shows the predicted cumulative magnitude distribution following from the preferred model, along with the observed distribution as measured by the catalog of Table 4. The contributions from characteristic and distributed earthquakes in the various zone types are also shown. The average rate of  $m \geq 6$  earthquakes is predicted to be about 0.61 per year for the next 30 yr, corresponding to an average recurrence time of 1.6 yr. This rate is about double the observed rate since 1850, which is 0.32 per year. The largest contribution to the total earthquake rate comes from the distributed earthquakes in type C zones, where the geodetic strain weighs heavily in the calculation. Although the strain rate in most type C zones is quite modest, their large area suggests that the cumulative probability of  $m \geq 6$  earthquakes is rather high. However, we note that type C zones are at the margin of, or even outside, the geodetic network, and the strain estimates are relatively uncertain there. Also, we assumed that the strain estimated by geodesy will be released completely as earthquakes. Some of the measured strain might be inelastic, so that it would not eventually result in earthquakes. The extent of inelastic strain is unknown, so we adopt the conservative view that all accumulated strain will be released in future earthquakes.

The difference between the predicted and observed rate of  $m \geq 6$  earthquakes might also be related to our

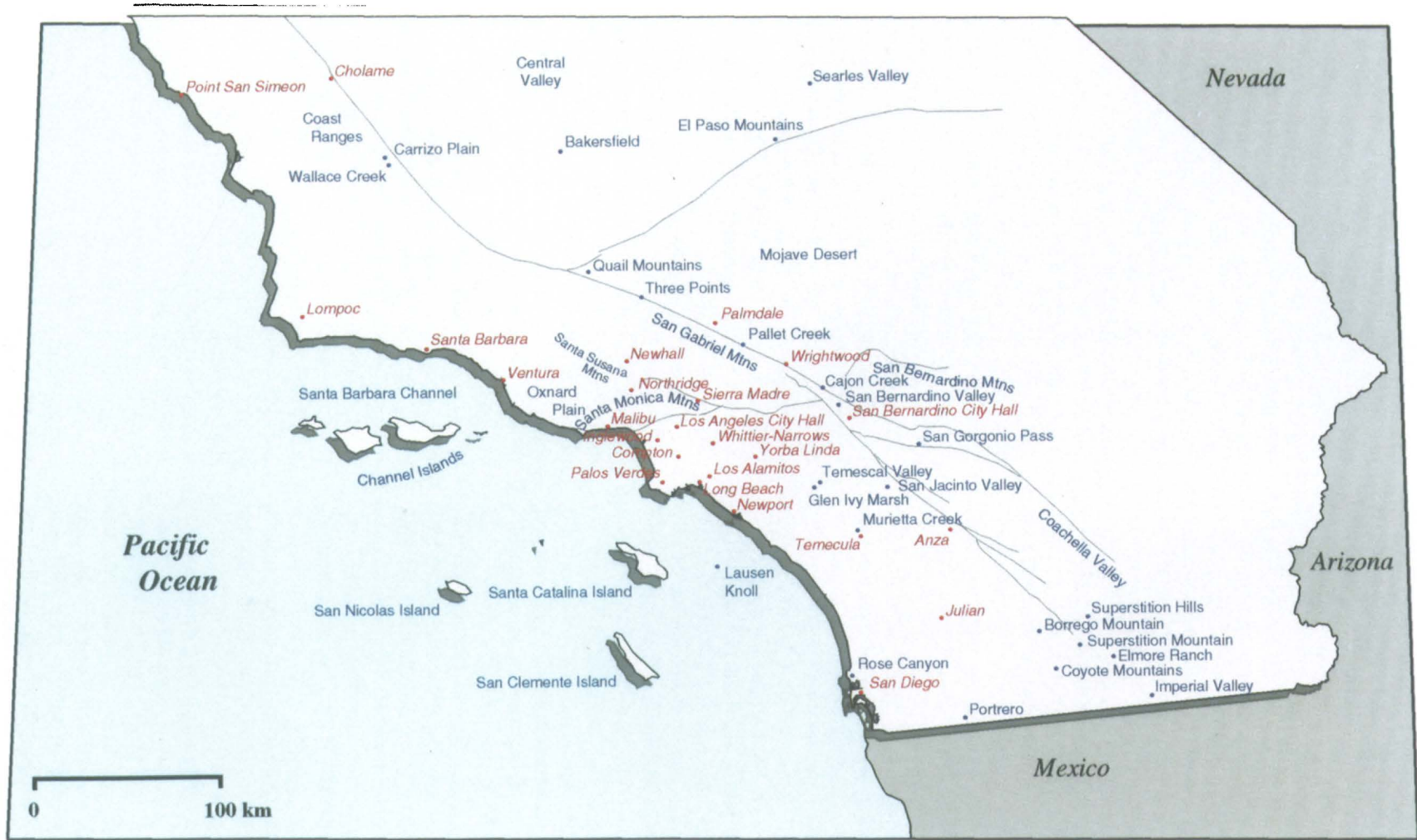


Figure 1. Map showing place names in southern California.

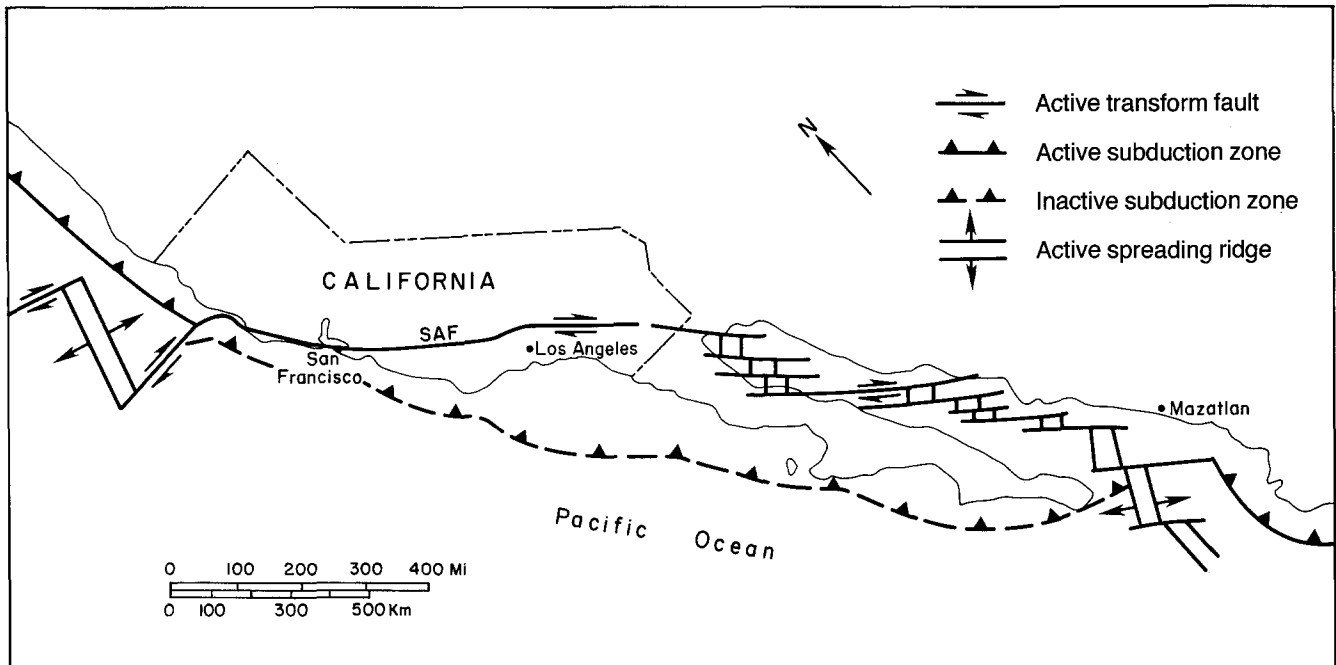


Figure 2. Map of ancient and modern plate boundaries in California.

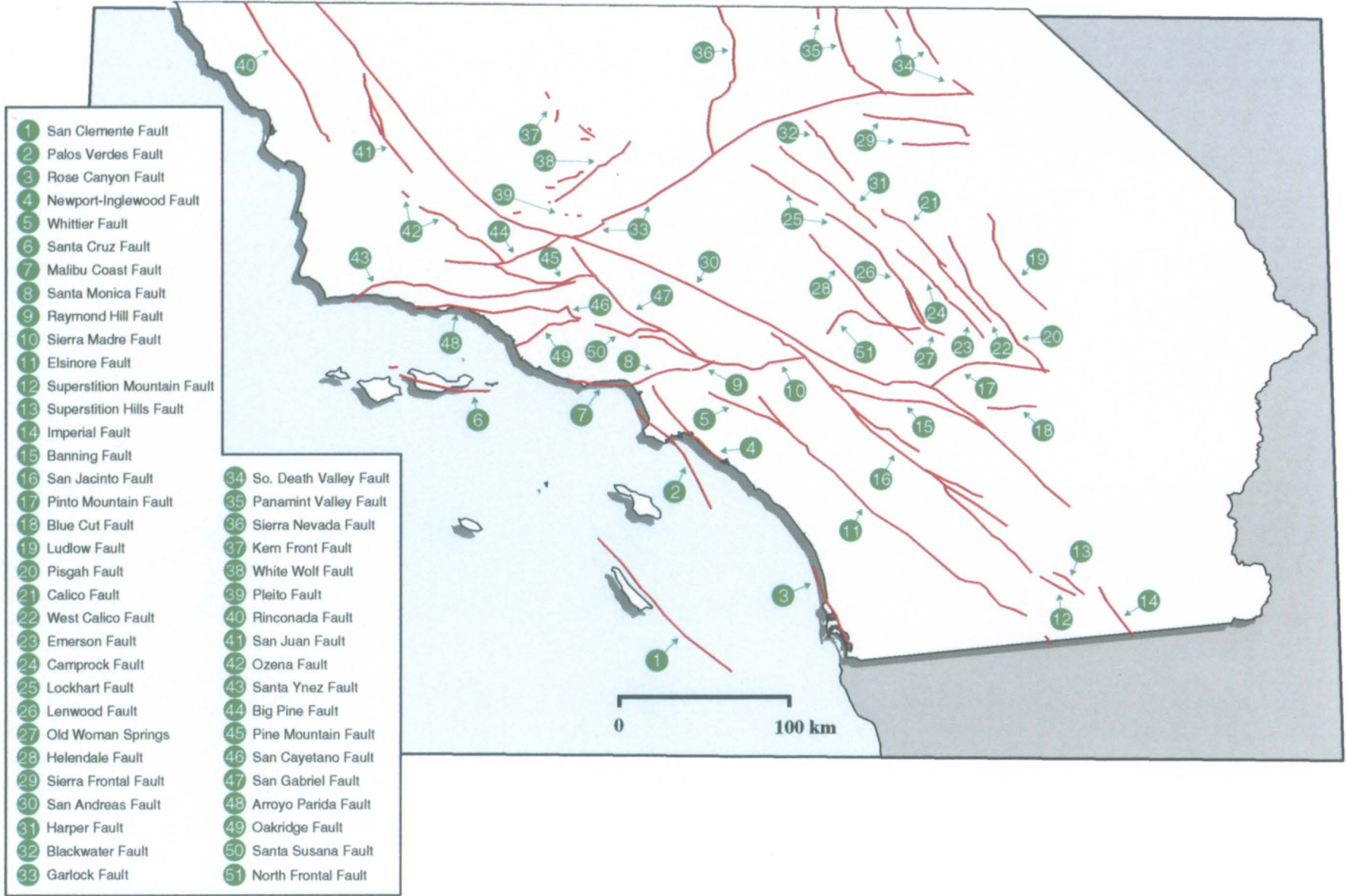


Figure 3. Major active surface faults in southern California.

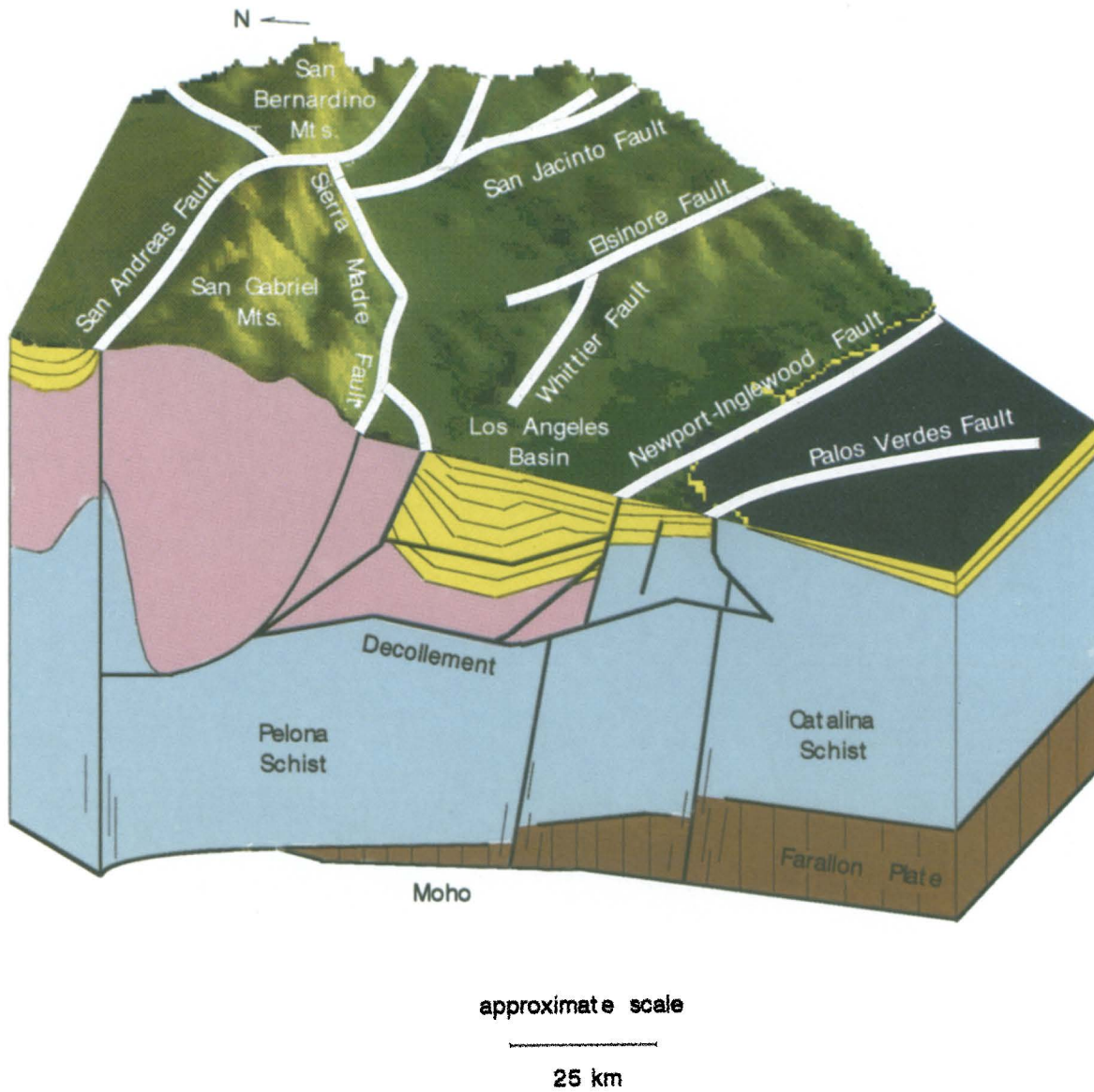


Figure 4. Cutaway block diagram of crust along profile from San Clemente Island to Mojave Desert.

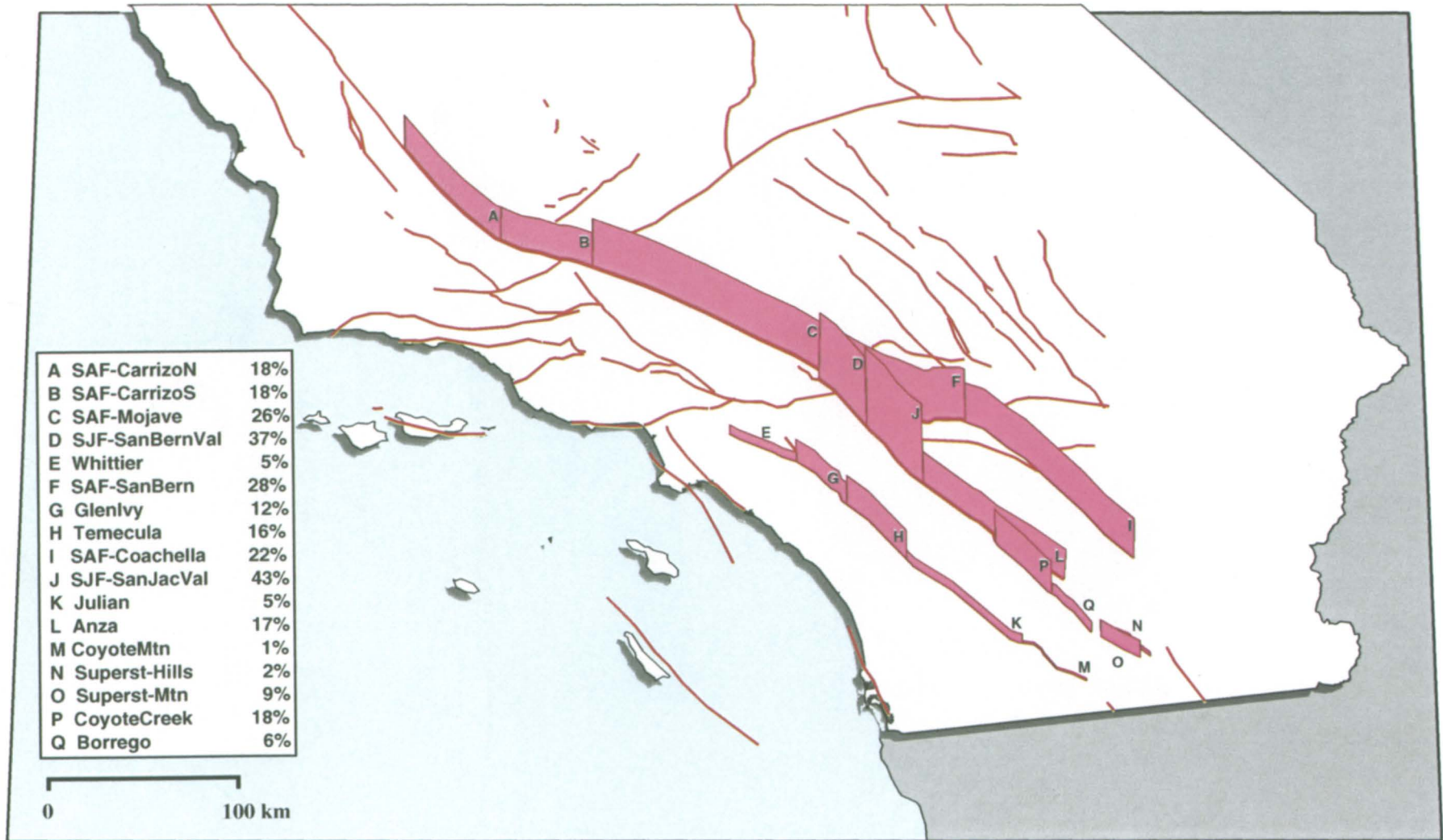


Figure 5. Fence diagram illustrating rupture probabilities for the time period 1994 to 2024 for fault segments associated with type A zones.

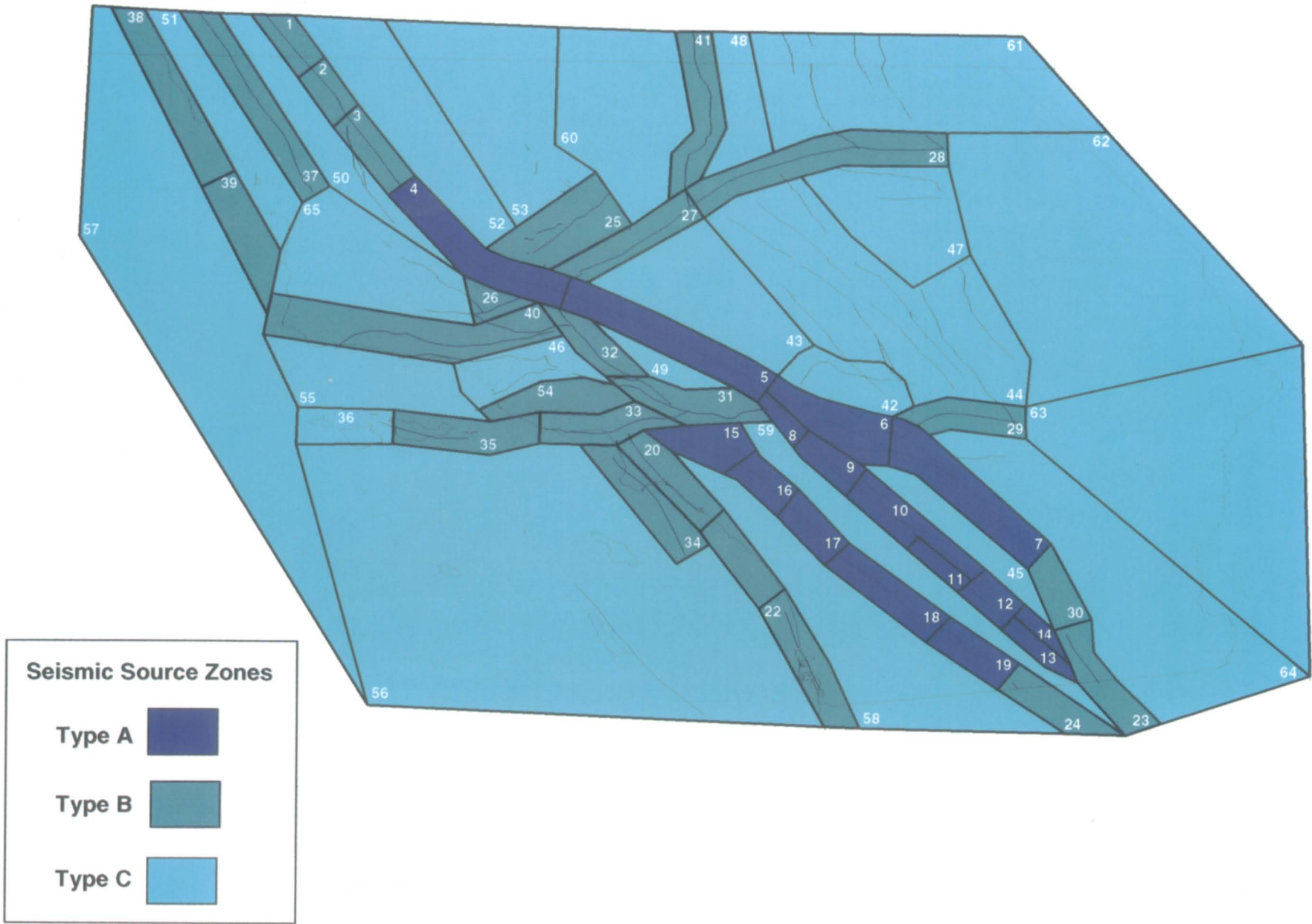


Figure 6. The 65 seismotectonic source zones for southern California. Zones are classified into type A, B, and C according to the quantity of available geologic data.

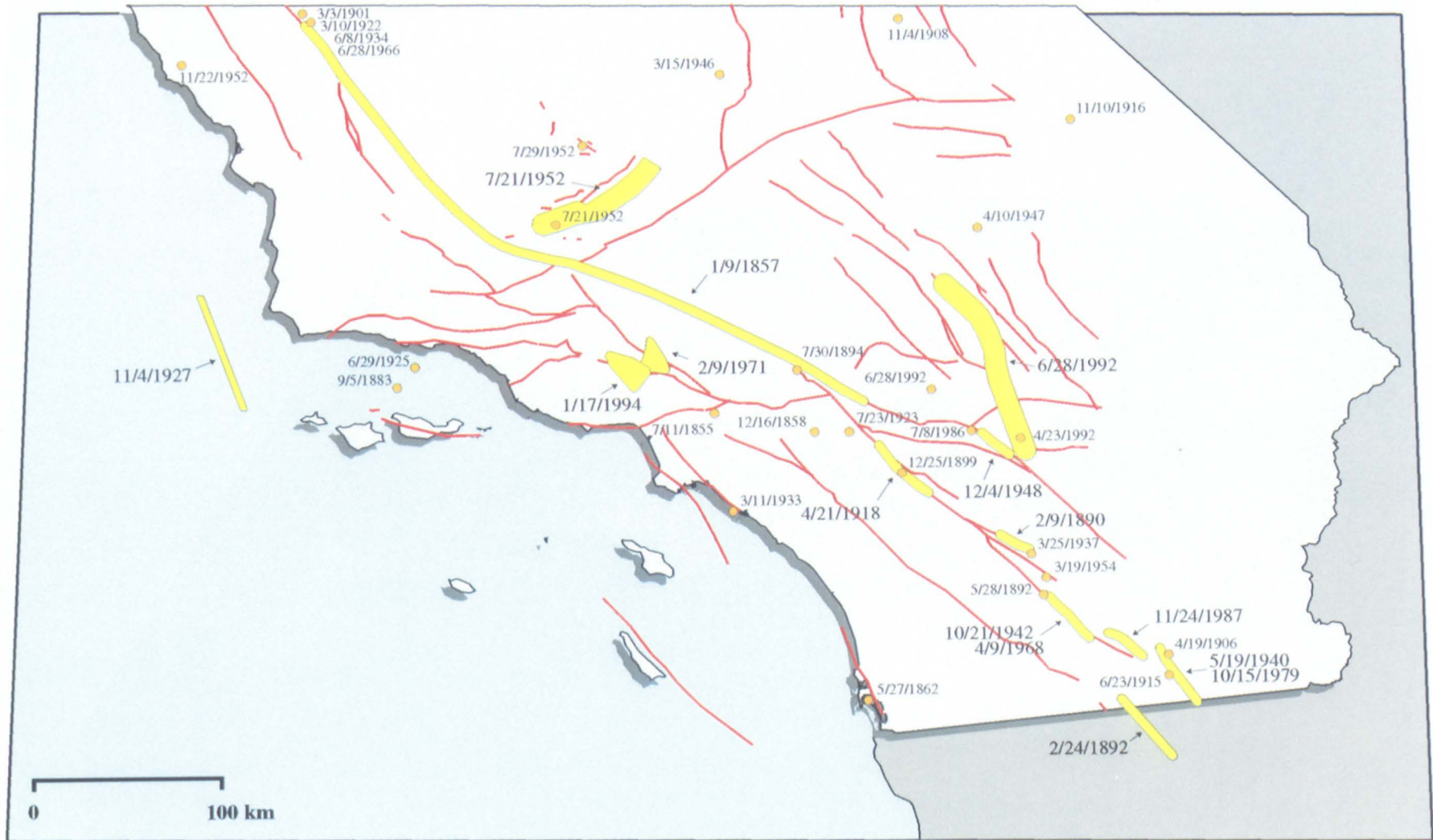


Figure 7. Map of earthquake epicenters listed in Table 4. If known, approximate rupture zones are shown in yellow.

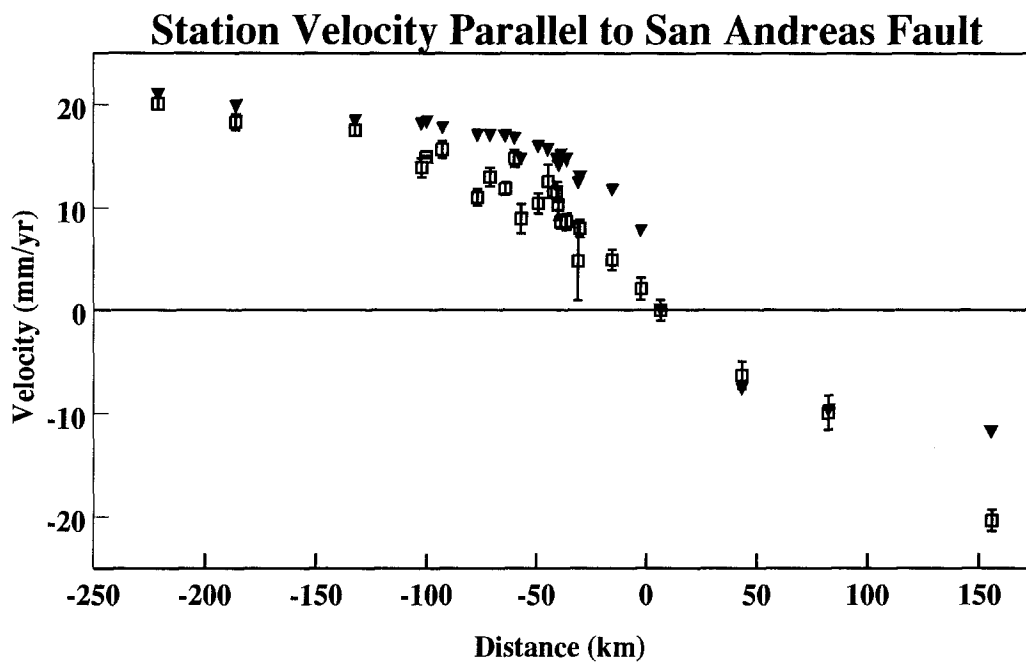


Figure 8. Predicted (triangles) and observed (squares) geodetic velocities across the Mojave segment of the San Andreas fault. Observed velocities estimated from GPS data, predicted velocities estimated from fault-slip rates.

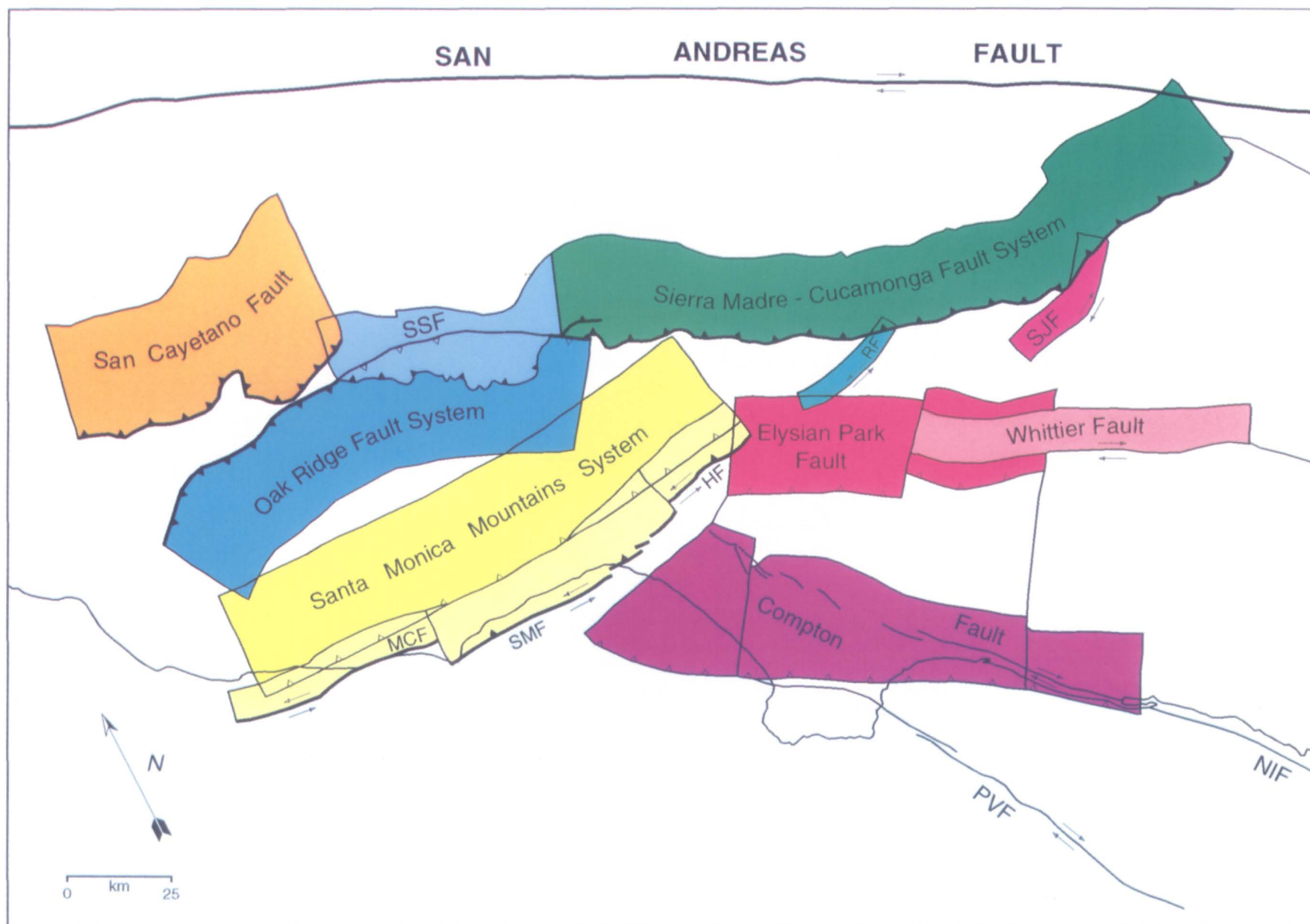


Figure 9. Exposed faults and buried thrust ramps in the greater Los Angeles basin.

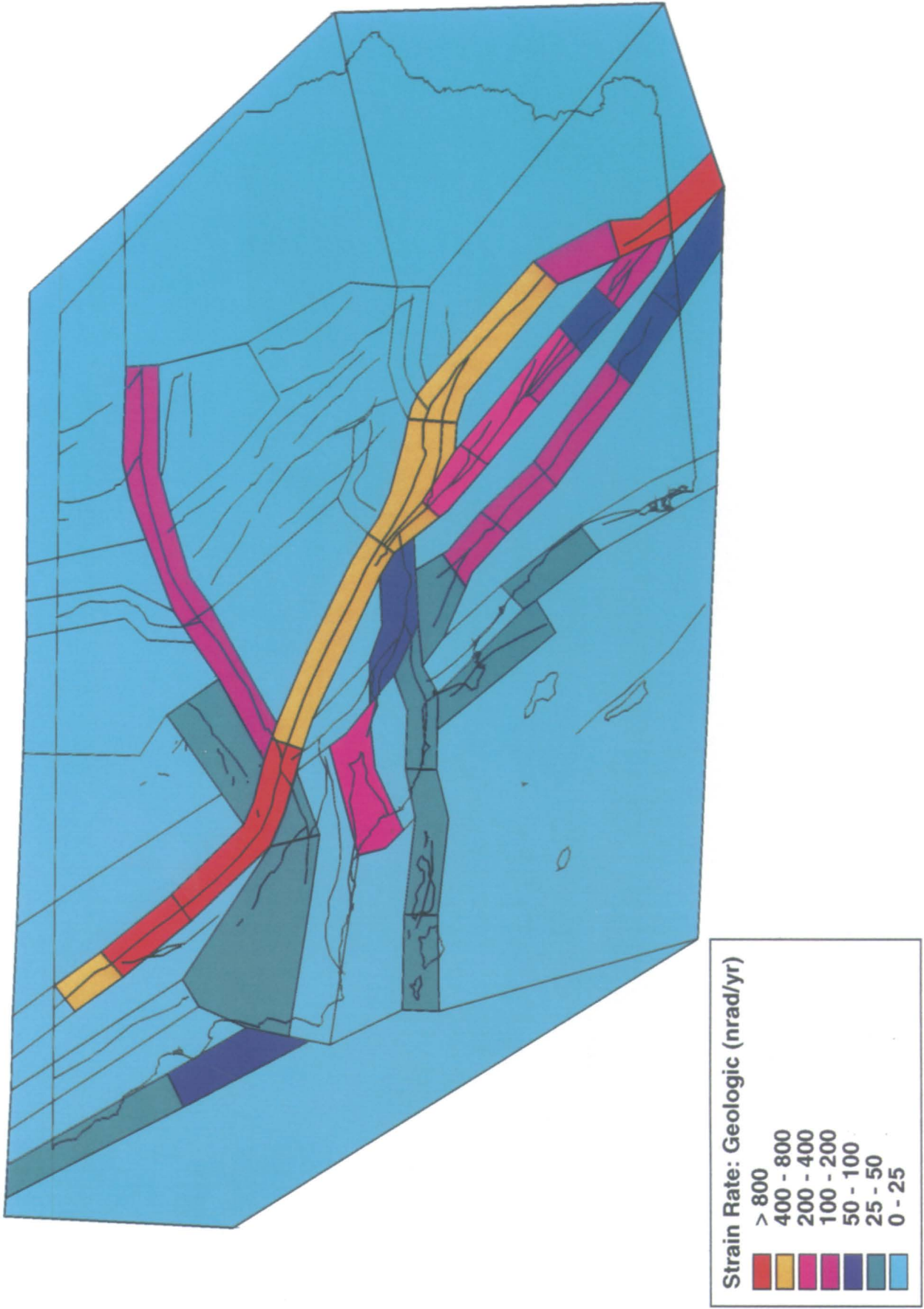


Figure 10. Strain rate in  $10^{-9}$  rad/yr estimated from fault-slip rates for each seismic-tectonic source zone.

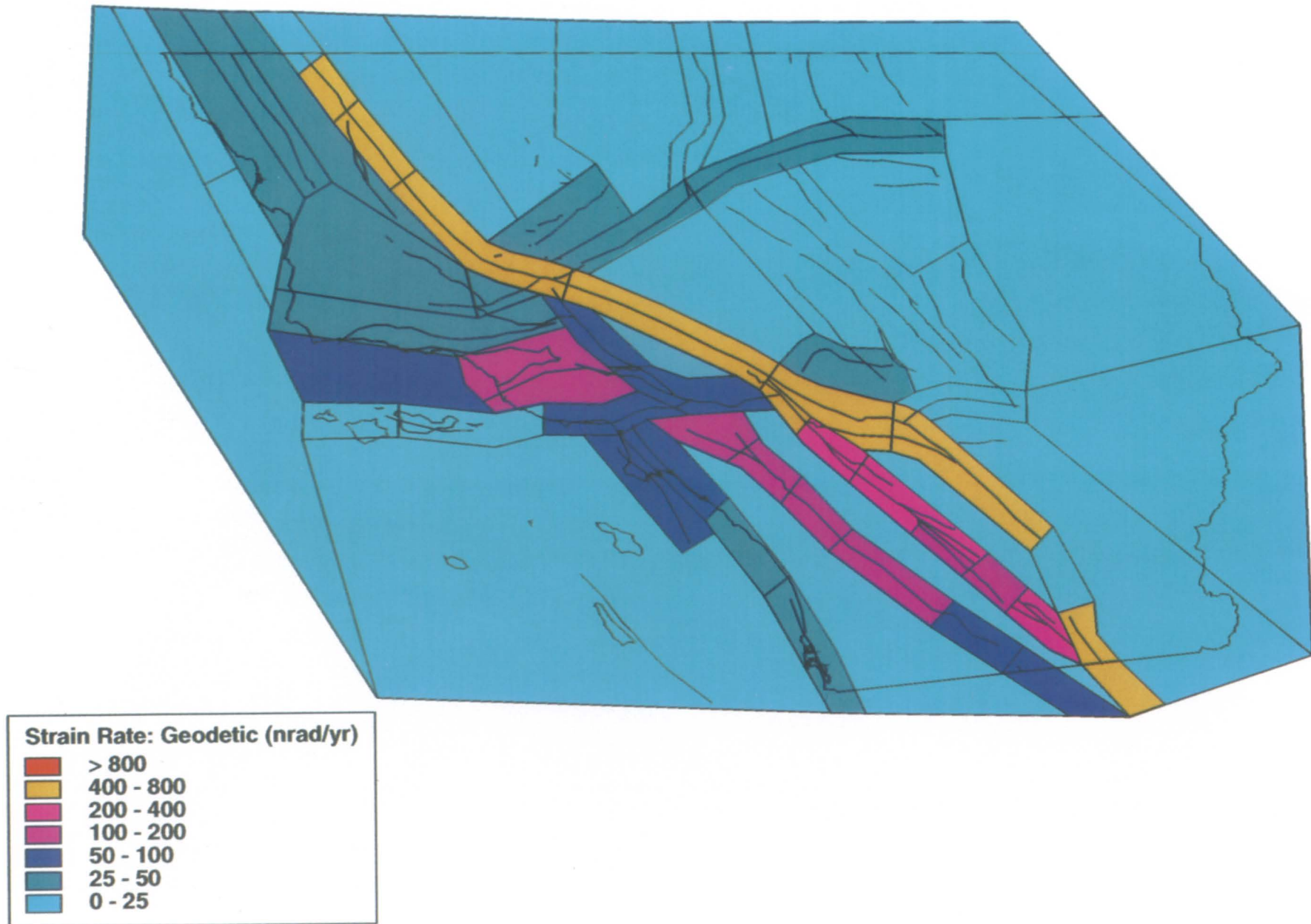


Figure 11. Strain rate in  $10^{-9}$  rad/yr estimated from GPS geodetic data for each seismotectonic source zone.

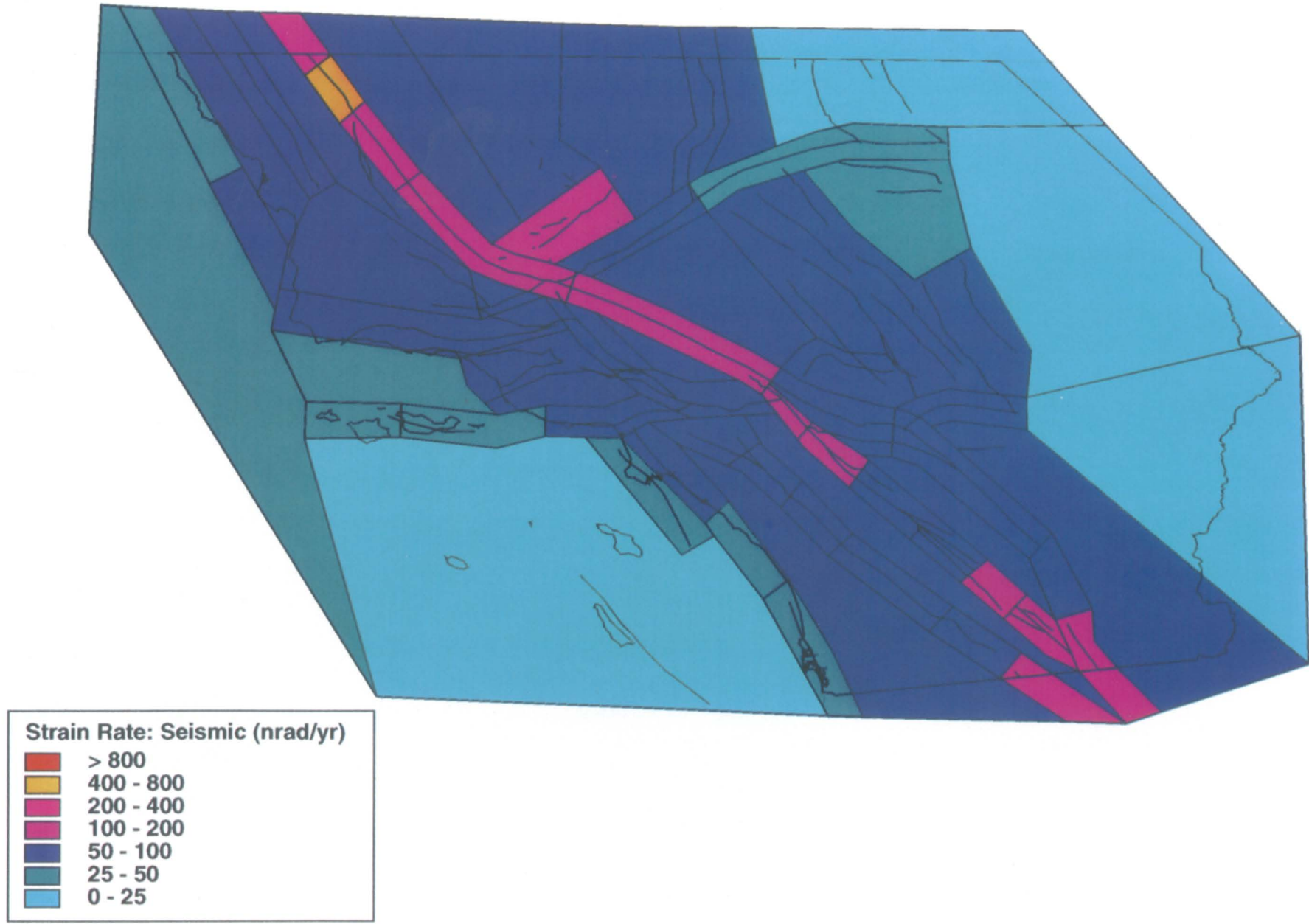


Figure 12. Strain rate in  $10^{-9}$  rad/yr estimated from the smoothed southern California earthquake catalog since 1850 for each seismotectonic source zone.

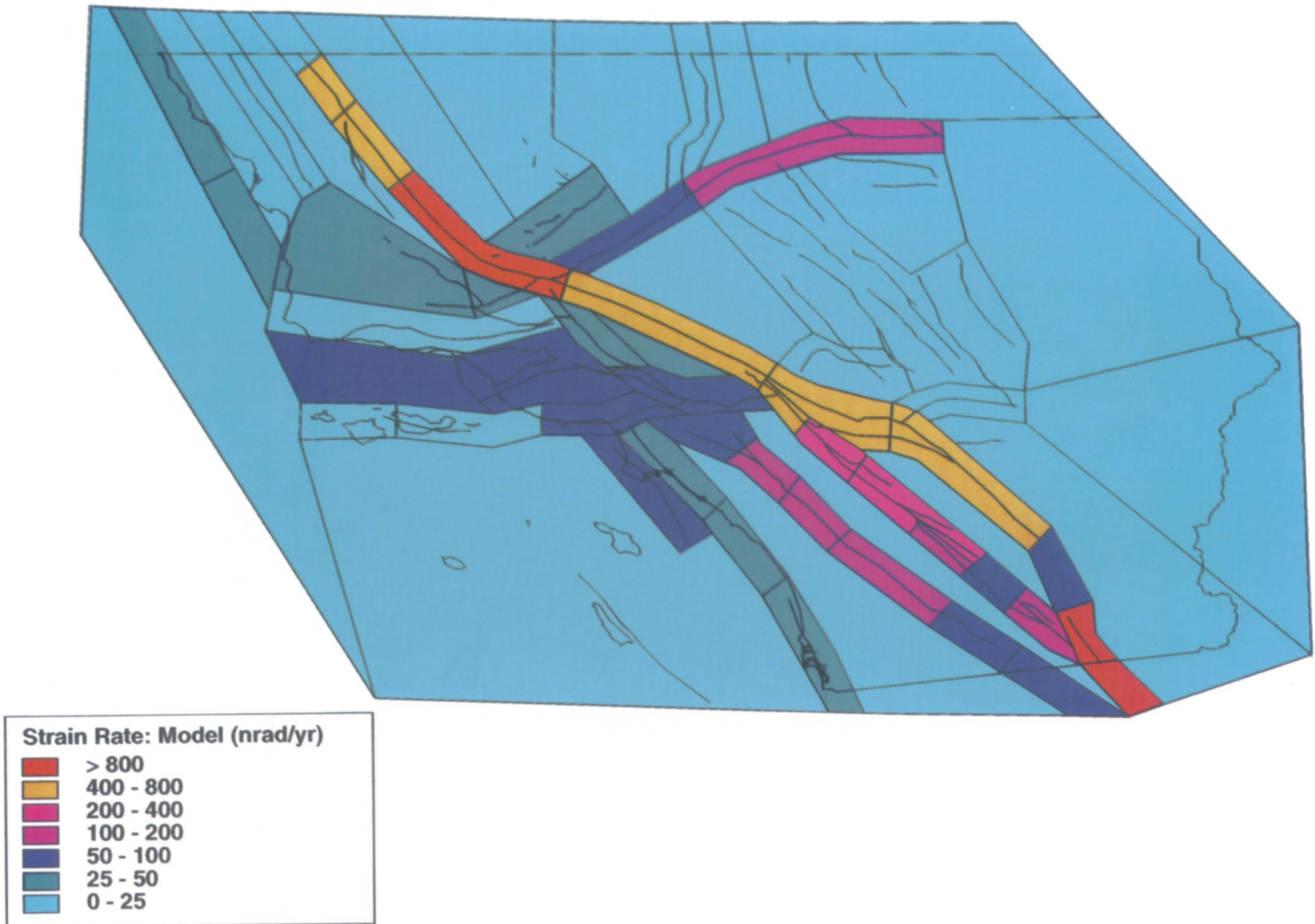


Figure 13. Strain rate in  $10^{-9}$  rad/yr calculated for the preferred model for each seismotectonic source zone.

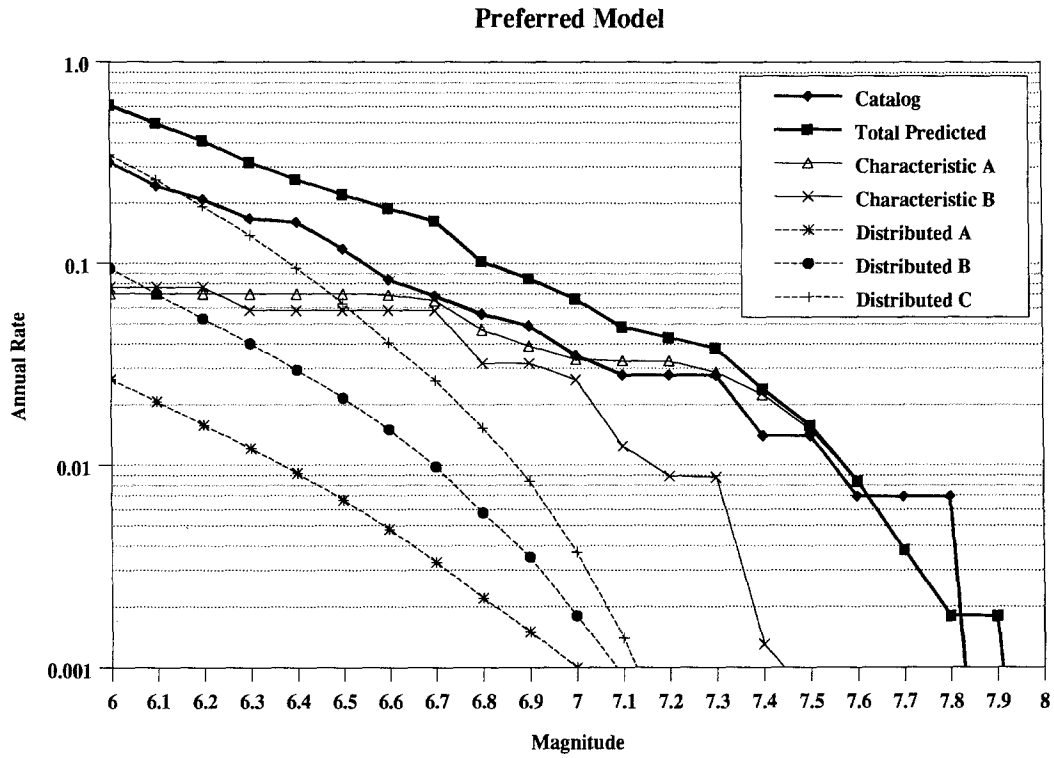


Figure 14. Annual rate of earthquakes with magnitude greater than  $M$  predicted for the preferred model, compared with the rate observed since 1850. Also, the contributions to the predicted rates from the type A, B, and C zones are shown separately for characteristic and distributed earthquakes.

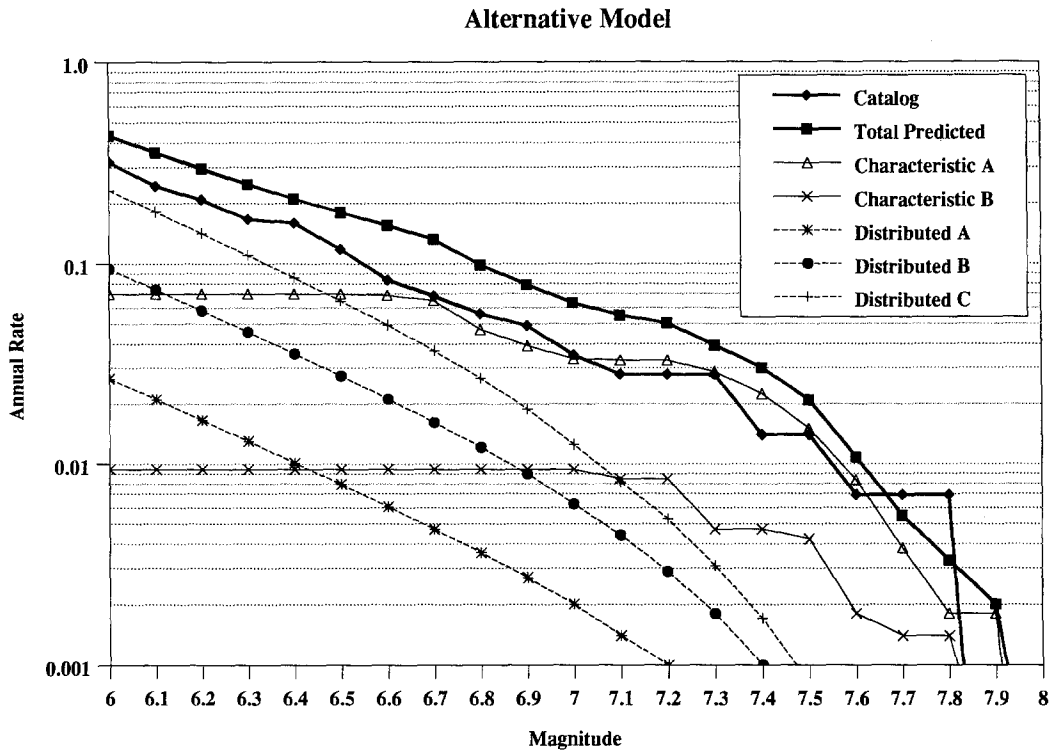


Figure 15. Annual rate of earthquakes with magnitude greater than  $M$  predicted for the alternative model, compared with the rate observed since 1850. Also, the contributions to the predicted rates from the type A, B, and C zones are shown separately for characteristic and distributed earthquakes.

### Los Angeles City Hall PGA (Rock Site) and 1 Second Spectral Acceleration (Soil Site)

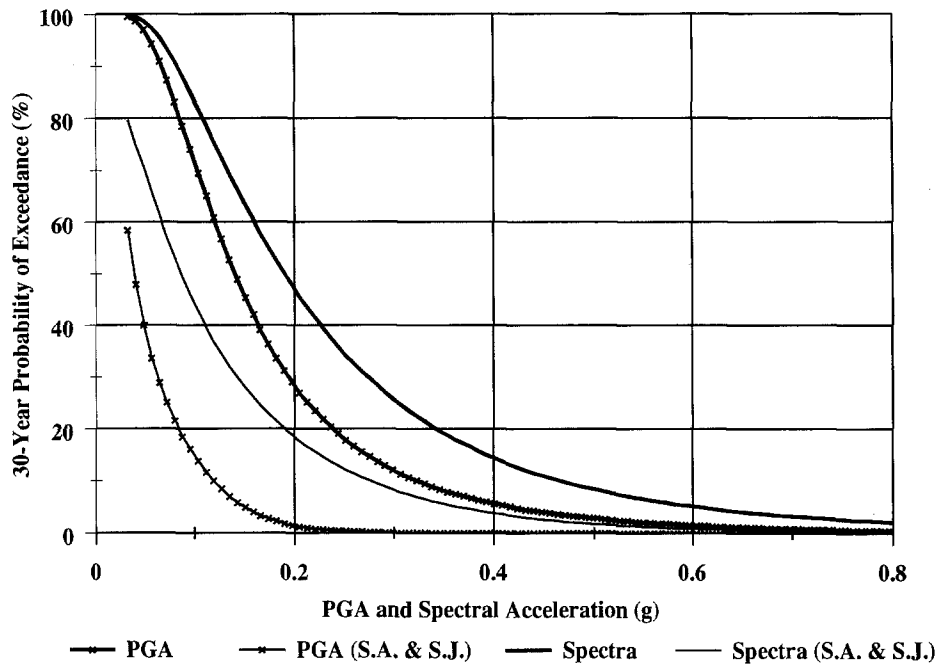


Figure 16. The 30-yr probability of peak ground acceleration exceeding a given value at the Los Angeles City Hall assuming a rock site. The contributions from events on the San Andreas and San Jacinto faults are shown separately. Also, the 30-yr exceedance probability is shown for the 1-sec-period spectral acceleration assuming a soil site.

### San Bernardino City Hall 1 Second Spectral Acceleration (Soil Site)

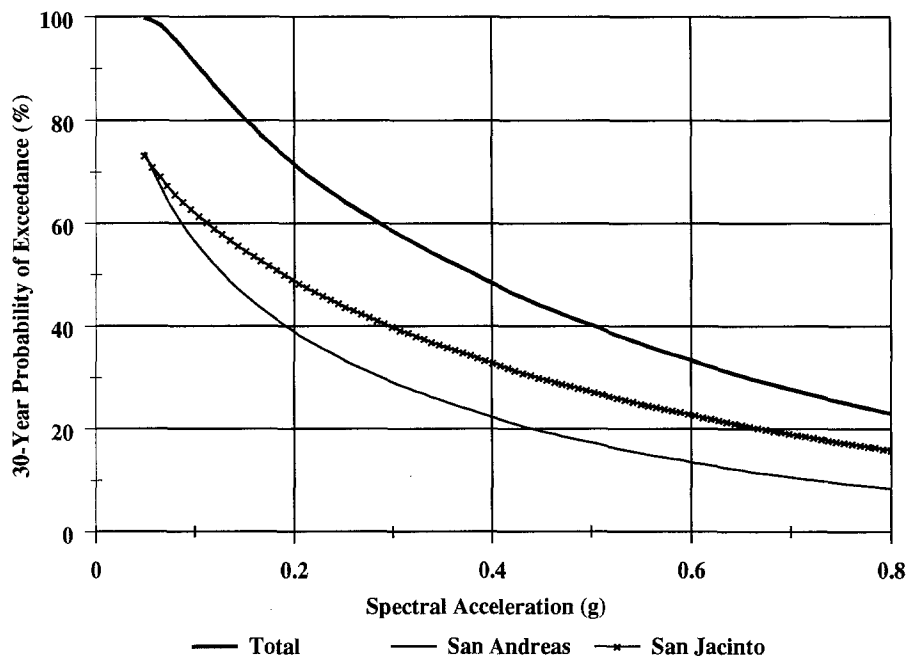


Figure 17. The 30-yr exceedance probability of the 1-sec-period spectral acceleration for the San Bernardino City Hall assuming a soil site.

### 30-Year Probability of Exceedance for 0.2 g

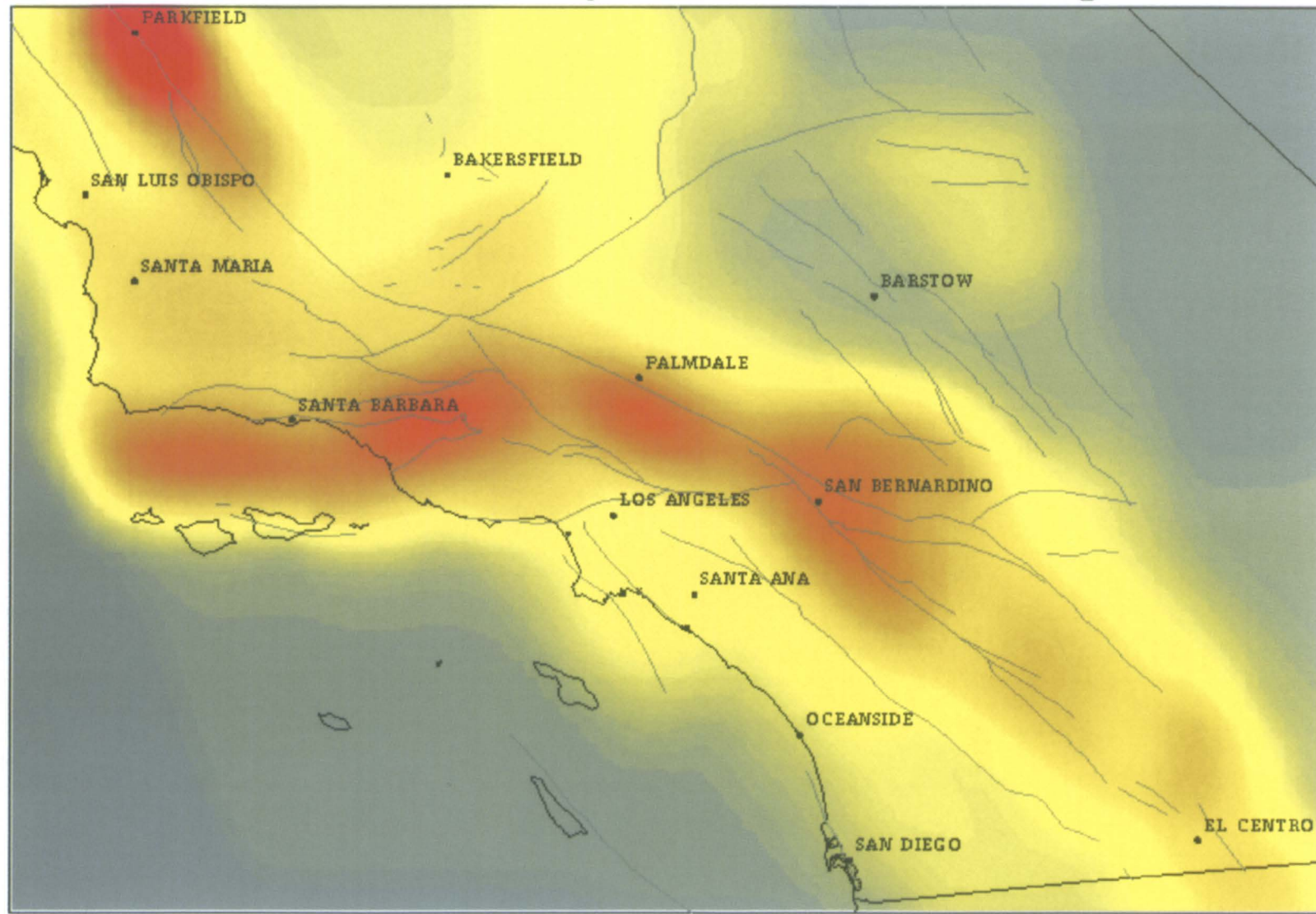


Figure 18. Map showing the 30-yr probability of the peak ground acceleration exceeding 0.2 g assuming a rock site.

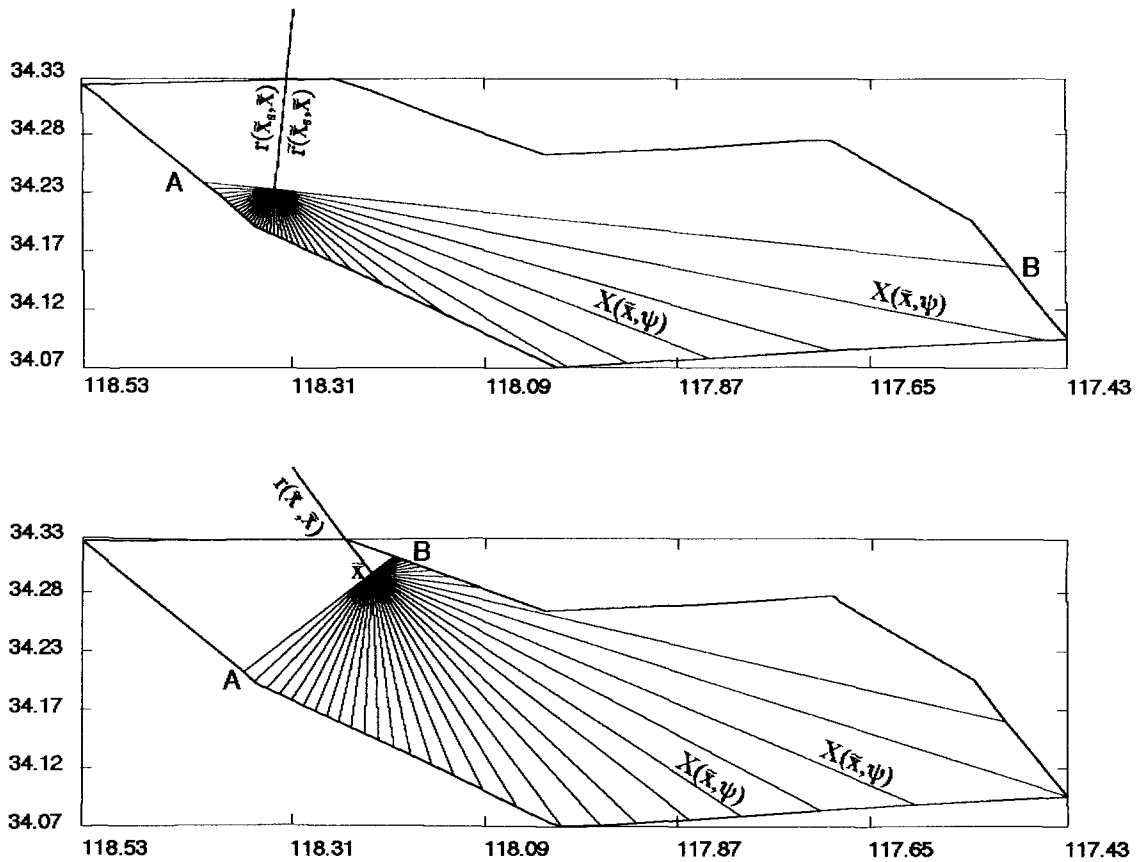


Figure 19. Procedure for calculating seismic hazard for a particular source zone. At each integration point  $\bar{x}$ , all vertical faults with surface traces that start or end at  $\bar{x}$  and are on the one side of the line AB, perpendicular to  $\bar{r}(\bar{x}, \bar{x})$ , share the same closest distance to the site. The distance from the integration point to the boundary in any direction,  $X(\bar{x}, \psi)$ , defines the longest possible rupture length at  $\bar{x}$  in that direction and is used to set the criteria for the occurrence of earthquakes with different rupture lengths. This contrasts with the point source model, which instead assumes a uniform probability of occurrence for earthquakes with different rupture lengths in all directions and at all points within the source zone.

assumption that the largest magnitude in any zone is limited by the length of surface fault traces. We adjust the estimated maximum magnitude to account for blind thrusts, but the 1992 Landers earthquake, which ruptured several apparently distinct fault segments, showed that fault length may not adequately constrain the maximum magnitude even in a strike-slip environment. Increasing the maximum magnitude in all zones would reduce the number of predicted  $m \geq 6$  earthquakes, but it would take a very large increase—nearly a full magnitude unit—to bring the predicted rate down to the observed level. The difference between the predicted and the long-term rates could be caused by natural variations in seismicity. The prediction is based on geological and geodetic data which reflect the long-term moment release, whereas the earthquake catalog covers a relatively brief time interval. Another Fort Tejon earthquake tomorrow would make up the deficit. A further consideration is that the predicted rate implicitly includes the contributions of aftershocks, which can relieve strain just as any other earthquake can. The catalog, however, may omit a number of  $m \geq 6$  aftershocks, especially in the period before 1932, which includes three of the five largest earthquakes, including the 1857 event. However, based on typical aftershock statistics, it is unlikely that missing  $m \geq 6$  aftershocks would make up more than 20% of the deficit.

The predicted rate of  $m \geq 7$  earthquakes is 0.067/yr, again about double the average rate since 1850 (0.035/yr). The predicted annual rate corresponds to a 30-yr probability of 86%. All of the above arguments regarding the comparisons of observed and predicted  $m \geq 6$  earthquakes also apply for  $m \geq 7$  events. Comparison is more difficult at  $m \geq 7$ , because the sampling is inadequate and the magnitude uncertainties before 1932 affect the results more. At  $m \geq 7$  the predicted rate is dominated by characteristic events in the type A and type B zones. The predicted rates would be reduced if we increased the estimated maximum magnitude substantially, or if we relaxed the constraints on the cascade model to include more interaction between segments. Either of these changes would replace several large earthquakes with a smaller number of even larger ones in the moment budget for the next 30 yr. At present, we lack any direct evidence to establish the maximum magnitude or the degree of segment interaction. Another possible modification, explored below, would be to use the Poissonian probability estimates, rather than the higher rates resulting from the lognormal model as assumed above. In this report, we accept the model presented in Tables 3 and 5 as the preferred model, and we use it in the probabilistic seismic hazard calculations below.

The preferred model predicts that great earthquakes like the 1857 event should be quite rare. Earthquakes of magnitude 7.8 or greater should occur at the rate of about two or three per 1000 yr, corresponding to a 6 to 9%

probability in 30 yr. Note that these estimates are particularly sensitive to the assumed maximum magnitude on many faults. The 1857 earthquake contributed 41% of the seismic moment release in the catalog, and only because of this large event are the seismic estimates of the moment rate comparable to those from plate tectonics and geodesy. In fact, 1857 was the only earthquake on the San Andreas in southern California since 1850 that expended significant seismic moment.

We also calculated seismic hazard parameters for an alternative model that conforms more to the observed distribution of earthquakes since 1850. For this model, we assume Poissonian behavior for cascades, with rates given in the last column of Table 3. We raised the maximum magnitude to 7.0, or 0.5 magnitude unit above the values predicted from the length of observed surface faults, whichever is greater. This allows for unanticipated earthquakes, and for the fact that the regression of magnitude versus fault length given by Wells and Coppersmith (1994) predicts the average magnitude, rather than the maximum magnitude. We also reduced the geodetic moment rate estimate in zones 35, 41, 44, 48, 52, 61, and 64 to values corresponding to maximum shear strain rates of 10 nanorad/yr. These zones presently have sparse geodetic coverage, and their estimated geodetic strain rates are very uncertain. Hazard parameters for this model are shown in Table 6, and the predicted magnitude distributions are given in Figure 15. The predicted rate of  $m \geq 6$  earthquakes is 0.43 per year, only slightly above the observed rate of 0.32 per year. For a Poisson process the relative uncertainty in the rate is the square root of the reciprocal of the number of events. Since the catalog contains only 49 earthquakes since 1850, the uncertainty in the average rate estimated from the catalog is 0.045 per year. Thus, the discrepancy between the alternate model and catalog rates is approximately two standard deviations. The predicted rate of  $m \geq 7$  earthquakes is 0.064 per year, compared to an observed rate of 0.035 per year. Since the observed rate is based on just five events, the uncertainty in the mean rate is about 0.015. Again, the discrepancy is about two standard deviations. Because the alternate model assumes a fully Poissonian process, and because the moment rate predicted by the model only exceeds the average rate from the earthquake catalog by about 25%, any significant difference in the rate of events must be related to the assumed magnitude distribution. According to the alternate model, the probability of an  $m \geq 7$  earthquake in southern California before 2024 is 85%.

#### Uncertainties

A formal estimate of the rate uncertainties for characteristic earthquakes can be obtained from the data in Table 2. We convert the uncertainty in each mean probability to a relative uncertainty, and multiply this by the conditional rate estimated for the lognormal model, to

estimate the standard deviation of each rate estimate. We then square and sum these values, with appropriate weighting, to get the variance of any weighted sum of the rates. The relative error in the total rate given in Table 2 is about 17%, and the estimated total cascade rates in Table 3 have about the same relative uncertainty. Because most of the  $m \geq 7$  earthquakes are characteristic earthquakes, this relative uncertainty of 17% will also apply to the rates of these large earthquakes. Thus, the 1- $\sigma$  range of predicted rates for the preferred model is 0.055 to 0.078 per year, corresponding to 30-yr probabilities in the range 81 to 90%. For the alternate model, the corresponding ranges are 0.053 to 0.075 events/yr, and 80 to 89%. These formal uncertainties reflect only errors in estimating displacements and slip rates, and to some extent the intrinsic variability of recurrence times about the median. The true uncertainties are undoubtedly much greater, as our calculations are based on several credible but unproven assumptions.

The close agreement between the preferred and alternative models at  $m \geq 7$  is fortuitous; the preferred model has more characteristic earthquakes in the type B zones, while the alternate model has more distributed earthquakes in the type C zones. Only at this magnitude level do the two models agree so closely, and this coincidence should not be interpreted to mean that the model is insensitive to the assumptions.

For  $m \geq 6$ , the yearly rates estimated by the preferred and alternate models differ strongly (0.614 versus 0.433), indicating that the predicted rate of moderate earthquakes depends very strongly on assumed maximum magnitude. Thus, a formal error estimate would not be very useful at this magnitude level.

### Probabilistic Seismic Hazard Analysis

The previous sections present information about the earthquake potential of specific faults and regions of southern California. The information includes estimated probabilities of large characteristic earthquakes on the major fault segments. These events capture one's attention because they cause damaging levels of ground-motion over wide areas. On the other hand, smaller events are more frequent and can occur anywhere, although their strong ground-motion effects will be less widespread. A person or structure located at a specified site in southern California is exposed to this spectrum of potential events.

It is the objective of probabilistic seismic hazard analysis (PSHA) to capture all contributions to a site's hazard, and to report various measures of the seismic hazard there. The results are presented in terms of the probability of the site's experiencing a ground motion of a specified level or larger in a specified future time window. We chose a 30-yr time window to illustrate the effects of the master model on PSHA in southern California. As one measure of the intensity of the ground

motion, we use the peak ground acceleration (PGA) at a level of 20%  $g$  (20% of gravity) and greater.

#### The Probabilistic Seismic Hazard Analysis Method

The PSHA computational method is conceptually simple. In essence, it sums the contributions to the site hazard (probability) from each square kilometer of the region around the site and for each magnitude level or, more precisely, each magnitude interval (e.g., 6.45 to 6.55). For example, the contribution at a particular site to the 30-yr probability from  $m = 6.5$  earthquakes in a particular square kilometer a distance  $R$  km away can be approximated by

$$\lambda_m \cdot 30 \cdot P[\text{PGA} > 0.2 | m = 6.5 \text{ and distance} = R].$$

The parameter  $\lambda_m$  is the mean annual rate per unit area of magnitude  $m$  events (here  $m = 6.5$ ). The values of  $\lambda_m$  are obtained from the seismicity information provided in later sections. The probability  $P[\text{PGA} > 0.2 | m = 6.5 \text{ and distance} = R]$ , which is read as "the probability that the PGA exceeds 0.2  $g$  given a magnitude 6.5 event at a distance of  $R$  km," is obtained from empirical and theoretical studies that predict how the ground-motion intensity decays with distance and how it increases with magnitude, coupled with empirical studies of the statistical variability of real observations about these predictions. This variability is quite large; it is not uncommon to observe ground-motion intensities more than twice as large or less than half as large as the predicted values.

Modifications to this procedure are necessary for large characteristic events on major fault segments (or cascading multiple segments). In effect, each such rupture is concentrated at the point on the fault closest to the site. In addition, if the non-Poissonian recurrence model is adopted, the product  $\lambda_{6.5} \cdot 30$  must be replaced by the 30-yr probability values in Table 2.

Finally, the simple summing of these hazard contributions is a valid approximation only when the final hazard is small (less than 10%). A better approximation for our analysis is

$$1 - \exp(-r \cdot T),$$

where  $r$  is the sum of the hazard rates (probabilities per year) and  $T$  is the time interval (30 yr in our example). The analysis procedure is easily automated, and many computer programs are available for these calculations. The specific procedure used in this report is described in Appendix E. The process can be repeated for different ground-motion levels, e.g., 0.1  $g$ , 0.2  $g$ , etc., leading to a decreasing plot of hazard versus increasing ground motion, or a "seismic hazard curve." Furthermore, the process can be repeated for a fine grid of sites to produce a site hazard map. PSHA can be applied to many dif-

ferent measures of ground-motion intensity depending on the application. Examples will follow.

The final product will be a probability that reflects all the uncertainties involved—namely, how many earthquakes will occur, how large they will be, where they will be, and to what degree the ground motions at the site will deviate from the predicted values. As we shall see below, the result can be readily dissected to display contributions to the site hazard from different hazard sources.

#### Specific Input to the Analysis

The input data are the predicted seismicity rates,  $b$  values, and limiting magnitudes for the 65 zones (Table 5) and the 30-yr probabilities for the specified characteristic earthquakes and cascades on the major faults (calculated from the annual rate given in Table 3). Recall that two alternative representations of these seismic recurrence models are presented. We focus on the preferred model in which the distributed seismicity is given by Table 5 and the characteristic earthquake probabilities are given by Table 3.

The site hazard calculations are based on empirical ground-motion prediction models by Geomatrix Consultants (1991) and Sadigh *et al.* (1986). They predict the peak ground acceleration at a site on “rock” or “soil” (engineering terms) at a specified distance from an earthquake of given magnitude. The local conditions may affect the level of ground motion; the two broad site classifications, rock and soil, each cover a spectrum of local geological conditions. The models also provide a probability distribution describing the variability of observations about these predictions; these variations are centered on the predicted value (i.e., the model is unbiased) and have a degree of variability measured by a standard deviation. The standard deviation of the natural logarithm of the PGA ranges between 0.69 and 0.38 from smaller to larger magnitudes for the rock site model. These models are currently in use and are selected as representative.

#### Seismic Hazard Curves for Downtown Los Angeles and San Bernardino

Seismic hazard curves for the Los Angeles City Hall site are shown in Figure 16. The upper dashed line is a plot of the 30-yr hazard versus peak ground acceleration, assuming a rock site. Note that at a level of 0.2  $g$  the 30-yr probability is about 30%. At acceleration levels potentially damaging to small modern buildings, the probability is less than a few percent. The lower dashed curve shows the fraction of PGA hazard contributed by the San Andreas and the San Jacinto alone. Their contribution is as much as one-third of the total probability for frequent low-level ground motions, but less than 10% for ground motions above 0.2  $g$ . Faults closer to Los Angeles City Hall, although less dramatic in many ways

and not capable of earthquakes as large as on the San Andreas and San Jacinto, are more likely to cause potentially damaging ground motions in the city. These conclusions are unchanged for soil sites.

The situation changes mildly for longer period motions which cause more damage to flexible multi-story buildings. Also, soil sites tend to enhance the effects of these motions. The solid curves in Figure 16 show the hazard associated with the 1-sec period “spectral acceleration” for a soil site. The San Andreas and San Jacinto contribute more to the 1-sec spectral acceleration than to the PGA at all levels; although they are farther away, they are likely sources of the large earthquakes that generate longer period seismic waves. Even so, the local sources dominate the 1-sec hazard for higher accelerations.

Figure 17 shows the 1-sec spectral acceleration hazard for the San Bernardino City Hall site, again presuming a soil site. The 30-yr hazard for ground motions greater than about 0.2  $g$  is several times larger here than in Los Angeles. The threat at virtually all levels is from the large fault systems, which pass near the city.

#### An Illustrative Seismic Hazard Map of Southern California

We have generated seismic hazard curves like those in Figures 16 and 17 for many sites across southern California, and the results for the 0.2  $g$  PGA (rock site) ground motion at each site are plotted and contoured in Figure 18. As seen in Figure 16, the probability that the peak ground acceleration exceeds 20% of gravity in the next 30 yr is about 30% at Los Angeles City Hall. Although the probability is significant throughout southern California, it exceeds 80% only in the Parkfield area (Fig. 18). The probability exceeds 60% in the Ventura and San Bernardino areas. A high-probability zone includes much of the Transverse Ranges fold and thrust belt between Santa Barbara and San Bernardino. The master model we are developing can produce a map like Figure 18 for any ground-motion parameter that may be useful.

The foregoing patterns of high seismic hazard change when we choose different mapping parameters. For example, when we contoured the 0.3-sec spectral acceleration for the 10% probability of exceedance in 50 yr, the high accelerations were concentrated along the San Andreas, San Jacinto, and Elsinore faults, rather than the east–west-trending zone between Santa Barbara and San Bernardino.

#### Conclusions and Future Needs

We reviewed the methods used by WGCEP (1988) for estimating the conditional probability of rupture for a fault segment, and we found it appropriate to revise the standard deviation of the logarithm of recurrence interval—a fundamental parameter. This parameter is

composed of two terms—one describes the intrinsic variability of earthquake recurrence and the other accounts for uncertainties in the input data. The intrinsic part is due to the erratic behavior of the dynamic process of earthquake rupture and unknown interactions from nearby faults. Based on new, high-quality paleoseismic data and advances in computer modeling of fault interactions, we now believe that earthquake recurrence is intrinsically more variable than was assumed in 1988. Increasing the variability reduces the periodicity. Consequently, we revised downward the conditional probabilities for some segments that have not ruptured recently. The largest reductions, still within the estimated errors, are for the Coachella Valley and Anza segments of the San Andreas and San Jacinto faults, respectively.

In addition to the time-predictable model used by WGCEP (1988), we considered a renewal model that does not assume a strong correlation between the previous displacement and time until the next earthquake. Furthermore, when we knew the dates of enough past earthquakes, we estimated statistical parameters directly from them. The 30-yr probabilities listed in Table 2 represent a weighted average of the three estimates (with weight proportional to the reciprocal of variance; i.e., assuming equal prior likelihood for each estimate).

The revised probability estimates are similar to those given in 1988, with a few exceptions. For the reasons mentioned above, the 30-yr probability is reduced from 0.4 to 0.22 for the Coachella Valley segment of the San Andreas, and from 0.3 to 0.17 for the Anza segment of the San Jacinto. On the other hand, the probability is increased from 0.1 to 0.43 for the San Jacinto Valley segment of the San Jacinto, partly due to the revision of the mean recurrence time to nearly half the 1988 estimate. For these revisions we followed the basic assumption of WGCEP (1988) regarding the existence of earthquakes characteristic to given fault segments. This assumption has been questioned by investigators who have found evidence for ruptures occurring over various combinations of contiguous segments. To allow for failure over multiple segments, we develop a “cascade” model in which the amount of slip is assumed to be characteristic to a given segment, but all earthquakes that can occur by combining contiguous segments are allowed. The model minimizes the total earthquake rate, subject to the geologically constrained rupture probability on each segment. This criterion brings the predicted annual rate for  $m \geq 7$  earthquakes into better agreement with the historical record since 1850.

At present, the above method of estimating probabilities of fault failure can be applied only to the San Andreas, San Jacinto, Whittier, and Elsinore faults due to the lack of data on other faults, including those responsible for the 1933 Long Beach, 1971 San Fernando, and 1994 Northridge earthquakes. To supplement the geologic data, we used the catalog of past earthquakes

and crustal deformation (geodetic) data from GPS networks in southern California. To combine the geologic, earthquake catalog, and geodetic data, we introduce seismotectonic source zones for earthquake source characterization. In the present report, we adopted 65 source zones as shown in Figure 6. Of the 65 zones, 41 are named after the fault they contain. Segments of the San Andreas, San Jacinto, and Elsinore, faults constitute 16 zones. We distinguish three types of source zones: type A zones each contain one major fault segment, with enough data for conditional probability analysis; type B zones contain well-known active faults for which segmentation and recurrence data are incomplete; and type C zones are not dominated by any single major fault, but may contain diverse and/or hidden faults. Our general strategy is to combine the contributions from faults with sufficient paleoseismic data and those from earthquake catalog data in such a way that the total displacement across southern California is consistent with the relative motion between the Pacific and North American plates. We also assumed that all the accumulated strain in the 11-km-thick brittle zone estimated from geodesy will be released by earthquakes.

Before integrating the three different data sets to produce a seismic hazard map, we compared what each data set is telling us about seismic sources in southern California. Crustal strain estimated from geology and that from earthquake catalog data show some markedly different patterns. The geology data show concentrated strain along the San Andreas and San Jacinto faults. The earthquake catalog data show significant strain release away from these major faults. The geodetic data show strain diffused outside the San Andreas fault zone (Fig. 8) as compared to the pattern expected from a simplified geologic fault model.

The sum of the predicted rupture rates on all characteristic fault segments exceeds 0.1 per year, which is greater than the rate of 0.03 to 0.04 per year for  $m \geq 7$  earthquakes in the catalog. By allowing for segment interactions using the cascade model (Table 3), the predicted rate of all characteristic earthquakes on those segments is reduced to about 0.071 per year as shown in Table 3 and Figure 14. Including characteristic and distributed earthquakes in all zones, and allowing for interactions with the cascade model, our preferred model predicts  $m \geq 7$  earthquakes should occur at a rate of 0.067 per year (Fig. 14), corresponding to a 30-yr probability of 86%. Note that the predicted rate of characteristic earthquakes exceeds that of  $m \geq 7$  events, because many of the characteristic magnitudes are less than 7. The predicted rate for  $m \geq 7$  exceeds the catalog rate mentioned above. The predicted rate can be further reduced if the values adopted for the maximum magnitude of distributed earthquakes are increased. Figure 15 shows the case where we adopted a maximum magnitude of either 7.0 or 0.5 magnitude unit above the geologically

estimated value, whichever is greater. Using the alternate model, the predicted rate for  $m \geq 7$  earthquakes is about 0.064 per year, corresponding to a 30-yr probability of 85%. The values for the preferred and alternate models are very similar at  $m \geq 7$ . This is a coincidence, as the uncertainties in the predictions are of the order of 15 to 20%.

We interpret the difference between predicted and observed rates of  $m \geq 7$  earthquakes to mean that earthquakes of this size have been less frequent over the last 150 yr than would have been expected based on observed fault lengths, slip rates, and accumulating strain. On the other hand, great earthquakes like the 1857 event should occur only about two or three times per millennium, and recurrence of such an event in the next 30 yr is relatively unlikely (6 to 9%). Thus, it appears that earthquake activity at  $m \geq 7$  has been anomalously low since 1850, although we had one great earthquake. Another great earthquake in the next few decades would help make up this apparent deficit in  $m \geq 7$  events.

The above calculated rates of 0.064 to 0.067 per year for  $m \geq 7$  earthquakes in southern California, however, are lower than the upper-bound estimate of 0.12 per year made in the first report (Phase I, WGCEP, 1992) in this series. Thus, the upper-bound estimate made on the basis of a recently increased level of seismicity is not considered to apply over the long term. The observed and calculated rates for southern California may be put into perspective by comparing them with the corresponding rates for the San Francisco Bay Region. According to the 1990 Working Group, the calculated 30-yr probability for an  $m \geq 7$  earthquake anywhere in the Bay Region is estimated as 67%, which corresponds to an annual Poissonian rate of 0.037 per year. This calculated rate is about 1.6 times the rate of 0.023 per year estimated from the catalog of earthquakes since 1836. Since the length of the plate boundary for southern California (about 500 km) is 2.5 times longer than that for the Bay Region (about 200 km) studied by the 1990 Working Group, the extrapolation of the 1990 Working Group's results to the same area as southern California would give 0.093 and 0.058 for the calculated and observed annual rates, respectively. This comparison shows that our predicted annual rate is consistent with that predicted for the Bay Region.

The predicted rate of 0.064 to 0.067 per year corresponds to a probability of 85 to 86% for the occurrence of a large  $m \geq 7$  earthquake in the next 30 yr somewhere in southern California. The probability of strong shaking at a given location, however, is not so high and varies from place to place. For illustration, we adopted a peak ground acceleration exceeding 0.2  $g$  as a criterion for strong shaking. Figure 18 shows the probability of experiencing a ground acceleration of 0.2  $g$  or higher in the next 30 yr for southern California. Although significant throughout southern California, the probability ex-

ceeds 80% only in the Parkfield area. The probability exceeds 60% in the Ventura and San Bernardino area, and a high probability zone (50 to 60%) coincides with the Transverse Ranges fold and thrust belt, which includes the epicentral region of the Northridge earthquake.

The model parameters in Tables 2, 3, and 5 represent the first generation master model for earthquake potential in southern California. The Northridge earthquake of 17 January 1994 was no surprise from the perspective of this model. The earthquake occurred in zone 54, a type B zone characterized by relatively high earthquake potential, falling in the top 13% of southern California in terms of moment rate per unit area. While the specific fault had not been known prior to the event, the location, magnitude, and style of the earthquake are consistent with our understanding of the regional geology and tectonics.

Additional research is needed in several areas to make seismic hazard estimation more reliable, precise, and pertinent to the user.

- We need to consider ground-motion parameters in addition to the peak ground acceleration when generating seismic hazard maps. In this report, we used peak ground acceleration as an illustration because of its relative insensitivity to local geologic site conditions. Our next target should be developing a similar characterization and consensus on local site effects, which is the prerequisite for considering other useful ground-motion parameters like response spectra at various frequencies. This research requires close cooperation between seismologists and geotechnical engineers.
- Seismic hazard estimates depend on the upper magnitude limit adopted for each seismotectonic source zone. We used the widely practiced method of relating earthquake size to the length of an independent fault segment, but the recent Landers earthquake demonstrated that several fault segments can break in a single earthquake rupture. We need to understand better the relationship between fault geometry and earthquake size, and more generally what limits the size of large earthquakes. This research must be multi-disciplinary, involving geologists, seismologists, geodesists, and rock mechanists.
- Despite progress in studying hidden faults (blind thrusts) in southern California, we still lack sufficient information to treat individual segments explicitly. We need to better understand the processes that control the magnitude distribution. We need to know if strain accumulating across basins containing one or more blind thrusts is being stored as elastic strain or is released aseismically. We also need a better understanding of the more shallow-dipping thrust ramps and detachment surfaces posited to exist beneath large parts of southern California—their relationship to the more steeply dipping, upper plate thrusts and strike-slip faults, and their

seismic potential. This research will also require cooperation among geologists, seismologists, geodesists, and rock mechanists.

- Geodetic and seismic data are potentially very important in assessing regional seismic hazard. We pushed the existing geodetic data base to the limits of its resolution, especially in the type C zones, where its influence is strong in assessing the hazard. We need wider geodetic coverage at increased resolution, especially away from the San Andreas fault. We also need a better understanding of the relationship between geodetic strain, active faults, and historical seismicity. This research must also be multi-disciplinary involving geologists, seismologists, geodesists, and hazard analysts.

### Acknowledgments

Activities of the Southern California Earthquake Center which led to this report are supported by National Science Foundation Cooperative Agreement EAR-8920136 and United States Geological Survey Cooperative Agreement 14-08-0001-A0899. Workshops addressing issues in this report were also supported by the California Department of Transportation, the County of Los Angeles, and the City of Los Angeles. This is SCEC Contribution Number 128.

### References

- Astiz, I. and C. R. Allen (1983). Seismicity of the Garlock fault, California, *Bull. Seism. Soc. Am.* **73**, 1721–1735.
- Bergmann, M., T. K. Rockwell, D. K. Miles, C. K. Hirabayashi, M. A. Hushebeck, C. C. Haraden, A. Thomas, and A. Patterson (1993). Preliminary assessment of the late Holocene slip rate for the Wildomar fault, Murrieta, California, Final technical report, *U.S. Geol. Surv. External Res. Prog. 14-08001-G2062*, 12.
- Biasi, G. P. and R. Weldon II (1994a). Quantitative refinement of calibrated <sup>14</sup>C distributions, *Quaternary Res.* **41**, No. 1, 1–18.
- Biasi, G. P. and R. Weldon II (1994b). Conditional probability of large earthquakes on the southern San Andreas fault from Paleoseismological evidence (submitted for publication).
- Bonilla, M. G. (1973). Trench exposures across surface fault ruptures associated with the San Fernando earthquake, in *The San Fernando, California Earthquake of February 9, 1971*, *U.S. Geol. Surv. Profess. Pap.* **773**, 173–182.
- Bowie, W. (1973). Comparison of old and new triangulation data in California, *U. S. Coast and Geod. Surv. Spec. Pub.* **151**, 1928, reprinted in reports on geodetic measurement of crustal movements, 1906–1971, National Geodetic Survey, Rockville, Maryland.
- Clarke, S. H., H. G. Greene, M. E. Field, and W. H. K. Lee (1983). Reconnaissance geology and geologic hazards of selected areas of the southern California borderland, *U.S. Geol. Surv. Open-File, Rept.* **78**, 62–83.
- Clarke, S. H., H. G. Greene, and M. P. Kennedy (1985). Identifying potentially active faults and unstable slopes offshore, in *Evaluating Earthquake Hazards in the Los Angeles Region: An Earth Science Perspective*, J. E. Ziony (Editor), *U.S. Geol. Surv. Profess. Pap.* **1360**, 347–375.
- Cornell, C. A. (1968). Engineering seismic risk analysis, *Bull. Seism. Soc. Am.* **58**, 1583–1606.
- Crook, R. Jr., C. R. Allen, B. Kamb, C. M. Payne, and R. J. Proctor (1987). Quaternary geology and seismic hazard of the Sierra Madre and associated faults, western San Gabriel Mountains, in *Recent Reverse Faulting in the Transverse Ranges, California, U.S. Geol. Surv. Profess. Pap.* **1339**, 27–64.
- Davis, P. M., D. D. Jackson, and Y. Y. Kagan (1989). The longer it has been since the last earthquake, the longer the expected time till the next? *Bull. Seism. Soc. Am.* **79**, 1439–1456.
- Davis, T. L. and J. S. Namson (1994). A balanced cross section analysis of the 1994 Northridge earthquake and thrust fault seismic hazards in southern California, *Nature* **372**, 167–169.
- Davis, T. L., J. Namson, and R. F. Yerkes (1989). A cross-section of the Los Angeles area: seismically active fold and thrust belt, the 1987 Whittier Narrows earthquake, and earthquake hazard, *J. Geophys. Res.* **94**, 9644–9664.
- Der Kiureghian and A. H. S. Ang (1975). A line source model for seismic hazard risk analysis, Technical Report UILU-ENG-75–2023, University of Illinois, Urbana, Illinois.
- Dolan, J. F., K. Sieh, T. K. Rockwell, R. S. Yeats, J. Shaw, J. Suppe, G. J. Huftile, and E. M. Gath (1994). Prospect for larger or more frequent earthquakes in the Los Angeles Metropolitan Region, California, *Science* **267**, 199–205.
- Dziewonski, A. M., G. Ekstrom, and M. P. Salganik (1993). Centroid-moment tensor solutions for January–March, 1992, *Phys. Earth Planet. Interiors* **77**, 143–150.
- Ellsworth, W. L. (1990). Earthquake history, 1769–1989, in *The San Andreas Fault System, California*, R. E. Wallace (Editor), *U.S. Geol. Surv. Profess. Pap.* **1515**.
- Feigl, K., D. Agnew, Y. Bock, D. Dong, A. Donnellan, B. Hager, T. Herring, D. Jackson, T. Jordan, R. King, S. Larsen, K. Larson, M. Murray, Z. Shen, and F. Webb (1993). Space geodetic measurement of crustal deformation in central and southern California, 1984–1992, *J. Geophys. Res.* **98**, 21677–21712.
- Fumal, T. E., S. K. Pezzopane, R. J. Weldon II, and D. P. Schwartz (1993). A 100-year average recurrence interval for the San Andreas fault at Wrightwood, California, *Science* **259** no. 5092, 199–203.
- Gath, E. M., T. Gonzalez, and T. K. Rockwell (1992). Evaluation of the late Quaternary rate of slip, Whittier fault, southern California, *U.S. Geol. Surv. Final Tech. Rept. NEHRP*, **24**.
- Geomatrix Consultants (1991). Seismic ground motion study for west San Francisco Bay Bridge, report to Caltrans, Division of Structures, Sacramento, California.
- Grant, L. B. and A. Donnellan (1994). 1855 and 1991 Surveys of the San Andreas fault: implications for fault mechanics, *Bull. Seism. Soc. Am.* **84**, 241–246.
- Grant, L. B. and K. Sieh (1993). Stratigraphic evidence for seven meters of dextral slip on the San Andreas fault during the 1857 earthquake in the Carrizo Plain, *Bull. Seism. Soc. Am.* **83**, no. 3, 619–635.
- Grant, L. B. and K. Sieh (1994). Paleoseismic evidence of clustered earthquakes on the San Andreas fault in Carrizo Plain, California, *J. Geophys. Res.* **99**, no. B4, 6819–6841.
- Gurrola, L. and T. Rockwell (1994). Paleoseismology of the Superstition Mountain fault, Imperial Valley, California. (Abstracts with programs), *Geol. Soc. Am.* **26**, 55–56.
- Hall, N. T., T. D. Hunt, and P. R. Vaughan (1994). Holocene behavior of the San Simeon fault zone, south-central coastal California, Geological Society of America Special Paper 292, 167–190.
- Hanson, K. L., J. R. Wesling, W. R. Lettis, K. I. Kelson, and L. Mezger (1994). Correlation, ages, and uplift rates of Quaternary marine terraces: south-central coastal California, Geological Society of America Special Paper 292, 45–72.
- Hauksson, E. and L. M. Jones (1989). The 1987 Whittier Narrows earthquake sequence in Los Angeles, southern California: seismological and tectonic analysis, *J. Geophys. Res.* **94**, 9569–9589.
- Hauksson, E. (1994). State of stress from focal mechanisms before and after the 1992 Landers earthquake sequence, *Bull. Seism. Soc. Am.* **84**, 917–934.

- Hauksson, E., L. M. Jones, and K. Hutton (1994). The 1994 Northridge earthquake sequence in California: seismological and tectonic aspects, *J. Geophys. Res.* (submitted for publication).
- Hudnut, K. W., M. H. Murray, A. Donnellan, Y. Bock, P. Fang, M. Cline, Y. Feng, Z. Shen, B. Hager, T. Herring, and R. King (1994). Coseismic displacements of the 1994 Northridge, California, earthquake (abstract), Seismological Society of America, Program for Northridge Abstracts, Pasadena, California.
- Hudnut, K. W. and K. E. Sieh (1989). Behavior of the Superstition Hills fault during the past 330 years, *Bull. Seism. Soc. Am.* **79**, 304–329.
- Huftile, G. J. (1992). Convergence rates across the Ventura Basin, California, *Ph.D. Thesis*, Oregon State University, Corvallis, Oregon.
- Hutton, L. K. and L. M. Jones (1993). Local magnitudes and apparent variations in seismicity rates in southern California, *Bull. Seism. Soc. Am.* **83**, 313–329.
- Kagan, Y. Y. (1993). Statistics of characteristic earthquakes, *Bull. Seism. Soc. Am.* **83**, 7–24.
- Kagan, Y. Y. and D. D. Jackson (1994). Long term probabilistic forecasting of earthquakes, *J. Geophys. Res.* **99**, 13685–13700.
- Klinger, R. E. and T. K. Rockwell (1989). Recurrent late Holocene faulting at Hog Lake in the Anza seismic gap, San Jacinto fault zone, southern California (abstracts with programs), *Geological Society of America, Cordilleran Section, 85th Annual Meeting of the Rocky Mountain Section*, Vol. 42, 102.
- Kostrov, B. V. (1974). Seismic moment and energy of earthquakes, and seismic flow of rock, *Izv. Acad. Sci. USSR. Phys. Solid Earth*, **1**, 23–40.
- Levi, S. and R. S. Yeats (1993). Paleomagnetic constraints on the initiation of uplift on the Santa Susana fault, Western Transverse Ranges, California, *Tectonics* **12**, 688–702.
- Lienkaemper, J. J. and W. H. Prescott (1989). Historic surface slip along the San Andreas fault near Parkfield, California, *J. Geophys. Res.* **94**, 17647–17670.
- Lisowski, M., J. C. Savage, and W. H. Prescott (1991). The velocity field along the San Andreas fault in central and southern California, *J. Geophys. Res.* **96**, 8369–8389.
- McGill, S. F. (1992). Paleoseismology and neotectonics of the central and eastern Garlock fault, *Ph.D. Thesis*, California Institute of Technology, Pasadena.
- McGill, S. F. (1994). Maximum age of the most recent earthquake on the Garlock fault in Searles Valley, California, *Bull. Seism. Soc. Am.* (in revision).
- McGill, S. F. and K. E. Sieh (1991). Surficial offsets on the central and eastern Garlock fault associated with prehistoric earthquakes, *J. Geophys. Res.* **96**, 21597–21621.
- McGill, S. F. and K. Sieh (1993). Holocene slip rate of the central Garlock fault in southeastern Searles Valley, California, *J. Geophys. Res.* **98**, 14217–14231.
- Millman, D. E. and T. K. Rockwell (1986). Neotectonics of the Elsinore fault in Temescal Valley, California, in *Guidebook and Volume, 82nd Annual Meeting of the Cordilleran Section of the Geological Society of America*, 159–166.
- Morton, D. M. and J. C. Matti (1987). The Cucamonga fault zone: geological setting and Quaternary history, *U.S. Geol. Surv. Profess. Pap.* **1339**, 179–203.
- Nishenko, S. P. and R. Buland (1987). A generic recurrence interval distribution for earthquake forecasting, *Bull. Seism. Soc. Am.* **77**, 1382–1399.
- Pacific Gas and Electric Company (1988). Final report of the Diablo Canyon Long Term Seismic Program, report to U.S. Nuclear Regulatory Commission.
- Patterson, A. C. and T. K. Rockwell (1993). Paleoseismology of the Whittier fault based on 3-dimensional trenching at Olinda Oil Field, Orange County, southern California (abstracts with programs), *Geol. Soc. Am.* **25**, no. 5, 131.
- Pinault, C. T. and T. K. Rockwell (1984). Rates and sense of Holocene faulting on the southern Elsinore fault: further constraints on the distribution of dextral shear between the Pacific and North American Plates (abstracts with programs), *Geol. Soc. Am.* **16**, 624.
- Reid, H. F. (1910). The mechanics of the earthquake, the California earthquake of April 18, 1906, report of the State Investigation Commission, Vol. 2, Carnegie Institution of Washington, Washington, D.C.
- Rockwell, T. (1988). Neotectonics of the San Cayetano fault, Transverse Ranges, California, *Geol. Soc. Am. Bull.* **100**, 500–513.
- Rockwell, T. K., E. M. Gath, and T. Gonzalez (1992). Sense and rate of slip on the Whittier fault zone, eastern Los Angeles basin, California, in *Proc. of the 35th Annual Meeting Association of Engineering Geologists October 2–9, 1992*, M. L. Stout (Editor), 679.
- Rockwell, T. K., M. E. Hatch, and D. L. Schug (1987). Late Quaternary rates of Agua Blanca and Borderland faults, *U.S. Geol. Surv. Final Tech. Rept.* **14-08-0001-22012**, 65, 2 plates.
- Rockwell, T. K., R. Klinger, and J. Goodmacher (1990). Determination of slip rates and dating of earthquakes for the San Jacinto and Elsinore fault zones, in *Geology around the Margins of the Eastern San Bernardino Mountains*, M. A. Kooser and R. E. Reynolds (Editors), Vol. 1, Inland Geological Society, Redlands, 51–56.
- Rockwell, T. K., R. S. McElwain, D. E. Millman, and D. L. Lamar (1986). Recurrent late Holocene faulting on the Glen Ivy North Strand of the Elsinore fault at Glen Ivy Marsh, in *Guidebook and Volume on Neotectonics and Faulting in Southern California, Cordilleran Section, Geological Society of America*, 167–1275.
- Rockwell, T. K. and A. P. Thomas (1994). Slip on the Imperial fault in the past 300 years at the U.S.–Mexico international border based on trenching, *J. Geophys. Res.* (submitted for publication).
- Sadigh, K., J. Egan, and R. Youngs. (1986). Specification of ground motion for design of long period structures (abstract), *Earthquake Notes* **57**, 13.
- Salyards, S. L., K. E. Sieh, and J. L. Kirschvink (1992). Paleomagnetic measurement of nonbrittle coseismic deformation across the San Andreas fault at Palmett Creek, *J. Geophys. Res.* **97**, no. B9, 12457–12470.
- Savage, J. C. (1991). Criticism of some forecasts of the National Earthquake Prediction Evaluation Council, *Bull. Seis. Soc. Am.* **81**, 862–881.
- Savage, J. C. (1992). The uncertainty in earthquake conditional probabilities, *Geophys. Res. Lett.* **19**, 709–712.
- Savage, J. C., W. H. Prescott, J. F. Chamberlain, M. Lisowski, C. and E. Mortensen (1979). Geodetic tilt measurements along the San Andreas fault in central California, *Bull. Seism. Soc. Am.* **69**, 1965–1981.
- Scholz, C. H. (1982). Scaling laws for large earthquakes: consequences for physical models, *Bull. Seism. Soc. Am.* **71**, 1–14.
- Seitz, G. J. and R. J. Weldon II (1994a). The paleoseismology and fault scarp morphology of the San Andreas Fault at Pitman Canyon, San Bernardino, California (abstracts with programs), *Geol. Soc. Am.* **26**, 90.
- Seitz, G. J. and R. J. Weldon II (1994b). The paleoseismology of the southern San Andreas fault at Pitman Canyon, San Bernardino, California, in *Guidebook, Annual Meeting of the Cordilleran Section of the Geological Society of American*, Vol. 27, 152–156.
- Sharp, R. V. (1981). Variable Rates of late Quaternary strike slip on the San Jacinto fault zone, southern California, *J. Geophys. Res.* **86**, 1754–1762.
- Shaw, J. H. (1993). Active blind-thrust faulting and strike-slip folding

- in California, *Ph.D. Thesis*, Princeton University, Princeton, New Jersey, 216 pp.
- Shaw, J. H. and J. Suppe (1994a). Active faulting and growth faulting in the eastern Santa Barbara Channel, California, *Geol. Soc. Am. Bull.* **78**, 700–721.
- Shaw, J. H. and J. Suppe (1994b). Earthquake hazards of active blind-thrust faults under the central Los Angeles basin, California, *J. Geophys. Res.* (submitted for publication).
- Shen, Z. K., D. D. Jackson, and X. Ge (1995). Crustal deformation across and beyond the Los Angeles basin from geodetic observations, *J. Geophys. Res.* (submitted for publication).
- Shimazaki, K., and T. Nakata (1980). Time-predictable recurrence model for large earthquakes, *Geophys. Res. Lett.* **7**, 279–282.
- Sieh, K. E. (1978). Slip along the San Andreas fault associated with the great 1857 earthquake, *J. Geophys. Res.* **68**, 1421–1448.
- Sieh, K. (1986). Slip rate across the San Andreas fault and prehistoric earthquakes at Indio, California, *EOS* **67**, 1200.
- Sieh, K. E. and R. H. Jahns (1984). Holocene activity of the San Andreas fault at Wallace Creek, California, *Geol. Soc. Am. Bull.* **95**, 883–896.
- Sieh, K., L. Jones, E. Hauksson, K. Hudnut, *et al.* (1993). Near-field investigations of the Landers earthquake sequence, April to July, 1992, *Science* **260**, 171–176.
- Sieh, K., M. Stuiver, and D. Brillinger (1989). A more precise chronology of earthquakes produced by the San Andreas fault in southern California, *J. Geophys. Res.* **94**, 603–623.
- Sims, J. D., J. C. Hamilton, and J. R. Arrowsmith (1993). Geomorphic study of earthquake offsets and subsequent landform response along the San Andreas Fault, Carrizo Plain, California, (supplement), *EOS* **74**, no. 43, 612.
- Stein, R. S. and R. S. Yeats (1989). Hidden earthquakes, *Science* **260**, 48–57.
- Stephenson, W. J., T. Rockwell, J. Odum, K. M. Shedlock, and D. Okaya (1994). Seismic-reflection and geomorphic characterization of the onshore Palos Verdes fault zone, Los Angeles, California, *Bull. Seism. Soc. Am.* (submitted for publication).
- Suppe, J. (1983). Geometry and kinematics of fault-bend folding, *Am. J. Sci.* **283**, 648–721.
- Suppe, J., G. T. Chou, and S. C. Hook (1992). Rates of folding and faulting determined from growth strata, in *Thrust Tectonics*, K. R. McKlay (Editor), Unwin Hyman, 105–121.
- Thatcher, W. (1979). Crustal movements and earthquake-related deformation, *Rev. Geophys. Space Phys.* **17**, 1403–1411.
- USGS Staff (1994a). Ground deformation in Granada Hills from the January 17, 1994 Northridge earthquake (abstract), Seismological Society of America, Program for Northridge Abstracts, Pasadena, California.
- USGS Staff (1994b). Ground deformation in Potrero Canyon from the January 17, 1994 Northridge earthquake (abstract), Seismological Society of America, Program for Northridge Abstracts, Pasadena, California.
- Vaughan, P. and T. K. Rockwell (1986). Alluvial stratigraphy and neotectonics of the Elsinore fault zone at Agua Tibia Mountain, southern California, in *Guidebook and Volume, 82nd Annual Meeting of the Cordilleran Section of the Geological Society of America*, Vol. 82, 177–191.
- Wald, D. J. and T. H. Heaton (1994). A multidisciplinary source analysis of the 1994 ( $M_w$  6.7) Northridge earthquake using strong ground motion, teleseismic, and geodetic data (abstract), Seismological Society of America, Program for Northridge Abstracts, Pasadena, California.
- Ward, S. N. (1994). A multidisciplinary approach to seismic hazard in southern California, *Bull. Seism. Soc. Am.* **84**, 1293–1309.
- Ward, S. and G. Valensise (1994). The Palos Verdes Terraces: bathtub rings from a buried thrust fault, *Geophys. Res.* **99**, 4485–4495.
- Weldon, R. J. II (1991). Active tectonic studies in the United States, 1987–1990, *Rev. Geophys.* **29**, 890–906.
- Weldon, R. J. and K. E. Sieh (1985). Holocene rate of slip and tentative recurrence interval for large earthquakes on the San Andreas Fault, Cajon Pass, southern California, *Geol. Soc. Am. Bull.* **96**, 793–812.
- Wells, D. L. and K. J. Coppersmith (1994). New empirical relationships among magnitude, rupture length, rupture width, rupture area, and surface displacement, *Bull. Seism. Soc. Am.* **84**, 974–1002.
- Wesnousky, S. G. (1986). Earthquakes, Quaternary faults and seismic hazard in California, *J. Geophys. Res.* **91**, 12587–12632.
- Working Group on California Earthquake Probabilities (1988). Probabilities of large earthquakes occurring in California on the San Andreas fault, *U.S. Geol. Surv. Open-File Rept.* 88–398.
- Working Group on California Earthquake Probabilities (1990). Probabilities of large earthquakes in the San Francisco Bay region, California, *U.S. Geol. Surv. Circ.* 1053.
- Working Group on California Earthquake Probabilities (1992). Future seismic hazards in southern California, Phase I: implications of the 1992 Landers Earthquake Sequence, *Calif. Div. Mines Geol. Spec. Pub.* 42 pp.
- Yeats, R. S. (1987). Late Cenozoic structure of the Santa Susana fault zone, *U.S. Geol. Surv. Profess. Pap.* 1339, 137–160.
- Yeats, R. S. (1988). Late Quaternary slip rate on the Oak Ridge fault, Transverse Ranges, California; implications for seismic risk, *J. Geophys. Res.* **93**, 12137–12149.
- Yeats, R. S. (1994). Oak Ridge fault system and the 1994 Northridge earthquake, *Nature* (in press).
- Yeats, R. S., G. J. Huftile, C. Hummon, C. Schneider, and H. Tsutsumi (1993). Northern Los Angeles fold-thrust belt, SCEC Annual Report, C28.
- Yeats, R. S., G. J. Huftile, and L. T. Stitt (1994). Late Cenozoic tectonics of the East Ventura Basin, Transverse Ranges, California, *Am. Assoc. Petroleum Geologists Bull.* **78**, no. 7, 1040–1074.

## Appendix A: Recurrence Models and Tabulations of Probabilities

The probability model assumes a lognormal probability density function of earthquake recurrence times  $T$  with mean  $\mu$ , median  $\hat{\mu}$ , and intrinsic (or aleatory) variability  $\sigma_{\ln T}$ , (strictly the standard deviation of the natural logarithm of the random recurrence interval  $T$ ) with probability density function  $f_T(t)$ :

$$f_T(t) = \frac{1}{t\sigma_{\ln T} \sqrt{2\pi}} \exp\left\{-\frac{[\ln(t/\hat{\mu})]^2}{2\sigma_{\ln T}^2}\right\}. \quad (\text{A1})$$

For the lognormal distribution

$$\mu = \hat{\mu} \exp(\sigma^2/2). \quad (\text{A2})$$

If  $\hat{\mu}$  (or equivalently  $\mu$ ) and  $\sigma_{\ln T}$  are precisely known, the conditional probability of recurrence in some time interval ( $t_e, t_e + \Delta T$ ) given the earthquake has not occurred prior to  $t_e$  is

$$P(t_e \leq T \leq t_e + \Delta t | T > t_e) = \frac{P(t_e \leq T \leq t_e + \Delta t)}{P(t_e \leq T \leq \infty)}, \quad (\text{A3})$$

where  $t_e$  is the elapsed time and

$$P(t' \leq T \leq t'') = \int_{t'}^{t''} f(t) dt. \quad (\text{A4})$$

However, due to current limitations,  $\mu$  and  $\sigma_{\ln T_i}$  are themselves uncertain and this introduces uncertainties into the probability calculation. To account for this, a distribution of the conditional probability is obtained by performing a large number of calculations for the conditional probability using values of  $\mu$  and  $\sigma_{\ln T_i}$  repeatedly drawn from distributions assigned to these parameters to reflect our current uncertainty in these values. The appropriate distributions on  $\mu$  and  $\sigma_{\ln T_i}$  are posterior distributions given the observation  $T > t_e$  (see Appendix A, Working Group, 1990, for a discussion of the posterior distribution of  $\mu$ . See also Davis, P. *et al.*, 1989). Distributions of the uncertain probabilities obtained by various methods are calculated by the procedure of Savage (1992), and from those distributions the mean probability and its standard deviation are then obtained (Table 2). Three specific methods are used to obtain fault-segment probabilities.

#### Paleoseismic Dates Method

For some fault segments, data for a sufficient number of recurrence intervals are available to estimate the recurrence parameters directly. Probabilities obtained from these recurrence data are designated as "Dates." The method is described in Savage (1991). Briefly, it involves finding the lognormal probability density function that best fits the observed recurrence data (see Nishenko and Buland, 1987). From this parent distribution  $n$  recurrence intervals are randomly drawn, where  $n$  is the number of recurrence observations in the original data, and from the drawn intervals a trial distribution is constructed and probabilities and their weights (given  $T > t_e$ ) are computed. This procedure is repeated a large number of times (3000 for the results presented here), each time employing a new set of recurrence times drawn from the parent distribution. These calculations yield distributions of both the uncertain probability and the uncertain parameters,  $\mu$  and  $\sigma_{\ln T_i}$ .

#### Time Predictable Model

Many fault segments do not have sufficient recurrence data to apply the paleoseismic dates method, but have data on displacement  $U$  in the last event and long-term fault-slip rate  $V$  which are used to obtain  $\mu$  and its uncertainty  $\sigma_m$ . Where those data are available, probabilities are obtained using two different approaches: the "time predictable" model which follows the method of the 1988 Working Group and the "renewal" model. As described in the body of the report, we assume  $\sigma_{\ln T_i} = 0.5 \pm 0.2$  for these models.

With the time-predictable probability model (Shimazaki and Nakata, 1980), the estimate of  $\mu$  appearing in equation (A1) pertains only to the next event and is based on the slip only of the previous earthquake. Specifically, as implemented here and previously (Working Group Reports, 1988, 1990), the mean of the expected recurrence interval for the next earthquake depends on the slip in the last event  $U_{\text{last}}$  and long-term fault-slip rate  $V$ :

$$\mu_{\text{next}} = U_{\text{last}}/V. \quad (\text{A5})$$

The uncertainty in  $\mu_{\text{next}}$  derives from the measurement uncertainty in  $U_{\text{last}}$  and  $V$ . Following the usual error analysis, the standard deviation of  $\mu_{\text{next}}$  is estimated by

$$\sigma_{\mu_{\text{next}}} = \mu_{\text{next}} \sqrt{\left(\frac{\sigma_u}{U_{\text{last}}}\right)^2 + \left(\frac{\sigma_v}{V}\right)^2}, \quad (\text{A6})$$

where  $\sigma_u$  and  $\sigma_v$  are the uncertainties (standard deviations) in measurement of  $U$  and  $V$ , respectively. Equation (A6) is evaluated using the current estimates of  $\mu_{\text{next}}$ ,  $U_{\text{last}}$ ,  $V$ .

#### Renewal Model

The renewal model assumes independence among recurrence intervals. In this model, the estimate of  $\mu$  now pertains to all events on a segment and is estimated from the mean of all earthquake slips  $\bar{U}$  on the segment,

$$\mu_{\text{all}} = \bar{U}/V. \quad (\text{A7})$$

Hence, analogous to equation (A6) the uncertainty on  $\mu_{\text{all}}$  is

$$\sigma_{\mu_{\text{all}}} = \mu_{\text{all}} \sqrt{\left(\frac{\sigma_{\bar{U}}}{\bar{U}}\right)^2 + \left(\frac{\sigma_v}{V}\right)^2}, \quad (\text{A8})$$

where  $\sigma_{\bar{U}}$  is the uncertainty on the mean slip  $\bar{U}$ . In addition to measurement error, the possibility of intrinsic event-to-event variation of  $U$  introduces the possibility of additional sampling error into the determination of  $\bar{U}$  giving for  $n$  slip events:

$$\sigma_{\bar{U}} = \sqrt{\frac{\sigma_U^2}{n} + \frac{\sigma_{U_i}^2}{n}}, \quad (\text{A9})$$

where  $\sigma_U$  is the uncertainty in measurement of  $U$  and  $\sigma_{U_i}$  is the intrinsic event-to-event variation of slip. Combining equation (A8) with equation (A9) gives

$$\sigma_{\mu_{\text{all}}} = \mu_{\text{all}} \sqrt{\frac{\sigma_U^2}{\bar{U}^2 n} + \frac{\sigma_{U_i}^2}{\bar{U}^2 n} + \frac{\sigma_V^2}{V^2}}. \quad (\text{A10})$$

There is, at present, little basis to fix  $\sigma_{U_i}$ . However, the observed variability of recurrence times and limited observations of recurring slip indicate  $U$  is not the same for all events. Savage (1992) implicitly assumes that the event-to-event variation of  $U$  follows the intrinsic variation of recurrence times

$$\frac{\sigma_{U_i}}{\bar{U}} = \frac{\sigma_{T_i}}{\mu_{\text{all}}}, \quad (\text{A11})$$

where  $\sigma_{T_i}$  is the standard deviation of the random recurrence interval  $T$  (i.e., from the standard relations for the moments of the lognormal distribution)  $\sigma_{T_i}^2 = \mu^2 \exp(\sigma_{\ln T_i}^2) - 1$ . We note that the assumption of equation (A11) has a physical basis if recurrence and slip are related and strictly follow either the time-predictable or slip-predictable models. For calculation of the renewal model probabilities we have followed Savage and adopted equation (A11). For all fault segments only the last slip was employed ( $n = 1$ ), giving the following from equations (A9) and (A10):

$$\sigma_{\mu_{\text{all}}} = \mu_{\text{all}} \sqrt{\frac{\sigma_U^2}{\bar{U}^2} + \frac{\sigma_V^2}{V^2} + \frac{\sigma_{U_i}^2}{\bar{U}^2}}, \quad (\text{A12})$$

which is evaluated using the current estimates of  $V$ ,  $\bar{U} = U_{\text{last}}$ ,  $\mu_{\text{all}} = \mu_{\text{next}}$ , and equation (A11).

### Discussion

The time-predictable and renewal models may be compared by constructing a marginal distribution in which  $\sigma$  represents the net standard deviation of recurrence time and is made up of two components: (1) the parametric (epistemic) uncertainty  $\sigma_\mu$  in the estimation of the mean  $\mu$  (e.g., uncertainty in measurement of  $U$  and  $V$ ) and (2) the intrinsic (aleatory) variability  $\sigma_{T_i}$  of recurrence times about the actual mean (Working Group, 1988):

$$\sigma = \sqrt{\sigma_\mu^2 + \sigma_{T_i}^2}. \quad (\text{A13})$$

As implemented here and by the 1988 and 1990 Working Groups, the time-predictable probability model does not strictly adhere to the time-predictable assumption, because an intrinsic variability of recurrence time about the estimated mean is permitted. If the time-predictable model

has some measure of validity, the intrinsic variability of the next recurrence interval is less than the overall event-to-event variability by some amount (i.e., for the next event  $\sigma_{T_i}|U_{\text{last}} \leq \sigma_{T_i}$ ). Hence, for the time-predictable model  $\sigma_{T_i}|U_{\text{last}}$  should replace  $\sigma_{T_i}$  in equation (A13) and in calculating probabilities using Equation (A1). However, in the absence of reliable information we assume that  $\sigma_{T_i}|U_{\text{last}} \leq \sigma_{T_i}$ . Hence, from equations (A6) and (A13) the net uncertainty for the next recurrence interval with the time-predictable method is

$$\sigma = \sqrt{\mu_{\text{next}}^2 \left(\frac{\sigma_U}{U_{\text{last}}}\right)^2 + \mu_{\text{next}}^2 \left(\frac{\sigma_V}{V}\right)^2 + \sigma_{T_i}^2}. \quad (\text{A14})$$

From equations (A10) and (A13) the net uncertainty for the renewal model is

$$\sigma = \sqrt{\frac{\mu_{\text{all}}^2}{n} \left(\frac{\sigma_U}{\bar{U}}\right)^2 + \mu_{\text{all}}^2 \left(\frac{\sigma_V}{V}\right)^2 + \frac{\mu_{\text{all}}^2}{n} \left(\frac{\sigma_{U_i}}{\bar{U}}\right)^2 + \sigma_{T_i}^2}. \quad (\text{A15})$$

In this report, only the slip in the last event was employed for calculations with the renewal model. Hence,  $n = 1$ ,  $\bar{U} = U_{\text{last}}$ , and  $\mu_{\text{all}} = \mu_{\text{next}}$ . Using those equalities and equation (A11) to evaluate  $\sigma_{U_i}/\bar{U}$  gives the net uncertainty for the renewal model:

$$\sigma = \sqrt{\mu_{\text{next}}^2 \left(\frac{\sigma_U}{U_{\text{last}}}\right)^2 + \mu_{\text{next}}^2 \left(\frac{\sigma_V}{V}\right)^2 + 2\sigma_{T_i}^2}. \quad (\text{A16})$$

In summary, because  $\mu_{\text{all}} = \mu_{\text{next}}$ , the models differ only in their net uncertainty as given by the doubling of the  $\sigma_{T_i}^2$  term in equation (A16) compared to equation (A14). This difference accounts for differences in probabilities obtained from the two models, listed in Table 2.

We differ on the relative merits of the renewal and time-predictable probability models. The issue hinges on the validity of the time-predictable assumption, which has not been definitively demonstrated. However, in using only the slip information in the last event, both models in effect employ the time-predictable assumption for estimating the mean recurrence time for the next event and further assume an intrinsic variation of recurrence times about that mean. If there is a time-predictable component to the intrinsic event-to-event variability of recurrence times (i.e.,  $\sigma_{T_i}|U_{\text{last}} \leq \sigma_{T_i}$ ), then the renewal model assumption of independence among intervals may overestimate net uncertainty. In principle, displacements and dates for several earthquakes on a fault segment could be used to evaluate the assumption of equation (A11) and to test for a time-predictable component to earthquake recurrence.

## Appendix B: Procedures for Constructing “Cascades” Model

We assume that each time a segment ruptures, whether alone or with others, it slips about the same amount. This is called the characteristic displacement for the segment. Given an assumed thickness of the ruptured part of the crust (11 km) and an assumed rigidity ( $3 \cdot 10^{10}$  Nm<sup>-2</sup>), we then calculate a characteristic seismic moment for each segment. The seismic moment for a cascade is then the sum of the characteristic moments for all segments involved, and the moment magnitude is calculated by the standard formula.

Preliminary tests showed that it is difficult to match the power law magnitude distribution without maximizing the number of large earthquakes, and minimizing the number of small ones. We use the following procedure:

1. List all possible earthquakes involving contiguous segments, in decreasing order of their moment magnitudes. Establish a minimum or “floor” rate for each possible event, equal to  $0.5 \cdot n/T$  for each type of event known to have occurred  $n$  times within the past  $T$  years, and equal to  $0.5 \cdot u$  for single segment events. Here  $u$  is the segment rupture rate. A zero is assigned to multi-segment ruptures never observed.
2. Compute the segment rupture rates implied by the minimum earthquake rates in step 1, and subtract these from the total rupture rates in Table 2.
3. Set the rate  $w$  of the largest possible earthquake equal to the smallest residual rupture rate on any segment composing the earthquake.
4. Decrease the residual rupture rates for all involved segments by  $w$ .
5. Repeat steps 3 and 4 for the next largest earthquake, and continue until all the rupture rates have been explained.

We show occurrence rates of all possible cascades in Table 3.

The procedure above minimizes the total earthquake rate on a fault, subject to the total rupture rate from Table 2, and the constraints in step 1, above. If we use the Poisson rupture rates in step 1 and adopt the characteristic displacement concept, then the procedure above also predicts correctly the long-term moment rate for the fault. Because the 30-yr conditional probabilities are generally higher than the long-term unconditional probabilities, the lognormal earthquake rates in Table 3 imply slip and moment rates higher than the long-term average.

## Appendix C: Geologic Data Base for Selected Faults in Southern California

### San Andreas Fault

In the WGCEP (1988) report, the central and southern San Andreas fault was divided into segments named

Cholame, Carrizo, Mojave, San Bernardino Mountains, and Coachella Valley. This nomenclature is retained for the present report. It is important to emphasize that although these segments are treated as independent sources of earthquakes, historical and paleoseismological observations show that ruptures may overlap and that some segments may both produce their own earthquakes and fail when large ruptures nucleate in an adjacent segment and propagate into them. For the San Andreas fault the present working group has made generally minor changes in estimates of slip rate and characteristic displacement. The most important changes are in developing a more extensive and precise earthquake event chronology at different locations along the fault.

*Cholame Segment.* The Cholame segment extends from Cholame southeastward for about 60 km. It lies between the Parkfield segment of the fault to the northwest, and the Carrizo segment, which experienced 7- to 11-m displacements in 1857, on the southeast. There are no independent slip-rate or recurrence data for this segment of the fault. However, there are alternative estimates of slip during the 1857 earthquake. Sieh (1978) concluded that the northwest 20 km of this section of the fault slipped about 3.5 m in 1857, with slip increasing to 9.5 m along the southeast 35 km of the segment. He suggested that the event prior to 1857 also produced about 3.5 m of slip along the northern half. Alternatively, Lienkaemper and Prescott (1989) concluded that slip during the 1857 earthquake averaged 6 m. The 1988 Working Group could not resolve this difference, and made a representative calculation using a median value of  $4.75 \pm 2.0$  m for the 1857 slip. They also adopted a slip rate of  $34 \pm 1.5$  mm/yr, based on extrapolation from the Carrizo segment. There have been no new slip-rate, earthquake recurrence, or characteristic displacement data for the Cholame segment since the 1988 report. The question remains open as to whether the Cholame segment produces its own event or only fails in conjunction with large 1857-type earthquakes. We adopt the 1988 characteristic displacement value but increase the uncertainty to  $\pm 5$  mm/yr to reflect uncertainties in interpretation. These values give an average recurrence interval of 140 (+93, -69) yr.

*Carrizo Segment.* The Carrizo segment of the San Andreas fault extends from about 145 km southeast of Cholame to Three Points. Along the northwestern part of the segment, near Wallace Creek, 1857 offsets of 8 to 10 m are reported and slip along most of this segment averaged 6 to 7 m (Sieh, 1978). In fact, the large and consistent amount of slip in 1857 distinguishes this part of the fault from the adjacent, and apparently lower, characteristic displacement Cholame and Mojave segments. The 1857 surface rupture clearly shows that slip during large earthquakes can extend beyond the boundaries of

this segment. The 1988 Working Group estimated recurrence for this segment using a slip rate of  $34 \pm 1.5$  mm/yr and a characteristic displacement of  $9.5 \pm 2.0$  m based on offsets associated with the 1857 earthquake and the two prior events at Wallace Creek (Sieh and Jahns, 1984). Since the 1988 report, new recurrence interval and characteristic displacement data have been developed. Two recent studies provide somewhat contradictory results. Sims *et al.* (1993) use offset stream and colluvial deposits exposed in trenches at Phelan Creek to interpret the occurrence of large earthquakes in 1857, 1505, 1367, 1231, and 1001. This history suggests an average recurrence interval of 212 (+190, -171) yr. Grant and Sieh (1994) trenched offset alluvial fan deposits at the Bidart site, located about 3 km from Phelan Creek. They present strong evidence that the penultimate Carrizo event occurred shortly after 1405 to 1510. This demonstrates at least one long interval of 350 yr, which is consistent with the late Holocene slip rate and the large characteristic slip. However, they conclude that the three prior events occurred between 1218 and the penultimate event, and interpret this as a temporal cluster.

Uncertainties also exist in estimates of characteristic displacement. The amount of slip during the past three earthquakes has been estimated at  $9.5 \pm 0.5$  m.,  $12.3 \pm 1.2$  m, and  $11.4 \pm 2.5$  m (Sieh and Jahns, 1984). Grant and Sieh (1993) used subsurface observations to measure 6.6 to 6.9 m for 1857 slip about 2.5 km south of Wallace Creek. Alternatively, Grant and Donnellan (1994) use monuments from an 1855 survey and a 1991 repeat survey to infer  $11.0 \pm 2.5$  m of right slip in the Carrizo Plain during the 1857 event. Finally, Grant and Sieh (1994) suggest that some of the events within their proposed cluster may have slip less than the 1857 offset. However, this interpretation is qualitative and is based on variations in the width of the zone of faulting rather than on measurement of actual offset.

Data and interpretations on the behavior of the Carrizo segment, which traditionally has been considered the most stable with regard to characteristic displacement and recurrence interval (large offsets and long intervals), are clearly in a state of flux. It is difficult for us to resolve both the differences and uncertainties in the paleoseismic recurrence intervals and characteristic displacement. For the present report, we prefer a slip rate of  $34 \pm 3$  mm/yr (Sieh and Jahns, 1984). The choice of characteristic displacement is somewhat equivocal, but we rely on the new subsurface data and estimate a value of  $7 \pm 4$  m. This encompasses the resurveying and would also allow for smaller slip events. These values yield a mean recurrence interval of 206 (+149, -125) yr. This calculated value is similar to the average recurrence interval using the preliminary event chronology.

**Mojave Segment.** The Mojave segment, as defined in the 1988 report and used here, extends southeastward

some 100 km from about Three Points to a few kilometers northwest of Cajon Creek. The northwest end of the segment is not well defined and represents a 40-km-long transition zone where slip increased from about 3 to 7 m in 1857. The southeastern end is the southern limit of the 1857 rupture. A primary characteristic of the Mojave segment is a relatively consistent 3 to 4 m of slip during the 1857 earthquake, although Salyards *et al.* (1992) estimate slip during the 1857 and two prior events at about 6 m per event near the south end.

The Mojave segment contains the Pallett Creek site, where paleoseismic evidence of 11 surface faulting earthquakes since about 529 A.D. has been identified in trenches. Sieh *et al.* (1989) present revised dates for these events. These dates indicate an average recurrence interval of 131 yr, but suggest that the interval between events ranges markedly from the mean value. Five intervals are less than 100 yr, three longer than about 190 yr, and the events could be partitioned into four groups or clusters with intervals of 200 to 330 yr between clusters. Since the 1988 report, there have not been any new paleoseismic studies initiated on the Mojave segment. However, dating of events at Wrightwood, 20 km to the south on the San Bernardino Mountains segment of the fault (see below), and reevaluation of the published Pallett Creek dates using Bayes' theorem to reduce the C-14 dating uncertainty (Biasi and Weldon, 1994a) provide new insights into the behavior of the Mojave segment. Biasi and Weldon (1994b) conclude that the past five events at Pallett Creek occurred in 1857, 1812, 1546, 1360, and 1087, with the dates of the three older events differing somewhat from Sieh *et al.*'s (1989) estimates. Of these, the 1360 and 1087 events do not appear to be correlative with Wrightwood. At least three Wrightwood events during the same time interval do not appear in the Pallett Creek record. This observation strengthens the interpretation that Pallett Creek and Wrightwood are at sites on the fault that experience overlapping ruptures. Because of this the event dates do not define the behavior of an individual rupture segment. The 1988 Working Group recognized that, paradoxically, the segment with the most paleoseismic data also appeared to exhibit great variability and uncertainty in behavior. Because of this the 1988 Working Group chose the direct method of calculating probabilities and used a slip rate of  $30 \pm 5$  mm/yr and a characteristic displacement of  $4.5 \pm 1.0$  m to calculate a recurrence interval. This segment of the fault lacks a well-constrained Holocene slip rate. For the present report we adopt the preferred value of 30 mm/yr from the 1988 report, but we increase the uncertainty to  $\pm 8$  mm/yr to accommodate possible rates from kinematic models (Weldon, 1991), although there are no new data. The uncertainty in the characteristic displacement is increased slightly to  $4.4 \pm 1.5$  m to take into account the paleomagnetic slip estimate at Pallett Creek. These values yield a calculated recurrence interval of 150 (+123,

–71) yr. Alternatively, using the newly revised dates for Pallett Creek, the average recurrence interval for a surface-faulting event passing through Pallett Creek is 134 yr since 644 A.D.

*San Bernardino Mountains Segment.* This segment, delineated by the 1988 Working Group, was recognized to be a structurally complex zone between the Mojave and Coachella Valley segments for which there were few data. They used 1812 as a tentative date for the most recent event, a long-term slip rate of  $24 \pm 3$  mm/yr (Weldon and Sieh, 1985), and a characteristic displacement of  $4 \pm 2$  m. The San Bernardino Mountains segment has received the most study since the 1988 report. At Wrightwood, Fumal *et al.* (1993) exposed the fault in a sequence of layered peat deposits. They show that the past five surface-faulting events occurred in 1857 and 1812 A.D., and about 1700, 1610, and 1470 A.D. Biasi and Weldon (1994b) modified the dates of the prehistoric events to 1693, 1587, and 1452, and added the date of a sixth event at 1192. At Pitman Canyon, 5 km south of Cajon Pass, Seitz and Weldon (1994a, b) identify the two youngest events on the fault. The most recent appears to correlate with the 1812 event at Wrightwood. The penultimate event post-dates 1659 and also appears to correlate with Wrightwood. In addition, they measure a displacement of a debris flow of 4 m during the most recent event and a cumulative offset of 7 to 8 m of right slip for these two earthquakes. The new paleoseismic data provide several important constraints for estimating behavior of the San Bernardino Mountains segment. It appears that the most recent event was in 1812, which defines an elapsed time of 181 yr. New observations of offset allow us to adopt a characteristic displacement of  $3.5 \pm 1.0$  m. Using a slightly modified slip rate of  $24 \pm 5$  mm/yr we calculate an average recurrence interval of 14 (+91, –60) yr. However, the event dates from Wrightwood, Pallett Creek, and Indio (see below) indicate a complex rupture history for the southern San Andreas fault. It appears that the San Bernardino Mountains segment (a) produces its own earthquakes (1812, 1546 to 1587, 1192), some of which extend to Pallett Creek and others that do not, and (b) slips when ruptures extend into it from the north (1857, 1360, 1087) or from the south (1693, 1452). Because of this fault interaction, calculating average repeat times from slip rate and characteristic displacement is a questionable approach to estimating conditional probability. The Wrightwood site has averaged one surface-rupturing earthquake every 133 yr since 1192. The most recent five events have been closer together, averaging 106 yr between events. For the present report we use the new paleoseismic data to define the average interval for surface-faulting events at this location.

*Coachella Valley Segment.* The Coachella Valley seg-

ment comprises the southern 100 km of the fault zone and extends from San Geronio Pass on the northwest to the Salton Sea on the southeast. This segment has the longest elapsed time of any on the fault zone, last experiencing a large event around 1680. The 1988 Working Group used the paleoseismic event times at Indio of 1680, 1450, 1300, and 1020 (Sieh, 1986) to arrive at an average recurrence interval of  $220 \pm 13$  yr. There have been no new paleoseismic studies on this segment since the 1988 report. However, the new dates at Wrightwood suggest that events occurring in 1690 and 1450 may have ruptured both the Coachella Valley and San Bernardino Mountains segments of the fault. Here we adopt the 1988 Working Group values, of slip rate, displacement, and previous dates.

#### San Jacinto Fault

The San Jacinto fault system has been an important source of moderate- to large-magnitude earthquakes in southern California this century. In 1988, the Working Group divided the fault into five segments using information on fault geometry, historical seismicity, and new slip-rate data. The segments, from north to south, were named San Bernardino Valley, San Jacinto Valley, Anza, Borrego Mountain, and Superstition Hills. Significant changes for the present report include modifying the segmentation model, increasing the slip rate on the fault, and changing estimates of characteristic displacements. These changes are described below.

*San Bernardino Valley Segment.* The San Bernardino Valley segment extends about 35 km from just south of the San Jacinto–Cucamonga fault intersection to the northern end of San Jacinto Valley. The main trace is the Claremont strand although there are parallel fault traces. The segment may have been the source of the 22 July 1899 earthquake ( $m = 6.4$ ) but has not clearly been the source of documented surface faulting. The most recent paleoseismic study in San Bernardino shows a very well-developed fault zone with a minimum late Holocene slip rate of 1.7 to 3.3 mm/yr. There is no earthquake event chronology for this segment.

The 1988 Working Group used a slip rate of  $8 \pm 3$  mm/yr, a calculated characteristic displacement of  $1.4 \pm 0.4$  m, and an elapsed time since 1890 to calculate 30-yr probabilities. For the present report we revise these values. The slip rate is increased to  $12 \pm 6$  mm/year, which is an extrapolation along the fault of the new slip rate data at Anza (see below). The characteristic displacement decreases slightly to  $1.2 \pm 0.3$  m. There are no independent data on characteristic displacement. The value is derived from Wells and Coppersmith (1994) and reflects a slightly shorter segment length than was used in 1988.

*San Jacinto Valley Segment.* The 1988 Working Group defined the San Jacinto Valley Segment on the basis of

microseismicity data and on the inferred extent of the  $m = 6.8$  21 April 1918 earthquake. The segment included the Claremont fault and parallel Casa Loma fault in the northern part, as well as the northern section of the Clark fault. They used a slip rate of  $11 \pm 3$  mm/yr, a calculated characteristic displacement of  $1.8 \pm 0.5$  m, and a 70-yr elapsed time to calculate a conditional probability.

For the present report we define the segment as extending about 45 km. It includes the Claremont and Casa Loma faults. The southern boundary zone of the segment is placed where the two faults merge to form the single Clark fault. The Clark fault is reassigned to the Anza segment (see below). As with the San Bernardino Valley segment, the slip-rate value is increased to  $12 \pm 6$  mm/yr to reflect the new data to the south. Similarly, the estimate of characteristic displacement is lowered to  $1.0 \pm 0.2$  m because of the shorter segment length. We use 75 yr as the time since the most recent event.

*Anza Segment.* As defined in the 1988 report, the Anza segment extended about 50 km from the inferred south end of the 1918 rupture just north of Anza. It is a structurally complex segment containing part of the Clark fault, the Coyote Creek fault, and the Buck Ridge fault. The Working Group recognized that the level of activity on the different strands might vary, but assumed most of it occurred on the Clark fault. They used a slip rate of  $11 \pm 3$  mm/yr, a characteristic displacement of  $1.4 \pm 0.4$  m, and an elapsed time of 96 yr assuming that a large earthquake in 1892 occurred on one of the strands. New slip-rate and earthquake recurrence data have been obtained on this segment. Rockwell *et al.* (1990) measured offsets of and dated late Pleistocene and Holocene alluvial fans near Anza. They conclude that a rate of  $12 (+7, -5)$  mm/yr is the best estimate of fault-slip rate. Klinger and Rockwell (1989) trenched the San Jacinto fault at Hog Lake near Anza. They observed three surface-faulting earthquakes since about 1210. Evidence suggests these events occurred about 1210, 1530, and 1750.

For the present report we consider the Clark fault, which extends about 90 km, as the Anza segment. The Coyote Creek fault is now treated as a separate segment. We adopt the new slip rate of  $12 (+7, -5)$  mm/yr. The characteristic displacement is calculated from Wells and Coppersmith (1994) and increased to  $3.0 \pm 1.0$  m because the segment has been lengthened. Using these values, the average repeat time for a magnitude 7.0 to 7.5 earthquake is  $250 (+321, -145)$  yr.

*Coyote Creek Segment.* This segment of the San Jacinto fault extends some 40 km from the intersection with the Clark fault in the north to the north end of the 1968 Borrego Mountain segment in the south. There are no independent fault parameters for this segment. The slip

rate of  $4.0 \pm 2.0$  mm/yr is extrapolated from the Borrego Mountain segment (see below). The calculated characteristic displacement, based on fault length and empirical regressions, is  $0.7 \pm 0.3$  m. This gives a mean recurrence interval of 175 (+158, -95) years. There has not been a large surface-faulting earthquake along this segment of the fault since at least 1892.

*Borrego Mountain Segment.* The Borrego Mountain segment is defined on the basis of the lateral extent of the  $m = 6.5$  1968 Borrego Mountain surface faulting. The 1988 Working Group considered the earthquake to be a characteristic event for this part of the fault. They used a geologically determined slip rate of  $4.0 \pm 1.0$  mm/yr (Sharp, 1981) and a characteristic displacement of  $0.7 \pm 0.1$  m to derive a mean recurrence of 175 yr. No new data have been developed on this segment. For the present report we retain the mean values, but increase the uncertainty on the slip rate and characteristic displacement by 0.1 mm/yr and 1.0 m, respectively.

*Superstition Hills Segment.* In the 1988 report, the Superstition Hills segment was composed of two parallel strands, the eastern Superstition Hills fault and the western Superstition Mountains fault. No slip-rate or recurrence data are available for either fault. On 23 November 1987 the Working Group discussed the segment and decided that the level of information was too poor to justify a conditional probability. On 24 November the fault ruptured in the  $m = 6.2$  Elmore Ranch and  $m = 6.6$  Superstition Hills earthquakes. The Elmore Ranch event was associated with 10 km of left-slip surface rupture on a northeast-trending fault zone conjugate to the main Superstition Hills fault. Twenty-seven kilometers of surface rupture occurred along the Superstition Hills trace, averaging about 0.5 m with a maximum surface slip of 0.9 m. Postearthquake studies provide information on earthquake recurrence, characteristic displacement, and slip rate. Trenching of the rupture (Hudnut and Sieh, 1989) exposed faulted deposits of the latest high stand of Lake Cahuilla, which occurred about 330 yr ago. Based on these trenches, Hudnut and Sieh (1989) conclude that for the past 330 yr the slip rate on the fault has been in the range of 2 to 6 mm/yr, the penultimate event occurred between about 300 and 150 yr ago, and slip during the penultimate event was about half the amount of the 1987 offset at that point on the fault. We use these new observations to estimate a slip rate of  $4.0 \pm 2.0$  mm/yr of the fault and characteristic displacement of  $1.0 \pm 0.3$  m for the fault. This gives a calculated average recurrence interval of 250 (+400, -133) yr. This value is consistent with the paleoseismic interval of 150 to 300 yr.

*Superstition Mountains Segment.* The Superstition Mountains segment is added to the San Jacinto fault zone

for the present report. It extends approximately 25 km southward from the south end of the 1968 Borrego Mountain surface rupture. Recent trenching by Gurrola and Rockwell (1994) at a site where the fault crosses the northern shoreline of Lake Cahuilla shows the occurrence of three surface-faulting events between 885 and 1440. The most recent event occurred about 1440, the penultimate event occurred between 1250 and 1300, and the third event back occurred between 885 and 1250. In addition, Gurrola and Rockwell measured a channel offset of  $2.0 \pm 0.3$  m associated with the most recent event.

There is no independent slip rate for this segment and we extrapolate the Borrego Mountain rate of  $4.0 \pm 2.0$  m. Assuming that the observed slip is characteristic for the fault, we calculate a recurrence interval of 500 (+650, -217) yr. Inspection of the preliminary event dates shows that individual intervals appear to range from about 200 to 400 yr. Simply using the time from 885 to the present and three intervals in the ensuing 1019 yr, we derive an average interval of 340 yr. Approximately 550 yr have elapsed since the most recent event on this segment.

#### Imperial Fault

The Imperial fault has produced two large historical surface-faulting events of  $m = 6.9$  in 1940 and  $m = 6.4$  in 1979. The 1979 event reruptured the northern 25 km of the 1940 event with a similar amount of surface offset. The 1988 Working Group noted that the long-term slip rate for the fault is not well determined and assumed a value of  $30 \pm 5$  mm/yr. They also used strong-motion estimates of deep slip of  $1.2 \pm 0.4$  m, as opposed to the average surface offset of 0.8 m, to calculate recurrence.

Subsurface investigations at the United States–Mexico border led Sharp (1981) to suggest that several hundred years had passed between the penultimate event and the 1940 earthquake. Based on relations between the fault and deposits of the last high stand of Lake Cahuilla, they conclude that only the 1940 Imperial Valley earthquake produced significant surface offset during the past 300 yr and that the penultimate event dates to about 1670. Rockwell and Thomas (1994) also suggest that the slip rate on the Imperial fault for the past 300 yr is only about 15 to 20 mm/yr, which is substantially less than the geodetic estimates. The Imperial fault appears to be a complex structure with possible multiple modes of behavior. There is no real basis for estimating repeat times for 1940-type events. It is possible that the northern part of the fault, which had a smaller offset in 1940, is failing at shorter intervals to fill a slip deficit. In the present report, we adopt the 1988 Working Group values to estimate an average recurrence interval of 40 (+24, -17) yr.

#### Whittier–Elsinore Fault

**Whittier Segment.** The Whittier segment extends 25 to 30 km from the Whittier Narrows in the north to the

Santa Ana River in the south. The slip rate for the Whittier fault has been determined near Yorba Linda. Rockwell *et al.* (1992) report a minimum dextral slip rate of 2.5 to 3.0 mm/yr, based on laterally displaced channels incised into a dated alluvial fan. The maximum age of the fan is determined from C-14 dating of land snails recovered from the surface of a buried soil (A horizon) below the uppermost fan deposit. Minimum slip is inferred from the deflection of small channels incised into the fan alluvium. Because the incisions are younger than the fan deposits, the slip rate is a minimum. Three-dimensional (3D) trenching by Gath *et al.* (1992) in the Olinda Oil field also established a minimum slip rate for the fault zone. They measure a rate of about 1 to 1.5 mm/yr on one of four strands of the fault. Two of the strands are well expressed geomorphically and have similar-sized stream deflections suggesting similar slip rates. Gath *et al.* infer a minimum rate for the entire fault zone of about 2 mm/yr.

The dates of the past two events and the amount of surface offset in the most recent event have been established at Olinda Oil field by 3D trenching (Patterson and Rockwell, 1993). The timing of the last two events is estimated at between 1400 and 2200 yr ago and 3000 and 3100 yr ago, respectively, based on C-14 dating of faulted and unfaulted alluvium. The characteristic displacement estimate is a minimum because investigation focused only on the main strand of the fault, and additional slip may have occurred on a more northerly trace. Nevertheless, at least 1.9 m of dextral slip was produced in the most recent event based on direct measurement of a laterally displaced channel.

We use these preliminary paleoseismic data to estimate a slip rate of  $2.5 \pm 1.0$  mm/yr. Although the observed displacement during the most recent event is a minimum value we use  $1.9 \pm 0.2$  m. These values give a calculated minimum recurrence interval of 760 (+640, -274) yr. Based on the initial dating, a minimum of at least 1400 yr has passed since the last large-magnitude strike-slip event on the Whittier fault.

**Glen Ivy Segment.** Paleoseismic studies at Glen Ivy Marsh provide new information on slip rate, recurrence, and characteristic displacement on this segment. An average slip rate of about 5.5 mm/yr, with a maximum range of about 2 to 9 mm/yr was determined by Millman and Rockwell (1986) based on correlating offset alluvial fan deposits and using the soils to estimate the fan ages. This rate has not been corroborated with radiometric dates on offset deposits.

Trenches at Glen Ivy marsh (Rockwell *et al.*, 1986) show that five and probably six earthquakes have disrupted the sediments there since about 1060, yielding an average recurrence interval of 150 to 200 yr. Age control is by C-14 dating of peat horizons that bracket individual events. The presence of nearly 40 peat horizons in about

3.5 m of section facilitated high-precision dating of some events. These events occurred in 1910, post-1660, 1360 to 1660, ~1300, 1260, and ~1060. The most recent surface rupture is associated with the 1910 Temescal Valley earthquake ( $m = \sim 6$ ). The surface displacement in this event (about 250 to 300 mm right lateral) was measured by excavating a circa 1890s concrete flume built across the fault in about 1890. A 1914 pipe is not offset laterally. More recent historical subsidence due to groundwater withdrawal has complicated the slip measurements. A channel displaced by the circa 1300 earthquake is laterally displaced about 50 cm on a secondary splay of the fault, but the net offset in that event could not be measured.

Using the Glen Ivy observations, we estimate a slip rate of  $5 \pm 2$  mm/yr. This is consistent with rates measured along the fault to the south. Because the characteristic displacement is not well constrained, we adopt a value of  $1.55 \pm 0.4$  m, halfway between that of the Whittier segment to the north and the Temecula segment to the south. However, the available data suggest displacement may have varied from event to event.

*Temecula Segment.* Recent trenching across the Wildomar fault in the Temecula segment has yielded a late Holocene slip rate for the principal strand. A fluvial channel, dated by C-14 at about 2000 to 2400 yr, is laterally displaced about  $10 \pm 1$  m and gives a slip rate of about 4.2 mm/yr (Bergmann *et al.*, 1993). This rate is a minimum because there are several minor strands of the fault that also have geomorphic expression. Nevertheless, it is similar to the rates determined at other locations along the fault.

Individual prehistoric earthquakes have not yet been directly dated along this fault segment. The historical record precludes a large earthquake since about 1818, when the Serrano family occupied the valley. Indirect evidence of recurrence from a trench across the Murrieta Creek strand, a minor fault that accommodates principally dip-slip in response to a series of small right steps along the Wildomar fault, suggests a maximum average recurrence interval of between 250 and 600 yr (Rockwell, personal comm.). As noted, the slip rate on this segment is measured at a minimum of 4.2 mm/yr. We have selected a rate of  $5.0 \pm 2.0$  mm/yr, which accounts for slip on additional minor strands and is consistent with the rate observed on other parts of the fault. Because there are no measurements of characteristic displacement, we have calculated a value of  $1.2 \pm 0.3$  m using the segment length and empirical relations of Wells and Coppersmith (1994). These yield an average recurrence interval of 240 (+260, -111) yr. A minimum of 175 yr has passed since the most recent large event on the segment.

*Julian Segment.* The Julian segment is the longest in-

dividual segment on the fault. It extends about 65 km. The northern end zone is a broad restraining bend and the southern end is a 4- to 5-km-wide dilational step to the Coyote Mountains segment. Paleoseismic data are sparse along this segment of the fault. Vaughan and Rockwell (1986) used soils to correlate and date displaced alluvial fan deposits. They determined a slip rate of  $5 \pm 2$  mm/yr, which is close to other rates for the fault zone. At present there are no data on characteristic displacements or recurrence intervals of individual earthquakes.

To calculate probabilities on this segment, we use the slip rate of  $5.0 \pm 2.0$  mm/yr and calculate a characteristic displacement of  $1.7 \pm 0.3$  m using segment rupture length. These values give a calculated repeat time of 340 (+290, -125) yr. The historical record in this region indicates a minimum elapsed time of 101 yr.

*Coyote Mountain Segment.* The Elsinore fault is well expressed in the Coyote Mountains as a narrow zone of faulting that laterally displaces alluvial deposits, and erosion features that vary in age from late Holocene to mid-Pleistocene. It is the southernmost segment of the fault within the continental United States. The segment length is 30 to 35 km. Both the northern and southern boundary zones are defined by releasing step-overs to the Julian and Laguna Salada segments, respectively.

The slip rate has been estimated at 3.5 to 5.5 mm/yr (Pinault and Rockwell, 1984), and more recently at about 3.5 mm/yr (Rockwell, 1991, personal comm.) based on offset Holocene deposits. Numerous small gullies along the fault indicate that the displacement during the most recent event varied between about 1.5 m along the southern part of the segment to a maximum of 2.8 m along the central portion of the segment. Older offset deposits also show a similar increase in slip toward the middle of the segment (Rockwell, 1991, personal comm.), suggesting that this displacement pattern is characteristic for the segment. Timing of the three most recent prehistoric earthquakes has been estimated with thermal luminescence dating of fissure fill deposits along the fault (Rockwell, 1991, personal comm.). These occurred at about 400, 1200, and 2000 yr ago. All of these age estimates have errors of several hundred years, but suggest repeat times for large earthquakes of about 600 to 1000 yr. For the Coyote Mountain segment we use the range of slip rates to derive a value of  $4.0 \pm 2.0$  mm/yr. The observed gully and stream offsets indicate a characteristic displacement of  $2.5 \pm 0.5$  m. From these we calculate an average recurrence interval of 625 (+875, -292) yr. Although the timing of individual events has large uncertainties, the calculated repeat time and the measured intervals are similar. Like the Julian segment, historical data indicate a minimum elapsed time of 101 yr.

### Cucamonga Fault

The Cucamonga fault is a major east-striking thrust fault that extends for 25 km along the south front of the eastern San Gabriel Mountains. The fault appears to be accommodating a portion of the convergence between the Transverse Ranges and Peninsular Ranges that occurs near the San Jacinto fault. Young faulting is expressed as a series of fault scarps in late Pleistocene–Holocene alluvial fans. Based on trenching and fault scarp profiling, Morton and Matti (1987) measured about 36 m of net surface displacement in the past 11,000 to 13,000 yr, and calculate a slip rate for the fault of 4.5 to 5.5 mm/yr. From scarp profiling they estimate a characteristic displacement of 2 m. They conclude that the most recent event on this fault occurred before deposition of a fan deposit that might be as old as 1000 to 1750 yr. Taking into account the uncertainties in C-14 dating, we assign a slip rate of  $4.0 \pm 2.0$  mm/yr to the fault.

### Garlock Fault

The Garlock fault is a 250-km-long left-lateral strike-slip fault that separates the Sierra Nevada and Basin and Range Province on the north and east from the Mojave block on the south. The Garlock fault changes character between its western and eastern ends. West of Koehn Lake the fault shows a relatively complex fault trace, produces continuous mild seismicity, and locally exhibits aseismic creep. The eastern portion of the fault produces very few small earthquakes, is not known to exhibit aseismic creep, and is characterized by a simpler fault trace (Astiz and Allen, 1983). A large step in fault trace also occurs at Koehn Lake. Wesnousky (1986) used these observations to divide the Garlock fault into eastern and western segments, and we use that segmentation here.

The Garlock fault has been the subject of numerous slip-rate studies during the past two decades. These are summarized by McGill (1992, 1994) and they show rates ranging from 1 to 11 mm/yr. McGill and Sieh (1991, 1993) observed geomorphic features along the eastern half of the fault and suggest that displacements during the past few earthquakes ranged from 4 to 7 m, 2 to 3 m, and 2 to 4 m near the El Paso Mountains, Searles Valley, and the Pilot Knob areas, respectively. They interpreted the Holocene slip rates at these same three sites at between 4 and 7 mm/yr, 4 and 9 mm/yr, and 3 and 9 mm/yr, respectively. Their slip rate estimate of 4 to 9 mm/yr at Searles Lake is the best documented.

Our preference is to assign the entire fault a slip-rate value of 4 to 11 mm/yr with a preferred rate of 7.5 mm/yr. The lengths of 100 and 130 km for the western and eastern segments give moment magnitudes of 7.3 and 7.5, respectively.

### Oak Ridge Fault

The Oak Ridge fault is a steeply south-dipping reverse fault bordering the south side of the Ventura basin.

The onshore segment of the fault is about 40-km long, extending from the intersection with the Santa Susana fault on the east to the Oxnard Plain. It is interpreted as continuing for about 50 km offshore into the Santa Barbara Channel. Based on cross sections from oil-well data, Yeats (1988) estimated the displacement of the top of the Pleistocene Saugus Formation and calculated a slip rate of 5.9 to 12.5 mm/yr since the end of Saugus deposition 200,000 to 400,000 yr ago. However, the slip rate is sensitive to the age of the top of the Saugus Formation. Levi and Yeats (1993) have reevaluated that age at 500,000 yr using paleomagnetic data. This yields a revised long-term rate of 4.8 to 5.0 mm/yr (Huftile, 1992; Yeats *et al.*, 1994). In this report, we adopt a slip rate of  $4.9 \pm 1.0$  mm/yr.

### Palos Verdes Fault

The Palos Verdes fault is a right-lateral oblique-slip fault extending approximately 115 km from Santa Monica Bay south to Lausen Knoll in the southern San Pedro Channel. The fault is onshore for only about 15 km along the northern flank of the Palos Verdes Hills. We recognize two segments. The northern segment is a broad zone of faulting in Santa Monica Bay (Clarke *et al.*, 1985); its southern end is defined by its intersection with the Redondo (submarine) Canyon fault. The southern segment has a major left step and bend north of the Los Angeles harbor where it splits into a series of subparallel strands.

The Palos Verdes fault has been modeled by Davis, T. *et al.* (1989) and Shaw and Suppe (1994b) as a south-west-dipping back thrust above a large blind thrust. However, recent geomorphic studies on an offset paleochannel in the Los Angeles harbor (Rockwell, 1991) are more consistent with the fault being dominantly a right-lateral strike-slip fault, with a slip rate of about 3 mm/yr. Other studies have estimated rates of vertical displacement on the fault but have provided little information on horizontal displacement. Vertical rates have ranged from about 0.2 to 0.7 mm/yr (Clarke *et al.*, 1983). However, Stephenson *et al.* (1994) show that onshore the ancestral channel of the Los Angeles River is incised into an 80 to 120 thousand-yr-old surface and is offset about 300 m. This gives a right-lateral slip rate of 2.5 to 3.5 mm/yr. Ward and Valensise (1994) model the uplifted marine terraces on the Palos Verdes Peninsula and calculate a vertical rate of 3 mm/yr associated with slip on a right oblique-slip fault. This occurs at a major restraining bend in the Palos Verdes fault and is consistent with at least 3 mm/yr of horizontal displacement. Finally, on the basis of regional considerations, 5 to 6 mm/yr of slip on the Agua Blanca fault appears to feed directly into the Coronado Bank fault (about 4 mm/yr) and Descanso–Rose Canyons faults (Rockwell, 1991, personal comm.; Rockwell *et al.*, 1987). This amount of slip is expected to be distributed between the Palos

Verdes and Newport–Inglewood faults because they are direct northward continuations.

Based on the available data, we assign a slip rate of  $3.0 \pm 1.0$  mm/yr to both segments of the Palos Verdes fault. At present there are no data on characteristic slip or on earthquake recurrence intervals.

#### San Cayetano Fault

The San Cayetano is a north-dipping reverse fault on the north side of the Ventura Basin. A 24-km-long western segment and 16-km-long Modelo lobe segment are defined by Huftile (1992). Along the western segment of the fault Rockwell (1988) used fluvial terrace deposits and alluvial fan surfaces to measure slip rates of  $1.05 \pm 0.2$  mm/yr at Sisar Creek,  $1.35 \pm 0.4$  mm/yr at Bear Canyon, and  $2.35 \pm 0.55$  to  $4.15 \pm 0.85$  mm/yr at Mud Creek. At Timber Canyon he measured a rate of  $3.6 \pm 0.4$  mm/yr and suggested that a long-term rate (180  $\pm$  20 ka) could be as high as  $8.7 \pm 1.9$  mm/yr. Huftile (1992) uses displacement of the top of the Saugus Formation and its revised age to calculate slip rates of 3.6 to 5.8 mm/yr for the western segment and 4.4 to 10.4 mm/yr for the Modelo lobe segment. Taking into account the range of rates and uncertainties, we adopt a slip rate of  $4.5 \pm 1.5$  mm/yr. There has been no surface-faulting event on this fault is at least the past 200 yr.

#### Sierra Madre Fault

The Sierra Madre fault extends for approximately 85 km along the base of the San Gabriel Mountains as a northeast-dipping reverse fault. The Cucamonga fault is the eastward extension of the Sierra Madre, and the northwest section of the Sierra Madre fault contains the rupture of the 1971 San Fernando earthquake. Along most of its length, there is very limited geomorphic evidence of Holocene slip. Also, there is no independent evidence for quantifying either slip rate or earthquake recurrence. On the basis of general geologic mapping and trenching, Crook *et al.* (1987) conclude that major earthquakes have not occurred for several thousand years, and possibly for as long as 11,000 yr. However, they note that it is anomalous that high parts of the San Gabriel Mountains are adjacent to segments of the fault where evidence of Holocene displacement is least persuasive.

On the north end of the Sierra Madre, trenching across the 1971 surface rupture (Bonilla, 1973), although open to interpretation, suggests recurrence intervals for San Fernando-type events could be as short as 200 yr. Because the ends of the Sierra Madre fault are so active, and because the San Gabriel Mountains are consistently high along their length, there is reason to conclude that most of the central section of the fault should have a rate of activity similar to the ends. Therefore, we extrapolate the Cucamonga fault rate of  $4.0 \pm 2.0$  mm/yr to the remainder of the Sierra Madre fault. The apparent ab-

sence of a well-defined geomorphic expression can be attributed to the occurrence of infrequent but very large displacement events, strong modification of scarps by erosional and depositional processes at steep range fronts, or the presence of associated blind thrusts along much of the fault's length. These alternatives need to be evaluated with additional geologic studies.

#### Santa Susana Fault

The Santa Susana fault extends along the southern edge of the Santa Susana Mountains from the San Fernando Valley in Los Angeles County approximately 40 km west-northwest into Ventura County. The extensive geological studies of the fault zone are summarized by Yeats (1987). Faulting is complex with numerous strands, and Yeats *et al.* (1993) divide the fault into three segments. Recent investigations by Levi and Yeats (1993) suggest the leading edge of the fault flattens to near horizontal due to gravitational and topographic effects, which may explain the apparent absence of Holocene surface faulting. The Santa Susana fault may have been the source of the 1893 Pico Canyon earthquake and the San Fernando lateral ramp of the fault was seismically active during and after the 1971 San Fernando earthquake (Yeats, 1987). Based on 4 km of displacement of the Saugus Formation in the past 500 ka, Yeats (1987) suggested a preliminary slip rate of 8 mm/yr. Revised rates for the Newhall–Portrero (northern) and Placerita (southern) segments are 2.0 to 2.3 mm/yr and 5.7 to 6.7 mm/yr (Huftile, 1992). For this report we use a slip rate of  $6.2 \pm 0.5$  mm/yr to characterize the Santa Susana fault. There are no independent data on recurrence interval.

#### San Simeon Fault

The San Simeon fault zone is the central part of the San Gregorio–Hosgri system of near-shore coastal strike-slip faults. The fault is 70- to 90-km long and locally extends onshore near Point San Simeon. Offset Pleistocene marine terraces (Hanson *et al.*, 1994) and offset Holocene deposits exposed in trenches (PG&E, 1988) indicate a right-lateral slip rate in the range of 0.5 to 6.0 mm/yr. To capture this range of uncertainty, we assign a slip rate of  $3 \pm 2$  mm/yr. Data from exploratory trenches and offset stream channels show multiple Holocene displacements of 1 to 2 m per event (PG&E, 1988; Hall *et al.*, 1994). Assuming a rupture of  $80 \pm 10$  km, we estimate a maximum earthquake of magnitude 7.1.

### Appendix D: Formulas Used to Construct Tables 5 and 6

1. Universal constants assumed for all zones  
rigidity  $\mu = 3 \cdot 10^{10}$  Nm  
elastic thickness  $H = 11$  km
2. Input data for each zone  
Geologic data: maximum magnitude  $m_x$ , length  $L$ ,

slip rate  $V$ , displacement  $d$ , and rate of characteristic earthquakes  $r_c$

Geodetic data: moment rate from strain  $\dot{M}_g$

Seismic data: yearly rate  $r$  of  $m \geq 6$  earthquakes for the whole catalog, and  $r'$  for the special catalog with characteristic earthquakes removed

### 3. Formulas used for all zones

Integrated moment over  $6 \leq m \leq m_x$ , per  $m \geq 6$  event, in units of Nm is calculated by the following formula:

$$C_d(m_x) = 2 \cdot 10^9 \cdot \frac{10^{0.5m_x} - 10^{0.5 \cdot 6}}{10^{-6} - 10^{-m_x}}$$

Moment per characteristic earthquake, in units of  $10^{15}$  Nm is given by

$$C_c(m_x) = 10^{1.5m_x + 9}$$

Cumulative rate of  $m \leq m_x$  earthquakes, is calculated by the following formula:

$$N(m, m_x) = f_d \cdot 10^{6-m} \cdot \frac{1 - 10^{m-m_x}}{1 - 10^{6-m_x}}$$

### 4. Calculated quantities for each zone

Calculated quantities, A zones

$f_d = r'$  rate of distributed earthquakes

$f_c = r_c$  rate of characteristic earthquakes

$M_m = \mu HLV + C_d \cdot f_d$  moment rate (model)

Calculated quantities, B zones

$f_d = r$

$f_c = \max[0, (0.5 \cdot \dot{M}_f + 0.5 \cdot \dot{M}_g - C_d \cdot f_d) / C_c]$

$M_m = C_c \cdot f_c + C_d \cdot f_d$  moment rate (model)

Calculated quantities, C zones

$f_d = 0.5 \cdot r + 0.5 \cdot \dot{M}_g / C_d$

$f_c = 0$

$M_m = C_d \cdot f_d$  moment rate (model)

Calculated quantities, all zones

$\dot{M}_f = \mu HLV$  moment rate (geol)

$\dot{M}_s = r \cdot C_d(8.22)$  moment rate (seis)

$a = 6 + \log(f_d)$   $a$  value for distributed events

In the A zones, characteristic and distributed earthquakes are treated separately. Characteristic frequencies are used as input to the cascades model. The rate of distributed earthquakes is determined by a smoothed catalog of earthquakes with characteristic earthquakes removed. The modeled moment rate will exceed the geologically determined rate by the contribution from distributed events. Note that the reported moment rate (model) is based on the long-term fault-slip rate, and as such it neglects the acceleration implied by the time-dependent modeling of characteristic earthquakes.

In the B zones, the moment rate is conserved by

introducing extra characteristic earthquakes. The target moment rate is the mean of the geological and geodetic rates. In the equation for  $f_c$ , the first two terms give the target moment rate, and the third (negative) term subtracts the moment rate already accounted for by distributed earthquakes. A positivity constraint is applied to account for the fact that the distributed earthquakes might by themselves imply more than the target moment rate; in that case  $f_c = 0$ , and the modeled moment rate may exceed the average of the geologic and geodetic moment rates.

In the C zones, the rate of characteristic earthquakes is constrained to zero. The rate of distributed earthquakes is taken as the mean of the observed (smoothed) seismicity rate and the rate needed to supply the geodetic moment-rate estimate. The value reported as  $\dot{M}_s$ , or "MR Seis," is the implied seismic rate assuming  $m_x$  as determined from global earthquake catalogs. The only seismicity data used in the model are in the rates  $r$  and  $r'$ , which are calculated with no assumption about the maximum magnitude. Thus, the modeled moment rate in the C zones will be less than the average of  $\dot{M}_s$  and  $\dot{M}_g$ , and it will depend on  $m_x$ . In fact,

$$\dot{M}_m = 0.5 \cdot \{ [C_d(m_x) / C_d(8.22)] \cdot \dot{M}_s + \dot{M}_g \}.$$

### Appendix E: Procedure for Calculating Seismic Hazard

The general methodology to calculate seismic hazard at a site is well established in the literature (Cornell, 1968). In this report, we used the line source model (Der Kiureghian and Ang, 1975) for characteristic earthquakes and 80% of distributed earthquakes in type A zones. For the rest of distributed earthquakes in type A zones and all earthquakes in type B and C zones, we modified the standard procedure in such a way that we can accommodate geologic constraints implied by the shape of each source zone as well as take into account the difference in focal mechanism; strike-slip or thrust.

In calculating ground motion, we used an empirical model by Geomatrix Consultants (1991) and Sadigh *et al.* (1986), in which strike slip, oblique slip, and thrust mechanisms are distinguished and the source to site distance is defined as the closest distance to the fault rupture surface. For the line source model, a spatial probability distribution function for the rupture length is calculated by moving the mid-point of a given length along the line source. Since our zone allows faults striking along various azimuths, this method become tedious. The usual approach in this case is to use point sources which tend to overestimate the source-site distance as compared to the line source model. In our model, which we call "three-dimensional probabilistic ground motion analysis (PGMA-3D)," we search for the feasible rupture areas within the source zone that share a common source-

site distance. A scanning of the source zone determines the ranges of azimuths that allow for the occurrence of earthquakes with specific rupture lengths that share a common source-site distance. This procedure provides the information on the spatial distribution of earthquakes with different rupture lengths within the seismic zone and the corresponding source-site distances.

We denote the distance between the site  $\bar{x}_s$  and an integration point  $\bar{x}$  on the earth's surface within a given source zone as  $r(\bar{x}_s, \bar{x})$ . As shown in Figure 19, it is the closest distance from the site to the surface traces of those rupture areas that start or end at  $\bar{x}$  and are on one side of the line perpendicular to  $\bar{r}(\bar{x}_s, \bar{x})$ . All vertical rupture areas that are to one side of the line AB, perpendicular to  $\bar{r}(\bar{x}_s, \bar{x})$ , and start or end at point  $\bar{x}$  have their closest distances to the site as  $\bar{r}(\bar{x}_s, \bar{x}) = \sqrt{r^2(\bar{x}_s, \bar{x}) + h^2}$ , where  $h$  is the depth to the seismogenic zone. The rupture areas on the other side of the line AB have shorter surface distances to the site than  $r(\bar{x}_s, \bar{x})$ . At each location, the source zone is searched, over different azimuths, for all possible rupture lengths that have  $r(\bar{x}_s, \bar{x})$  as their closest surface distances to the site. As was discussed earlier, all lines to one side of the line AB, i.e.,  $X(\bar{x}, \psi)$  in Figure 19 are feasible candidates.  $X(\bar{x}, \psi)$  is the longest possible rupture length from  $\bar{x}$  along azimuth  $\psi$  that has  $r(\bar{x}_s, \bar{x})$  as its closest surface distance to the site. A comparison between a rupture length ( $l$ ) and  $X(\bar{x}, \psi)$  determines if an earthquake with the rupture length  $l$  can occur within the region along the azimuth  $\psi$  starting or ending at  $\bar{x}$ . The objective is to construct spatial probability density functions for the rupture lengths. Let us define the function  $\phi(\bar{x}|l)$  as

$$\phi(\bar{x}|l) = \frac{1}{\pi} \int_{\psi_{AB}}^{\psi_{AB} + \pi} H[\lambda(l) \cdot X(\bar{x}, \psi) - l] d\psi, \quad (\text{E1})$$

where  $\psi_{AB}$  is the azimuth of the line AB at  $\bar{x}$ , and  $H[ ]$  is the Heaviside function:

$$H[\lambda(l) \cdot X(\bar{x}, \psi) - l] = 0$$

$$\text{if } l > \lambda(l) \cdot X(\bar{x}, \psi) \quad \text{and}$$

$$H[\lambda(l) \cdot X(\bar{x}, \psi) - l] = 1 \quad \text{if } l \leq \lambda(l) \cdot X(\bar{x}, \psi). \quad (\text{E2})$$

The  $\lambda(l)$  is a factor that allows a fraction of the rupture length to extend the boundaries of the region; i.e., for  $\lambda(l) > 1$ ,  $\phi(\bar{x}|l) = 1$  if  $l \leq \lambda(l) \cdot X(\bar{x}, \psi)$  for all azimuths and  $\phi(\bar{x}|l) = 0$  if  $l > \lambda(l) \cdot X(\bar{x}, \psi)$  for all azimuths. A spatial probability density function for the rupture length

can be constructed by taking the ratio of  $\phi(\bar{x}|l)$  to the integration of  $\phi(\bar{x}|l)$  over the entire area source,

$$f_s(\bar{x}|l) = \frac{\phi(\bar{x}|l)}{\int_S \phi(\bar{x}|l) d\bar{x}}, \quad (\text{E3})$$

where  $S$  represents the source area. For a uniform spatial distribution of all rupture lengths over the entire source  $f_s(\bar{x}|l)$  becomes a constant. In that case, the rupture lengths do not play any role in the PGMA of the source zone, which is equivalent to the point source model. This condition can be simulated by selecting a large value for  $\lambda(l)$ , i.e., allowing the rupture lengths to go beyond the boundaries of the source zone. In other words, the point source model is a special case of PGMA-3D when earthquakes with portions of their rupture lengths outside the source zone are included in the PGMA.

Following the traditional formulation of the PGMA, the probability that the ground motion at a site  $\bar{x}_s$  exceeds a specific level  $y$  from earthquakes within the source  $S$  is formulated as

$$P(Y > y | \bar{x}_s, S) = \int_S \int_M \int_L P[Y > y | m, \bar{r}(\bar{x}_s, \bar{x})] f_s(\bar{x}|l) f_M(m) f_L(l|m) d\bar{x}. dl. dm, \quad (\text{E4})$$

where  $P(Y > y | m, \bar{r}(\bar{x}_s, \bar{x}))$  is the probability that the ground motion at the site will exceed  $y$  from a magnitude  $m$  earthquake at a distance of  $\bar{r}(\bar{x}_s, \bar{x})$ . The term  $f_s(\bar{x}|l)$  is defined by equation (E3). The term  $f_M(m)$  is the magnitude density function and  $f_L(l|m)$  is the probability density function for the rupture length as a function of magnitude. For the cases of the nonvertical rupture areas,  $\bar{r}(\bar{x}_s, \bar{x})$  becomes a function of the dipping angle and azimuth. For dipping faults the term  $f_s(\bar{x}|l)$  is the same as is described by equation (E3); but at each location the closest distance is computed taking the dip and strike of the fault rupture area into account.

For the majority of our 65 seismic zones, the fault is assumed to be vertical strike-slip. Table 7 lists the fault type, dip direction, dip angle, and range of strike direction for seismic zones with nonvertical and/or oblique slip. This table is based on a consensus among geologists who participated in an SCEC workshop held at USC on 25 February 1994.

#### Appendix F: Joint Commentary of the National Earthquake Prediction Evaluation Council and the California Earthquake Prediction Evaluation Council

This joint statement of the two earthquake predictions evaluation councils addresses the suitability of the

conclusions presented in this report for application to public policy and compares them to the existing earth science basis for public policy. It also presents some caveats that should be considered when the conclusions are applied to policy.

The scientific conclusions that drive policy applications must follow from a broad consensus within the earth science community, based on objective, internally consistent analyses that use appropriate data sets and methodologies. This critique by the two councils further extends the report's peer review process. An advanced draft of the report was circulated to the members of both councils. This resulting commentary compares the reports conclusions on damaging earthquake potential to the results of earlier studies that have supported public policy.

## Background

The 1988 Working Group report presented long-term 30-yr probabilities for the occurrence of  $m \geq 7$  earthquakes on segments of the San Andreas fault and  $m \geq 6.5$  on the San Jacinto fault. After the June 1992 Landers/Big Bear earthquakes, an earlier (November 1992) report in this series reexamined  $m \geq 7$  earthquake probabilities in southern California over a 1- to 5-year time frame, specifically considering implications for increased hazard following the 1992 events. The present report reappraises the 30-yr probabilities of  $m \geq 7$  earth-

quakes in southern California using new data and revised, expanded methodologies.

## Comparing Conclusions

### Comparing San Andreas/San Jacinto Independent Segment Probabilities with Earlier Studies

The probability estimates of the largest (characteristic) earthquakes to be expected on individual southern San Andreas or San Jacinto fault segments range from about 10 to 40% in the 1988 report compared with about 6 to 43% (with uncertainties between 6 and 18%) for those same segments in this report (Table 2). Although methods and data sets differ somewhat, the present authors do not consider the differences between their 1994 probability estimates for individual segments of the San Andreas/San Jacinto fault system and the 1988 conclusions significant. Single segment probabilities in the 1994 report are presented between 1 and 24% (with 3 to 15% uncertainties) for two additional segments of the San Jacinto fault and for portions of the Whittier/Elsinore faults (Table 2) that were not considered in the 1988 report.

*Policy Implications.* This study assesses the southern San Andreas and San Jacinto segments using important data acquired after 1988 and refinements in analysis. It is the first comprehensive evaluation of these fault segments since 1988. The results are reassuring. The priorities currently given to earthquake preparedness are not likely to change significantly in response to the 1994 conclusions, except perhaps for some fine tuning at the local scale. These conclusions may help the private sector refine the geographic focus of their earthquake preparations.

### Comparing the Independent Segment Probabilities with the 1994 Cascade Model

In addition to the independent segment probability estimates, the present authors have developed a cascade model that accounts for the interactive rupture of multiple segments during individual earthquakes (Table 3). Multiple-segment earthquake estimates reduce the number but increase the average size of ruptures expected during the next 30 yr compared to predictions for independent-segment events. The present report estimates that, if segments are independent, there is an aggregate 66% probability that at least one characteristic earthquake will occur on one of the four southern San Andreas segments in the next 30 yr. This compares with a 53% probability estimate that a multiple-segment earthquake will occur at least once during the same period according to the cascade model.

*Policy Implications.* Both the independent-segment and cascade model analyses estimate a significant likelihood

Table 7

Zone Number	Range of Strikes	Dip and Dip Direction
15	N to N90W	45 E and NE
20	N to N90W	45 W and SW
26	N30E to N90E	45 N and NW
	N30W to N90W	45 N and NE
31	N30E to N90E	45 N and NW
	N30W to N90W	45 N and NE
32	N to N90W	45 N and NE
33	N30E to N90E	45 N and NW
	N30W to N90W	45 N and NE
34	N to N90W	45 W and SW
35	N30E to N90E	45 N and NW
	N30W to N90W	45 N and NE
40	N30E to N90E	45 N and NW
	N30W to N90W	45 N and NE
46	N30E to N90E	45 N and NW
	N30W to N90W	45 N and NE
49	N30W to N90W	45 N and NE
54	N30E to N90E	45 S and SE
	N30W to N90W	45 S and SW
55	N30E to N90E	45 S and SE
	N30W to N90W	45 S and SW
65	N30E to N90E	45 S and SE
	N30W to N90W	45 S and SW

of large damaging events. The present rationales for earthquake preparedness in areas adjacent to the San Andreas, San Jacinto, and Whittier/Elsinore faults are not significantly modified by the cascade model conclusions.

#### Southern California Earthquake Regional $m \geq 7$ Probability Estimates

From a more regional perspective, this report addresses that portion of the state south of latitude  $36^\circ$  with a "preferred" model which apportions the seismic moment budget for all of southern California among 65 source zones using geologic (including paleoseismic), geodetic, and earthquake catalog data. This holistic analysis is based upon the comprehensive concept of the SCEC master model. Rules are established to partition the seismic moment among the 65 zones categorized into A, B, and C types, depending upon the amount of geologic data available for combining with geodetic and earthquake catalog sources. The preferred model predicts a rate of 0.067 events/year for  $m \geq 7$  earthquakes in southern California, corresponding to a 30-yr probability of 86%. This value exceeds the 1988 southern California estimate of about 50 to 60% that only considered the aggregated San Andreas and San Jacinto probabilities in southern California. While the present estimate raises the probability somewhat, it expands the area of consideration.

*Policy Implications.* The regional  $m \geq 7$  probability estimates of this report underscore the need for continuing earthquake preparedness efforts in urban areas. They further justify the need for earthquake preparedness activities in the more rural areas of southern California which were not considered in the 1988 report.

#### Using the Regional Preferred Model in Probabilistic Seismic Hazard Analysis for Public Policy

The preferred model characterizes the 65 source zones using standardized rules for partitioning seismic moment rate. The manner of establishing the boundaries and partitioning the seismic moment are inevitably somewhat arbitrary. Greater confidence in characterizing the seismic sources using these procedures might have resulted from a close correspondence between the predicted seismic rate for large events such as  $m \geq 7$  and the historically observed rate. Although not emphasized in this report, there is a disparity between the observed moment release represented by seismic activity since 1850 and the larger moment accumulation budget during that period, calculated from the currently observed rate of plate movement. The long-term nature of this disparity is difficult to quantify. An important qualification to the results of the preferred model results from the observed rate of  $m \geq 7$  earthquakes since 1850 (0.035 events/yr): only about half the calculated preferred model rate (0.08

events/yr). As the authors point out, there are changes that can be made in the approach such as adjusting the cascade analysis to lower the rate of  $m \geq 7$  events to be closer to the observed value. By making some of these changes, an alternative model (Table 6) comes closer (0.065 events/yr compared to 0.035 events/yr observed), but still leaves a significant gap. As the authors point out, an unknown but significant portion of the cumulative plate motion budget in southern California can be taken up by anelastic deformation and not entirely released by earthquakes. Additionally, given the limited temporal extent of the earthquake catalog, we cannot rule out the possibility that future very large earthquakes will more closely balance the observed and calculated moment release rates.

Comparing the calculated and observed seismic rates of  $m \geq 7$  earthquakes does not definitively test the validity of the model. In the absence of such a test, another approach should be used to evaluate the suitability of the preferred model to public policy applications. To be used in public policy, a seismic hazard model should not yield maps with patterns of ground motion that are severely affected by the choice of seismic zone characteristics that are relatively unconstrained by data. Studies are needed to show the sensitivity of seismic hazard analyses to variations in the selection of seismic source boundaries and parameter values.

Another limitation of the preferred model is the present lack of consensus on how to characterize some types of seismic sources such as blind thrusts.

*Policy Implications.* At present, caveats must be applied to the ways in which detailed conclusions of this report are used for particular sites. The appropriateness of the rules and the assumptions used in defining and partitioning seismic moment among the source zones should be further examined to see how variations in the least-constrained parameters affect the overall patterns of ground motion.

#### Continuing Investigations are Recommended to Emphasize the Following Issues

- Blind thrust geometry and slip rates, and their incorporation into the preferred model methodology.
- The intrinsic variability in characteristic earthquake recurrence rates and its significance in probability analyses.
- Further acquisition and appraisal of geologic evidence that significantly modifies earlier paleoseismic interpretations such as that concerning the Carrizo segment of the San Andrea fault.
- The assumptions used in the distribution of seismicity and the sensitivity of the seismic rate and hazard maps to reasonable variations in these assumptions.

- The geographic characterization of type C seismic source zones and the sensitivity of predicted seismic rate and seismic hazard maps to variations in their definition.

In the meantime, from a public policy point of view, the maps derived from the preferred model can be used to characterize regional seismic hazard in southern California. Like any other single model, the preferred model should be used with professional caution and appropriate sensitivity studies when applied to site-specific geotechnical estimates for earthquake resistant design of individual structures.

Despite inevitable uncertainties, this report significantly advances the characterization of southern Cali-

fornia seismic sources using regional geologic, geodetic, and earthquake catalog observations. The earth sciences and the citizens of California are in debt to SCEC and its investigators for this effort. This line of investigation is promising and should continue.

Tom McEvelly, Chair  
National Earthquake Prediction  
Evaluation Council

Jim Davis, Chair  
California Earthquake Prediction  
Evaluation Council

Manuscript received 7 October 1994.